University of Southampton

Faculty of Natural and Environmental Science

School of Ocean and Earth Sciences

Quaternary Fire Activity in Northern Africa reconstructed from charcoal records in marine sediments

Volume 1 of 1

by

Harriet Ruth Moore

MSci Geology

ORCID ID http//orchid.org/0000-0002-1292-1953

Thesis for the degree of Doctor of Philosophy

March 2019

University of Southampton

Abstract

Faculty of Natural and Environmental Sciences

School and Ocean and Earth Sciences

Thesis for the degree of Doctor of Philosophy

Quaternary Fire Activity in Northern Africa reconstructed from charcoal records in marine sediments

by

Harriet Ruth Moore

Fire in the Earth's ecosystems is a significant driver of ecological change, fires remove dead biomass and prevent the reestablishment of woody plants acting to maintain and/or expand the high light environments. Frequent fires, create positive feedbacks that affect the environment by driving it towards increasingly arid conditions, by promoting the fire and often arid adapted grasses. The increased fire activity during the Late Miocene is hypothesized to have led to the large scale, global near synchronous expansion of C_4 tropical grasses and consequently, the evolution of the savanna biomes.

Little, however, is known about the role of fire activity in the geologic past. Existing terrestrial and lacustrine records are often discontinuous due to periods of erosion or non-deposition, cover limited time intervals, may have poor age control and can be strongly biased by very local events. Marine sediments provide an underexploited resource to circumvent these issues. In this thesis, I present a number of new reconstructions of regional fire activity spanning several Quaternary glacial-interglacial cycles, reconstructed from deep sea sedimentary cores located on the Northwest African Margin. These new records allow me to shed light on long-lived patterns of palaeo-fire activity in response to intervals of climate change documented across northern Africa at both orbital and millennial time-scales.

Chapter 4 explores the factors that determine the validity of fire activity reconstructions from marine sediments by examining inter-site discrepancies in charcoal recovery and comparing the results of three distinct techniques to reconstruct fire activity, including both geochemical and

optical approaches. I report major differences in charcoal concentration between different sites along the northwest African margin, and suggest that oxidation could be a potential control on charcoal preservation in certain locations. In addition, I show that there can be large discrepancies in reconstructions of fire activity using optical and geochemical methods, with the optical method of charcoal extraction revealing more charcoal flux variability than geochemical techniques.

Chapter 5 examines the evolution of spatial variability in fire activity along a transect (9°N-21°N) along the Northwest African Margin over the last 50 kyr. This interval covers events driven by both high- and low- latitude climatic forcing which occur over millennial and orbital timescales respectively. Each of the three sites in the transect shows a different relationship between hydroclimate and fire activity. The northern site exhibits a pattern of increased fire activity in response to increased humidity. In direct contrast, the southern site displays reduced fire activity when humidity increases. The central site (15°N) displays peak fire activity during intermediate humidity, with a reduction in fire activity during both arid and humid climate intervals. I attribute this to the proximity of this site to the highly rainfall sensitive grassy-woody savanna boundary, which experiences major changes in floral assemblage and therefore fuel loads associated with even small changes in rainfall. Greater aridity leads to a contraction of vegetation cover and a reduction of fuel loads, whilst increased humidity produces a floral assemblage that generates more moisture rich fuel loads, consequently in both cases resulting in decreased fire activity.

Chapter 6 presents a long record of fire activity response to climatic changes through the Last Glacial Cycle (140-0 kyr before present) at Site Ocean Drilling Program (ODP) 658 (21°N). In general, a clear relationship between fire activity and precipitation is clearly observed, higher fire activity is observed when humidity increases due to the greater availability of biomass, supported by the higher precipitation levels facilitated by the northward displacement of the Intertropical Convergence Zone (ITCZ). However, during the times of highest humidity (African Humid Periods 5 and 1), fire activity is dampened. I discuss three possible hypotheses to explain this suppression of burning: 1) High-latitude climate forcing exerted a secondary control on vegetation through remnant effects of the glacial, 2) Changes in atmospheric carbon dioxide exerts a secondary control on fire activity by promoting forest growth at the expense of grasslands, 3) The most extreme insolation peaks triggers conditions that were sufficiently humid to encourage the expansion of wetter-adapted less flammable ecosystems with higher fuel moisture contents.

Chapter 7 compares and contrasts charcoal flux records from two glacial-interglacial cycles experiencing similar orbital geometry: the Last Glacial Cycle (MIS 1-5, 0-140 ka) and the Mid-Brunhes (MIS 9-11, 300-450 ka). The same relationship between precipitation and fire activity as observed in the Last Glacial Cycle is present through the Mid-Brunhes, with fire activity increasing with increasing humidity, except during peak interglacials. The absence of strong charcoal flux peak associated with MIS 11, a major interglacial associated with only weak insolation forcing, implies that it is the interglacial state rather than insolation forcing that is responsible for the suppression of burning during interglacials. This result is enigmatic, however, my favoured hypothesis to explain the low fire activity observed, is the development of a wetter less flammable vegetation assemblage leading to a smaller moister fuel source that experiences less climatic curing during interglacials. Also due to the similarity in the deglaciation from MIS 2 where there is the potential for a human impact and MIS 11 without a human impact in fire activity in the charcoal flux trends this study allows me to suggest that there is no or minimal anthropogenic forcing of fire activity during the Holocene.

Table of Contents

Table of Tables

Table of Figures

A.1.1 List of Accompanying Materials

Due to the size of the data sets generated as part of these studies, all data is submitted electronically in the form of a CD.

Research Thesis: Declaration of Authorship

Print name: Harriet Ruth Moore

Title of thesis: Quaternary Fire Activity in Northern Africa reconstructed from charcoal records in marine sediments

I declare that this thesis and the work presented in it are my own and has been generated by me as the result of my own original research.

I confirm that:

1. This work was done wholly or mainly while in candidature for a research degree at this University;
2. Where any part of this thesis has previously been submitted for a degree or any other qualification at this University or any other institution, this has been clearly stated;
3. Where I have consulted the published work of others, this is always clearly attributed;
4. Where I have quoted from the work of others, the source is always given. With the exception of such quotations, this thesis is entirely my own work;
5. I have acknowledged all main sources of help;
6. Where the thesis is based on work done by myself jointly with others, I have made clear exactly what was done by others and what I have contributed myself;
7. None of this work has been published before submission

Signature: Date:

Acknowledgements

A thesis is made by more than just one person, it's my name is on the cover but there are so many people that I need to give heartfelt thanks to because without them, my PhD and this thesis wouldn't have reached completion.

Firstly, thanks to my supervisors Paul Wilson and Anya Crocker at the University of Southampton for your help and support and pushing me to be a better scientist over the last four years. To Colin Osborne and David Beerling at the University of Sheffield for your enthusiasm about my data and Claire Belcher at the University of Exeter for teaching me about charcoal. A special mention also to Nele Meckler for sharing her invaluable XRF data for ODP 658 from which I based my sampling plans.

Thank you to the captain, the crew and scientific party of Ocean Drilling Program Leg 108 and the captain and crew of RV Meteor cruise M65/1 during which GeoB9508-5 and GeoB9528-3 for retrieving the sediment I've worked on. I would like to thank the ODP core repository and GeoB core repository at the MARUM – Centre for Marine Environmental Sciences at the University of Bremen, Germany for providing me with the sedimentary material I worked on. To Walter Hale, Holger Kuhlmann and Alex Wülbers at the Bremen Core Repository for help with sampling.

To those brave enough to deal with HF, thanks to Shir Akbari, John Marshall, Dave Carpenter and Ian Harding for help in the palynology labs and chats about charcoal and gossip. Also, to Tanya Beattie, thank for your help in collecting reflected light images of my charcoal on the Zeiss and for the encouragement in the labs, the laughs and shared pain at wearing full PPE for hours in a hot many windowed laboratory during the summer whilst sieving.

My grateful thanks to Elizabeth Mullinger, Alice Cardy and Megan Spencer for running the ODP Site 658 samples for TOC. Special thanks to Vicki in addition to your help generating the TOC values and for so much more, for being a sympathetic ear and for the giggles and gripes sessions. Thanks for being a good friend.

Unreserved thanks to the wonderful NOC IT for dealing with all my technical issues, especially Chris who rescued my laptop from death and healed to the point it was able to limp through the last couple months of this PhD so I could get this thesis written up.

My thanks to all the members past and present of the Palaeoresearch group for their support and guidance and shared comradery. To office mates graduated and yet to graduate thanks for a wonderful work environment. Particularly to Tim van Peer for his help with figures, encouragement and F1 chats and keeping me amused in the office. Thanks to Anieke Brombacher for tea breaks, advise on both science and life and for games of squash. Also, to Emma Chambers for willing me on.

To the varying members of the "Lunch Bunch" for their daily funny stories, bonkers conversations, you were a welcome mid-day distraction. To Dan Doran for the use of the kettle and cups of tea and letting me hide in the rock prep lab when I needed a change scenery whilst I was writing up.

To Gabriella Jardine a great housemate, thanks for girly nights in with a film or binging Netflix and bottle of wine or a G&T or two, and for our shopping trips where we were a bad influence on each other for the social aspect of PhD life. To my non-science friends Claire, Adele, Rosanna and Moni for being supportive, positive influences and giving me pep talks and reminding me that there is life outside of academia.

To the Moore Tribe because you have had to put up with pints of tears and hours of scientific explanations and wiggly lines. You are the best. You kept me grounded and remined me that it's all going to be ok. Thanks for the being there for me when I needed you, your years of encouragement, unceasing support and always being on my side.

Lastly but by no means least, to my Matt who has kept me sane. Thank you for coping with me when I've been stressed out and sometimes irrational, for supplying me with food so I didn't need to worry about cooking. Thanks for the massages and countless hugs, for letting me rant when I needed to and mopping up my tears. Thanks for so being wonderful.

So here it is 272 samples and 169,106 individual charcoals counted later, my thesis.

Definitions and Abbreviations

NOC	National Ocean Oceanography Centre
DIS	Bremen Core Repository Drilling Information System
ODP	Ocean Drilling Program
MIS	Marine Isotope Stage
SEDIS	Scientific Earth Drilling Information Services
IODP	Integrated Ocean Drilling Program
GPTS	Geomagnetic Polarity Timescale
mbsf	Meters below sea floor
mcd	Meters composite depth
yr	Years
kyr	Thousands of years
ka	Thousands of years ago
Ma	Millions of years
Myr	Millions of years ago
NWAM	North West African Margin
NWA	North West Africa
NAS	North African Savanna
NETW	North East Trade Winds
AEJ	African Easterly Jet
MAP	Mean Annual Precipitation
ITCZ	Intertropical Convergence Zone
AMOC	Atlantic Meridional Overturning Circulation
SST	Sea Surface Temperature
$\delta^{18}O$	Ratio of ^{16}O to ^{18}O

$\delta^{13}C$	Ratio of ^{12}C to ^{13}C
$\delta^{13}C_{org}$	Ratio of organic ^{12}C to ^{13}C
$\delta^{15}N$	Ratio of ^{14}N to ^{15}N
$\delta^{15}N_{org}$	Ratio of organic ^{14}N to ^{15}N
$\%C_{org}$	Percentage organic carbon
%N	Percentage Nitrogen
%TOC	Percentage Total Organic Carbon
TOC	Total Organic Carbon
TIC	Total Inorganic Carbon
AOM	Amorphous Organic Matter
C:L	Ratio of Carbon to *Lycopodium*
C/N	Ratio of Carbon to Nitrogen
Nd	Neodymium
H_2O_2	Hydrogen Peroxide
HCl	Hydrochloric Acid
HF	Hydrofluoric Acid
$K_2Cr_2O_7$	Potassium Dichromate
AHP	African Humid Period
GSP	Green Sahara Period
H	Heinrich Events
IRD	Ice Rafted Debris
YD	Younger Dryas
B/A	Bølling-Allerød Interstadial
G-IG	Glacial – Interglacial Cycle
LGC	Last Glacial Cycle
LGM	Last Glacial Maxima
PGC	Penultimate Glacial Cycle
PGM	Penultimate Glacial Maxima

BC	Black Carbon
OREC	Oxygen Resistant Elemental Carbon
pCO_2	Atmospheric Carbon Dioxide
pO_2	Atmospheric Oxygen
LR04	Benthic Global Oxygen Isotope Stack (Lisiecki and Raymo, 2005)
NPP	Net Primary Productivity
JJA	June, July and August
XRF	X-ray fluorescence
(V)PDB	(Vienna) Pee Dee Belemnite standard

Chapter 1 Introduction

Fire has been a major driver of environmental change since at least the Silurian (Glasspool et al., 2004), acting as a mechanism to induce floral turnover or to maintain and expand some of the planet's vegetation zones, notably savanna ecosystems. The specific fire activity associated with a particular biome is strongly influenced by vegetation density, plant type and climate particularly precipitation and temperature. The size and global distribution of fire-regulated ecosystems are therefore highly sensitive to changes in climate. A more active fire cycle has been hypothesized to have facilitated the near-synchronous global C_4 tropical grassland expansion marking the evolution of the savanna biome during the late Miocene (8-5 Ma)(Beerling and Osborne, 2006; Cerling, 1992; Hoetzel et al., 2013; Keeley and Rundel, 2005; Osborne, 2008; Scheiter et al., 2012). While the behaviour and ecological impact of fire in modern systems can be observed and is well understood, relatively little known about fire activity and its impacts in the geological record. In order understand the role of fire in past ecosystems it required an investigation of the differing result obtained by different charcoal extraction methods and the reproducibility of these finding.

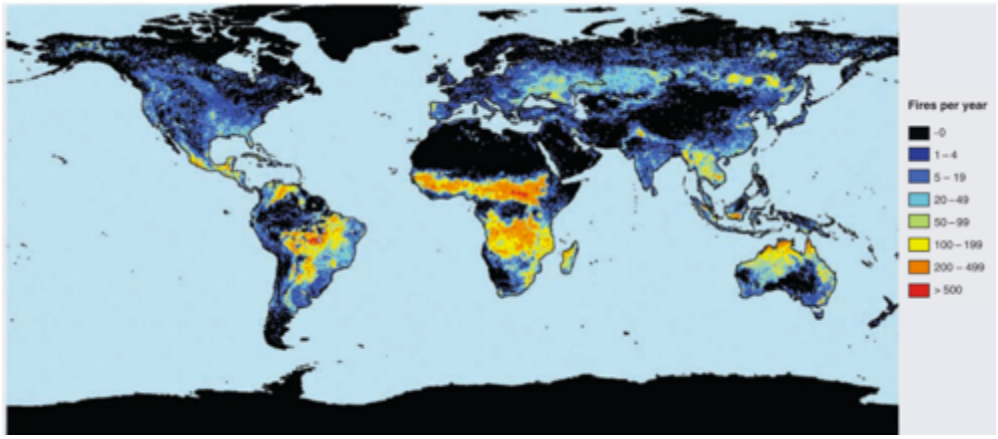

Figure 1.1 Global Fire Map: Annual average number of fires observed by satellite (Bowman *et al.,* 2009, Giglio *et al.,* 2006).

Palaeowildfire activity has previously been studied to investigate the relationship between hydrology and climate forcing, using charcoal flux as a proxy for fire activity, across glacial-interglacial cycle and humid and arid millennial climate events across North America (Flannigan et al., 2000; Marlon et al., 2009; Umbanhowar, 2004), Southern Africa (Daniau et al., 2013, 2010, 2007; Hoetzel et al., 2013), North Africa (Bird and Cali, 1998) and globally (Herring, 1985; Justino et al., 2010; Power et al., 2008). Despite being the locus of some of the highest fire activity globally (Figure 1.1). Northern Africa is comparatively less well-studied (Bird and Cali, 1998). Furthermore, this status is likely to have been long-lived because floral assemblages on North Africa have remained

broadly consistent, despite multiple documented latitudinal migrations, since at least ca. 660 ka (Dupont, 1993). These records however, currently span short geological intervals and examine a local fire activity signal, given the observable modern day climatic and floral variability of Africa I would expect to see pronounced spatial variability in the geological past which thus far has not been documented in the literature. The shorter length of the published charcoal records also prevents the identification of long-term patterns and trends or cyclic behaviours in fire activity.

Today, human activity is the main driver of fire activity in northwestern Africa but an understanding of the underlying climatic forcing functions remains important, not least because the 21st Century rainfall climate of the Sahel, a vital farming region where the majority of the inhabitants are dependent on subsistence agriculture, has an uncertain future (Cincotta et al., 2000; De Rouw, 2004; Oweis and Hachum, 2006). Thus, environmental changes leading to the expansion or contraction of fire-regulated ecosystems occurring in this region will have wide reaching socio-economic impacts on food and water security for the citizens of the region (Cincotta et al., 2000; Laris and Wardell, 2006; Vierich and Stoop, 1990). It would be intriguing to assess the whether an anthropogenic signal could be unpicked from an underlying natural signal or if the onset of human fire activity could be identified in a new higher resolution record of past burning.

1.1 North African Savanna

The North African Savanna (NAS) is located between 5-15°N and acts as a buffer between the hyper-arid sparsely vegetated Sahara Desert to the north and dense tropical forests to the south (Dupont, 2011, 1993). The term savanna encompasses a broad range of environments, defining any ecosystem with a C_4 grassy understory with a variable C_3 woody cover component (0-80%) (Hirota et al., 2011; Ratnam et al., 2011; Scholes and Archer, 1997). The North African Savanna (NAS) is sub-divided into two, differentiating between two functionally contrasting ecosystems; a grassy and woody savanna (Figure 1.2). The grassy savanna prevails under more arid conditions where Mean Annual Precipitation (MAP) falls between about 110 and 650 mm/yr and is located between about 15 and 10°N, (Sankaran et al., 2005). The floral assemblage of the grassy savanna is dominated by tropical grasses but also comprises a smaller woody component (0-40% canopy cover), this environment is climatically maintained (Accatino et al., 2010; Sankaran et al., 2005). The woody savanna is located south of the grassy savanna between about 10 and 5°N under where more humid conditions prevail (MAP ~650-1100mm/yr) (Accatino et al., 2010; D'Onofrio et al., 2018; Hoffmann et al., 2012; Scholes and Archer, 1997). The higher precipitation supports a larger woody

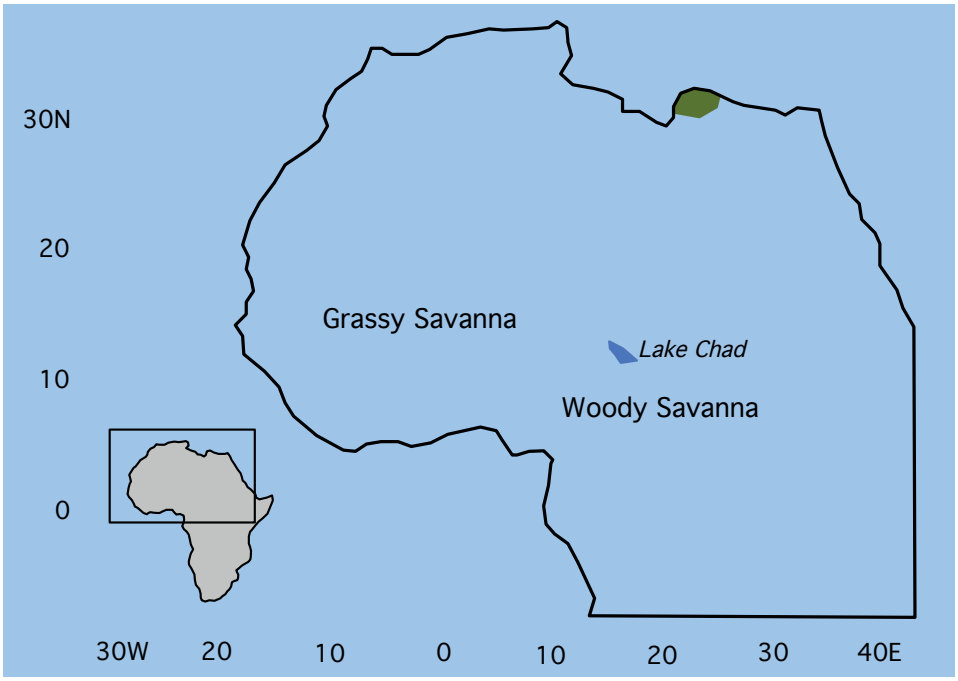

Figure 1.2: Schematic of the North African Savanna. Schematic map of the major North African vegetation bands, adapted from Sarnthein *et al.,* (1989).

component (40-80%) which, without regular disturbance by fire and/or herbivore grazing, would result in grass exclusion and canopy closure (reversion to forest)(Accatino et al., 2010; Archibald and Hempson, 2016; Bond et al., 2005; Cochrane, 2003; Sankaran et al., 2005). Thus, regular burning is an intrinsic feedback mechanism to maintain the high light environment required by tropical grasses by destroying woody saplings and preventing forest encroachment (Accatino et al., 2010; Sankaran et al., 2005). This positive feedback loop increases the tropical grass habitat increasing the fire susceptibility and thus fire activity of the region, this mechanism drives the ecosystem towards increasing dominance of arid-adapted flora (Beerling and Osborne, 2006; Keeley and Rundel, 2005). In this way, frequent fires selectively promote the growth of fire-adapted flora (Beerling and Osborne, 2006; Keeley and Rundel, 2005).

Today, the NAS experiences some of the highest fire activity globally (Figure 1.1) with fire reoccurrence intervals typically between 1-5 years (Keeley and Rundel, 2005). A strong annual link is observed in the NAS between burning and precipitation. Fires ignited naturally by lightning strikes begin early in the dry season (October-November) at the southern fringes of the Sahara (17°N) and after a short period of climatic curing progresses southward as the dry season advances (Carmona-Moreno et al., 2005; Cooke et al., 1996; Harrison and Sanchez Goñi, 2010; Stott, 2000).

Climatic curing is defined as the time requirement needed for the biomass to desiccate and become sufficiently flammable facilitate successful ignitions during warm dry weather. Thus, the NAS is highly sensitive to changes in the hydrological cycle unlike the Earth's other biomes African vegetation is precipitation- rather than temperature-dependant (Dupont, 1993; Dupont et al., 1989). Consequently, African biomes have distinct parallel latitudinal distribution (Figure 1.2) falling along precipitation gradients (Dupont, 1993; Dupont et al., 1989), dictated by the mean annual location of the Intertropical Convergence Zone (ITCZ).

1.2 Intertropical Convergence Zone

The Intertropical Convergence Zone (ITCZ) supplies Northern Africa with >60-90% of its annual rainfall (Shanahan et al., 2015). The ITCZ comprises a band of low pressure where the northern and southern hemisphere trade winds converge, producing a belt of intense rainfall close to the equator (Schneider et al., 2014; Waliser and Gautier, 1993). Annually the ITCZ shifts position migrating towards the warmer hemisphere, reaching a northern position of 9°N during boreal summer and a southern position of 2°N during boreal winter (Schneider et al., 2014; Waliser and Gautier, 1993). This yearly progression produces the seasonal precipitation cycle of wet summers (July-August) and dry winters (December-February)(Mohtadi et al., 2016; Shanahan et al., 2015).

Over geological timescales, the latitudinal extent of this seasonal migration in the ITCZ has undoubtedly changed in response to changes in the inter-hemispheric temperature gradient (Earth's thermal equator) induced either or by orbitally driven changes in incident solar radiation associated with the strengthening/weakening of Atlantic Meridional Overturning Circulation (AMOC) caused by changes in latitudinal ocean heat transport (Barker et al., 2010; Broecker and Putnam, 2013). During times of insolation maxima and strong AMOC, the northern hemisphere is warmed, dragging the ITCZ to higher latitudes during boreal summer than during insolation minima and times of weak AMOC, thereby increasing rainfall across northern Africa- causing the so called African Humid Periods (AHPs) and Green Sahara Periods conditions (Ehrmann et al., 2016; Jolly et al., 1998; Shanahan et al., 2015; Skonieczny et al., 2015) (e.g., MIS 5e and Bølling-Allerød (B/A) (Barker et al., 2010; Rohling et al., 2013, 2002). Under the inverse conditions arid conditions occurs e.g. the Last Glacial Maximum (LGM), Heinrich (H) Events, Younger Dryas (YD) and the 8.2kyr climate events, rainfall delivery to northern Africa is reduced (Bouimetarhan et al., 2012; Maslin et al., 2014; McGee et al., 2014; Shanahan et al., 2006; Stager et al., 2011). Recent studies invokes ITCZ expansion and contraction on millennial timescales rather than ITCZ migration in response to sea

surface temperatures (SST) on the north western African margin (NWAM) (Collins et al., 2010; Singarayer et al., 2017) but the overall association between a warmed northern hemisphere and humid conditions on northern Africa is not changed. This relationship is demonstrated clearly in the deposition of organic-rich sedimentary layers or sapropels in Mediterranean Sea sediments when freshwater flux into the basin through North African wadi systems and the Nile is high, increasing surface buoyancy and reducing deep-water formation generating anoxic conditions and increased the preservation of organic material and the deposition of a sapropel layer (Ehrmann et al., 2016; Grant et al., 2016; Melki et al., 2010; Rohling et al., 2015; Toucanne et al., 2015; Williams, 2009). Sapropel deposition has been occurring for the at least the last 8 Ma occurring at ~20 kyr intervals, given the requirement for their formation sapropels have been used to infer corresponding AHPs back into the Late Miocene (Larrasoaña et al., 2013). Currently, unlike the well documented sapropels from which many of the older APHS are inferred, the less well studied AHPs are not formally documented therefore the exact number or timing of these potential AHP's are unknown (Larrasoaña et al., 2013).

1.3 Arid Climate Events

1.3.1.1 Heinrich Events

Elevated levels of ice rafted debris (IRD) define Heinrich Events (H) (Heinrich, 1988; Hemming, 2004; Maslin et al., 2001, 1995). H events are associated with high melt water flux events and massive iceberg calving from the Laurentide Ice Sheet into the North Atlantic Ocean, cooling the northern hemisphere inducing colder SSTs on the northwest African margin displacing the ITCZ south (Broecker et al., 1992; Heinrich, 1988; Hemming, 2004; Maslin et al., 2001, 1995; Niedermeyer et al., 2009). Heinrich Event 1 (HE1)(16-17 ka) is the largest of these events records in palaeo-archives.

Heinrich Events are intervals of pronounced aridity on Northern Africa (Bouimetarhan et al., 2012; Collins et al., 2013; Mulitza et al., 2008; Tjallingii et al., 2008), these so called 'Mega-droughts' are indicated by large increases in offshore dust fluxes, doubling pre- and post- event specific arid events (Collins et al., 2013; Mulitza et al., 2008). These intervals are associated with the drying out of North African lakes (Lamb et al., 2007; Marshall et al., 2011; Shanahan et al., 2006; Stager et al., 2011, 2002; Verschuren et al., 2009) and a southward displacement of the palaeo-Sahara-Sahel boundary by 3-7° (e.g. from 19-12.5°N during H1), depending on the severity of the event (Collins et al., 2013).

1.3.1.2 Younger Dryas and 8.2 ka Event

Colder conditions prevailed across much of the northern hemisphere during YD (12-13 kyr) and 8.2 ka (8.0-8.4 kyr) large melt water pulses from ice margin lake on North America, produced colder sea surface temperatures and reduced seas surface salinities in the North Atlantic displacing the ITCZ south towards the equator (Alley et al., 1997; Alley and Ágústsdóttir, 2005; Magny and Bégeot, 2004; Weaver et al., 2003; Weldeab et al., 2007; Zhao et al., 1995).

During the YD and 8.2 ka event dust flux increases (Adkins et al., 2006; Mulitza et al., 2008; Tjallingii et al., 2008; Zielhofer et al., 2017) indicating prevailing arid conditions across northern Africa, evidenced by widespread low-stand lake conditions across the region including; Lake Bosumtwi, Lake Challa, Lake Tana and Lake Victoria (Gasse, 2000; Stager, Mayewski and Meeker, 2002; Alley and Ágústsdóttir, 2005 and references therein; Shanahan *et al.*, 2006; Lamb *et al.*, 2007; Verschuren *et al.*, 2009; Marshall *et al.*, 2011).

1.4 Humid Climate Events

1.4.1 Bølling-Allerød

The B/A interstadial (~14.7-12.9 ka) (Bond et al., 1999; Dansgaard et al., 1993) is suggested to have been driven by a melt water pulse from the Antarctic ice sheet into the Southern Ocean (Barker et al., 2010; Weaver et al., 2003) producing a relatively warm phase in the northern hemisphere and a northerly displacement of the ITCZ. The warmer conditions are marked by reduced sea-ice cover and warmer sea surface temperatures (SSTs) in the North Atlantic Ocean (Bradtmiller et al., 2016; Weldeab et al., 2007), with an almost synchronous 9°C warming of air temperatures above Greenland (Severinghaus and Brook, 1999) and a ~20m rise in sea level within 500 yrs of this event (Weaver et al., 2003). At this time northern Africa experiences a period of higher humidity as indicated by an increase in humid taxa in the pollen records (Dupont, 2011), and marine sites on the northwest African margin record an increase in humidity indices at GeoB7920-2 and a reduction in dust and terrigenous flux offshore to Ocean Drilling Program (ODP) site 658 (Adkins et al., 2006; Tjallingii et al., 2008).

1.4.2 African Humid Periods and Green Sahara Periods

Orbitally forced insolation-driven penetration of the ITCZ to higher latitudes across the modern-day Sahara Desert region is largely controlled by precession minima resulting in a northwards shift in the position of the vegetation zones across Africa (Claussen and Gayler, 1997; Collins et al., 2010; DeMenocal et al., 2000; Dupont, 1993; Larrasoaña et al., 2003; Ritchie et al., 1985; Rohling et al., 2015; Shanahan et al., 2015). In this way, AHP conditions are closely associated with the development of Green Sahara Period (GSP), the terms AHP and GSP are often used interchangeable, I use GSP specifically to refer to increased vegetation coverage. The GSP describes an interval when the Sahara Desert was extensively covered by scrubby vegetation and gallery forests developed along waterbodies activated by the increased rainfall (Hély et al., 2014, 2009; Watrin et al., 2009). The floral assemblage of the GSP associated with AHP1 (5.5-15kyr) is noted to have a non-analogous floral assemblage compared to modern African ecosystems (Hély et al., 2009; Watrin et al., 2009). Investigation of pollen samples from 73 terrestrial sites, each site representative of in-situ palaeo-floral assemblages, these site cover a latitudinal range of between 4.3°S and 25.5°N in Western Africa, that encompassed the modern biomes of the Sahel, Grassy Savanna, Woody Savanna and the Rainforest indicated that during AHP 1 humid taxa are found 9-5°N of their current position to coexist with arid and desert taxa, having migrated along river systems (Hély et al., 2009; Watrin et al., 2009). Notably an increase in tropical tree pollen at higher latitudes during this interval is documented in these records, transport as a driver is discounted as tropical trees are entomophilous (low pollen producers) and the pollen that is produced is sticky and is poorly dispersed by wind due to its shape therefore remaining close to source (Dupont, 1993), however a small degree of pollen transport can't be discounted. A straightforward north-south migration of the African biomes therefore may be an oversimplification. Consequently, I infer a non-analogue floral scenario for all AHPs.

1.4.3 AHP-1 or *the* African Humid Period

The most recent African Humid Period (AHP1) is often referred to in the literature as '*the* African Humid period' (5.5-15kyr), this term is misleading, as multiple AHPs have been inferred to have occurred at least since the late Miocene (8 Ma)(Larrasoaña et al., 2013, 2003; Maslin and Christensen, 2007) but it is by far the best-studied of the AHPs. Rock art and carvings discovered in the central Sahara during the late 1850's, and subsequently dated to mid - AHP1 at ~10 ka, indicate that this region was a verdant landscape that supported megafaunal assemblages including

hippopotamus, elephant, giraffe, crocodiles as well as fish not associated with the modern Sahara Desert (Figure 1.3)(Barnett, 2002; di Lernia and Gallinaro, 2010; Dumont, 2017; Gallinaro, 2013).

Figure 1.3: Art work from the Central Sahara dating to the African Humid Period (AHP1). http://freevst.x10.mx/sahara/sahara_world/sahara_history/rock%20art%2001.jpg

1.5 Plant Photosynthetic Pathways

Two major photosynthetic pathways are used by plants– the ancestral C_3 or Calvin cycle photosynthetic pathway and C_4 or Hatch-Slack Cycle which evolved during the Oligocene (Cerling et al., 1993; Ehleringer et al., 1991; Osborne, 2008; Waller and Lewis, 1979). These photosynthetic pathways are adapted to different growing season conditions, therefore expansions and contractions of C_3 and C_4 coverage have been documented in the geologic past, e.g. the Late Miocene (8-5 Ma) (Cerling, 1992; Ehleringer et al., 1997; Osborne, 2008; Osborne and Beerling, 2006), across the last glacial-interglacial transition (20 ka) and during GSPs (Kuechler et al., 2013).

C_3 plants are most competitive under cooler growing season temperatures (<25°), low light and high rainfall (>1100mm/yr MAP) and high atmospheric carbon dioxide (pCO_2)(>500ppmv). C_4 plants are more competitive under warmer growing season temperature (>25°C), higher light conditions, lower rainfall (350-1100cm)(Aldersley et al., 2011; Boom et al., 2002; Ehleringer and Cerling, 2001; Ségalen et al., 2007; Waller and Lewis, 1979). C_4 plants also have a competitive advantage at lower pCO_2 (<500 ppmv) because this photosynthetic pathway evolved to reduce water loss through open

stomata during pCO_2 uptake during respiration because pCO_2 is more effectively concentrated and processed (Bond et al., 2003; Cerling et al., 1993; Dupont et al., 2013; Hoetzel et al., 2013; Sage, 2001; Ségalen et al., 2007). As a result, C_4 plants have a water use efficiency that is 2-3 times greater than that of C_3 plants (Bobe, 2006; Bond et al., 2005; Hoetzel et al., 2013; Keeley and Rundel, 2005). Their rapid regenerative capacity and high water efficiency enable C_4 plants to generate large amounts of dry flammable fuel (Bond et al., 2005; Keeley and Rundel, 2005) allowing them to dominate in frequently burnt ecosystems (Beerling and Osborne, 2006; Bobe, 2006; Bond et al., 2005; Furley et al., 2008; Hoetzel et al., 2013; Keeley and Rundel, 2005). C_3 plants produce smaller amounts of biomass that typically have a higher moisture content and are therefore less flammable (Dupont, 2011; Niedermeyer et al., 2010; Ripley et al., 2010). The proportion of C_3 to C_4 plants within an ecosystem therefore directly impacts biome flammability.

As the two photosynthetic pathways fractionate carbon differently the $\delta^{13}C$ values for the plant waxes can be differentiated, grassy C_4 plants have an average $\delta^{13}C$ values of -13‰, whereas C_3 plants have an average $\delta^{13}C$ values of -26‰ (Ascough et al., 2009). These $\delta^{13}C$ values are retained in charcoal following combustion and in biomarkers i.e. plant wax, $\delta^{13}C$ is therefore a highly useful proxy for past vegetation (Ascough et al., 2011; Castaneda et al., 2009; Das et al., 2010; Krull et al., 2003; Kuechler et al., 2013).

Fire acts as a key feedback mechanism regulating C_3 woody coverage by preventing sapling growth and removing dead biomass (Bond et al., 2005; Higgins et al., 2000; Keeley and Rundel, 2005), thereby creating and/or maintaining a high-light conditions required by grasses and preventing forest encroachment in savanna environments (Beerling and Osborne, 2006; Keeley and Rundel, 2005; Osborne, 2008).

1.6 Fire

Natural wildfire ignition is largely controlled by lightning strikes, although volcanic activity, meteorite fall, spontaneous combustion and sparks produced during rock falls all potentially contribute to a relatively small number of ignitions (Cope and Chaloner, 1980; Patterson et al., 1987; Shinneman and Baker, 1997). Human activity can act to both increase or suppress fire (Bowman et al., 2011; Power et al., 2008), however it is generally accepted that increased fire activity marks the onset of anthropogenic forcing on fire activity. The timing of the onset of human-

controlled fire activity is debated. Fire activity is seen to increase between 70-4kyr whilst annual burned area in Africa probably peaked between 40-4 kyr (Archibald et al., 2012). Schreuder *et al.*, (2019) invoke human hunting practices to explain an increase in burning at *ca.* 55 ka, whereas a later estimate of *ca*. 8 ka is posed when significant human habitation is implied for Central and Western North Africa (Manning and Timpson, 2014; Osborne et al., 2008; Sereno et al., 2008). An anthropogenic impact on fire activity is postulated after 4 ka when models incorporating the physics of fire spread, the human effect on different aspect of fire spread and palaeoecology (Archibald, Staver, and Levin 2012 and references therein) suggest fire was beginning to be used for significant large-scale land clearance and the initiation of agropastorialism i.e. the cultivation of crops or the domestication of cows (Archibald et al., 2012). I consider an anthropogenic impact unlikely before 4ka because of a lack of habitation in the study region before this point coupled with the smaller fires. i.e. cooking fires generate insufficient large amounts of charcoal to alter the natural charcoal signal. Whereas, land-clearance dramatically increases charcoal production whilst agropastoralism acts to reduce charcoal production by reducing fuel levels and removing ignitions points (trees) by the destruction of saplings by grazing and human activity. These human actions were capable to sufficiently distort and mask or distort the underlying natural fire activity signal.

1.6.1 Floral adaptions to fire frequent environments

Plants in biomes experiencing frequent fires have developed traits to survive regular burning. In order to take advantage of the increased light availability and additional nutrients following wildfire, certain plant species are adapted to flower immediately after a fire event, i.e. tropical C_4 savanna grasses, or re-sprout from protected buried vegetative structures in the first growing season following the burning event (Keeley and Fotheringham, 2000). Selective promotion of fire adapted species by a heightened fire activity drives the ecosystem towards increasingly arid, C_4 plant dominated states (Beerling and Osborne, 2006; Bobe, 2006; Furley et al., 2008; Hoetzel et al., 2013; Keeley and Rundel, 2005).

1.6.2 Fire Hypothesis

The large global near-synchronous C_4 grassland expansion, observed in $\delta^{13}C$ proxy records during the late Miocene between 5-8 Ma (Beerling and Osborne, 2006; Cerling, 1992; Ehleringer et al., 1997; Hoetzel et al., 2013; Osborne, 2008; Osborne and Beerling, 2006), is hypothesized to have been facilitated by a more active fire cycle, evidenced by charcoal particles identified in the Atlantic

Ocean and the Niger Delta dating to this interval (Bond, 2015; Hoetzel et al., 2013; Morley and Richards, 1993). Additionally, the growth of C_4 grasses was aided by lower pCO_2 increasing the relative competitiveness of C_4 to C_3 plants (Cerling et al., 1997; Ehleringer et al., 1997; Osborne, 2008). The promotion of C_4 plants at the expense of the C_3 vegetation increased dry biomass generation producing a larger fuel source, elevating the annual fire potential of the biome (Keeley and Fotheringham, 2000). The prevention of woody plant growth and the destruction of established woody plant seedling by regular fires, promotes C_4 plant growth by sustained and/or expanding the availability of high light-environments, as well as other fire adapted flora (Figure 1.4)(Bond et al., 2005; Furley et al., 2008; Hoetzel et al., 2013; Keeley and Rundel, 2005; Osborne and Beerling, 2006). Evapotranspiration rates and cloud formation is slow in areas of low tree cover reducing regional precipitation (Shukla and Mintz, 1982). C_4-habitat area and fire susceptibility is therefore promoted in a positive feedback loop (Figure 1.4)(Bond et al., 2005; Furley et al., 2008; Keeley and Rundel, 2005; Osborne and Beerling, 2006). In this way regional vegetation $\delta^{13}C$ values become progressively more negative indicative of increasing C_4 floral component (Cerling et al., 1997).

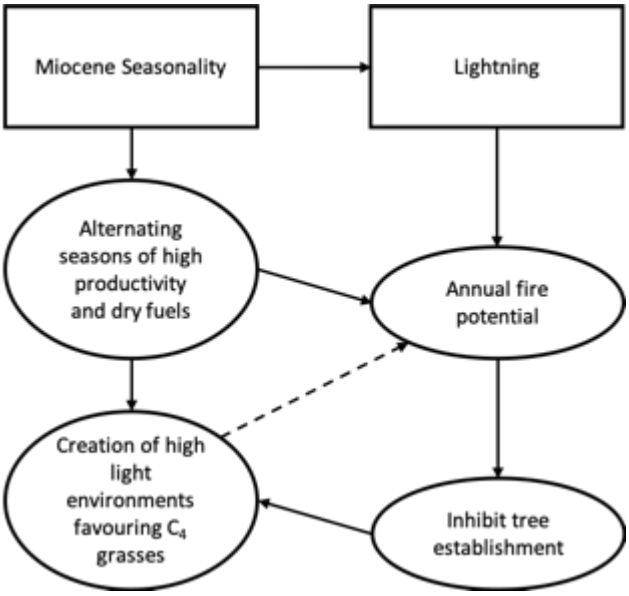

Figure 1.4: The Fire Hypothesis as a positive feedback driver driving wetter ecosystems towards more arid conditions during the Miocene, facilitating C_4 grass expansion. Adapted from Keeley and Rundel, (2005).

1.6.3 Fire activity influence on the hydrological cycle

The hydrological cycle can be modified as a result of smoke production (Andreae et al., 2004; Beerling and Osborne, 2006; Fromm et al., 2005). Smokey and pyro- clouds produced during

burning changes latent heat transport to the free troposphere, which significantly alters tropical circulation (Andreae et al., 2004). Cloud longevity can be sustained by smoke aerosols, rainfall is less frequent but more intense, promoting regional aridity (Koren et al., 2004). Both of these mechanisms have the potential to promote greater regional aridity and therefore favour C_4 plant growth. Additionally, thunderstorms caused by pyroclouds, likely increase lightning activity and consequently the potential for an increased number of wildfire ignitions (Andreae et al., 2004; Beerling and Osborne, 2006; Fromm et al., 2005), thereby increasing regional fire activity and the promotion of arid C_4-dominant biomes (Beerling and Osborne, 2006; Bond et al., 2005; Keeley and Rundel, 2005).

1.6.4 Flammability

The flammability and fire activity of an ecosystem is strongly influenced by vegetation distribution, abundance and assemblage and the proportion of C_3 to C_4 plants (Belcher *et al.*, 2010). Biome flammability is controlled by the inter-dependence of ignitability, combustibility and sustainability. The ignitability is defined by the ease by which biomass catches fire which, in turn, is controlled by fuel moisture content. Fuel moisture is determined by the proportion of C_3 to C_4 vegetation, because C_3 plants typically produce wetter less flammable fuels than C_4 plants (Dupont, 2011; Niedermeyer et al., 2010; Ripley et al., 2010). Resultantly, C_4 dominated floral assemblages are inherently more flammable. Combustibility refers to the intensity by which fuel burns, while sustainability refers to the degree to which burning is maintained over time (Simpson et al., 2016).

Ecosystem flammability can also be influenced indirectly by soil nutrients (Bond et al., 2005), temperature (Pausas and Ribeiro, 2013), pCO_2 (Bond et al., 2003) as they affect plant growth and C_3:C_4 competitiveness (Ehleringer et al., 1997; Ehleringer and Cerling, 2001; Sage, 2002; Waller and Lewis, 1979). Mammal herbivory can also influence flammability, in particular grazing herbivores help to maintain the grassy, highly flammable environments (Archibald and Hempson, 2016). Atmospheric oxygen levels (pO_2) also influence flammability, however this is effect limited to the deep geologic past (Belcher and McElwain, 2008; Belcher *et al.*, 2010). Wildfire is not sustained until pO_2 reaches 18.5% (Belcher *et al.*, 2010).

1.6.5 Fire Proxies

Fires are ephemeral events not, in themselves, preserved in the geologic record. Yet certain combustion products may signal their past activity. Charcoal is generally considered to be highly resilient and can be preserved for millions of years in terrestrial and marine geologic archives (Ascough et al., 2011, 2010; Belcher and McElwain, 2008; Bird and Cali, 1998; Glasspool et al., 2004; Herring, 1985; Parkin et al., 1970; Patterson et al., 1987; Scott, 2010). Combustion produces a large number of products i.e. combustion continuum (Czimczik et al., 2002; Masiello and Druffel, 1998; Thevenon et al., 2010) (Figure 1.5) encompassing a large range of particle sizes and degrees of charring. The term charcoal is therefore often used as a 'catch-all'. More specific terminology is applied to the combustion particles based on extraction method (Czimczik et al., 2002; Masiello and Druffel, 1998; Thevenon et al., 2010). Terms include, biochar, Black Carbon (BC), soot, Oxygen Resistant Elemental Carbon (OREC), and pyrogenic carbon (Bird and Ascough, 2012; Bird and Cali, 1998; Bird and Gröcke, 1997; Herring, 1985; Preston and Schmidt, 2006; Thevenon et al., 2010). The vast terminology used in the literature limits comparisons that can be made between 'charcoal' studies employing different terminology and extraction methods (Scott, 2010).

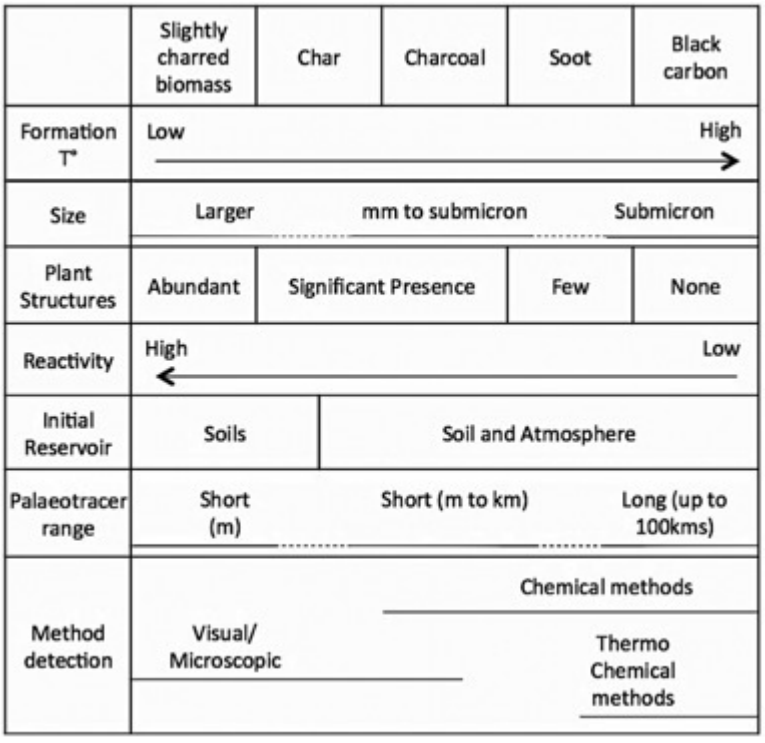

Figure 1.5: The charcoal continuum. The pyrogenic carbon combustion continuum and the corresponding quantification techniques (Modified from Masiello 2004; Thevenon *et al.,* 2010).

1.7 Thesis Objectives

The overall objective of this thesis is to shed new light on past fire activity in northern Africa through the study of charcoal in marine sediments from the northwest African margin. It comprises four main chapters:

1) A validation analysis of charcoal flux as proxy for fire activity. In this study I investigate charcoal recovery at three marine drill sites and assess the reproducibility of geochemically based and optical methods for determining charcoal content in deep sea sediments.

2) Spatial analysis of fire activity on the northwest African margin. In this study I investigate variability in fire activity for a transect of three sites using charcoal flux records, to determine regional differences in fire activity in response to orbital and millennial scale climate events.

3) Temporal analysis of fire activity on northern Africa across the Last Glacial Cycle (0-140 ka). In this study I investigate fire activity variability using marine charcoal flux records, to reconstruct patterns of past burning across orbital and millennial scale climate events.

4) Temporal analysis of fire activity in northern Africa. In this study I investigate the temporal similarities and dissimilarities in fire activity between charcoal flux records for two orbitally similar glacial cycles, the Last Glacial Cycle (0-140 ka) and the Mid-Brunhes Interval (300-450 ka).

Chapter 2 Materials and Methods

2.1 Materials

Previous workers have investigated methods of material quantification on palynological slides including counts by area or counts against a known amount of exotic material in a process called spiking (Finsinger and Tinner, 2005; Matthews, 1969; Patterson et al., 1987; Swain, 1973; Tolonen, 1986 and References Therein). In addition, multiple systems of charcoal classification based on morphology and reflectance criteria are published in the literature (Crawford and Belcher, 2014; Enache and Cumming, 2006; Jensen et al., 2007; Patterson et al., 1987) these classification schemes reference the particular material recovered in that specific study.

I chose to classify the charcoal recovered in my studies against my own set of morphological and reflectance criteria and test the method employed as no comparable study is present in the literature. Unlike the majority of studies and method investigations for charcoal which use material collected close to source from lacustrine and terrestrial archives, the marine charcoal I use is deposited at a greater distance from source and undergone greater transportation and therefore has suite of different morphology than those described by other authors as well as experiencing different depositional conditions.

2.1.1 Charcoal

Charcoal is often used as a catch all term for a large range of combustion products that are produced during burning (the combustion continuum), encompassing combustion products ranging in size and degree of charring Cha(Figure 1.5). Charcoal is specifically defined here as a carbon-rich terrestrially derived material produced by total combustion by either natural or anthropogenic mechanisms (Bird and Ascough, 2012; Keeley and Rundel, 2005). Charcoal fluxes are used here as a proxy for fire activity, higher charcoal fluxes are indicative of higher fire activity (Winkler, 1985).

2.1.2 Fire Activity

There are a large number of factors that dictate the amount of charcoal recovered in palaeo-archives, ranging from amount of charcoal produced which is affected by size and moisture content of the fuel source, the number of fire events that produced the charcoal recovered and the distance between the fire and the study site.

I therefore use the term fire activity when discussing the changes in charcoal flux in order to avoid assumptions about the frequency, size contributions and fire proximity to the study site, because of the uncertainty in source and the number of individual fire events associated with using palaeo-archives (Crawford and Belcher, 2014; Marlon et al., 2009).

2.1.2.1 Charcoal Archives

The majority of charcoal records presented in the literature are generated from terrestrial sediment archives, including lacustrine deposits. Typically, these archives contain the largest charcoal fragments and highest concentrations of charcoal particles due to their potential proximity to the sources of charcoal. Continental records, however, typically only preserve a locally representative signal of palaeo-wildfire. In addition, generating proxy records from terrestrial archives can be problematic because they are susceptible to stratigraphic discontinuities, age control is often difficult and they can be limited in geological range. Marine settings provide a way to circumvent these problems as deep-sea sediment sequences can provide longer, more continuous proxy archives that benefit from tighter age control when compared to terrestrial records. Marine sediments also typically receive charcoal inputs from a larger geographic area, giving a more regionally-integrated signal.

North Africa is the world's largest source of mineral dust, responsible for half of all global atmospheric dust, all sourced from North African deserts, with estimates of dust transport ranging from 160-760x10^6 tonnes per year (Engelstaedter and Washington, 2007; Goudie and Middleton, 2001; McGee et al., 2013; Ridley et al., 2012). The high assumed preservation potential of charcoal (Scott, 2010) and the transportation of terrestrial material, including charcoal from the African continent by wind out over the Atlantic Ocean (Figure 2.1), suggest that marine sediment cores are an underutilized resource for conducting marine charcoal derived fire activity studies. A small number of studies show that there is the potential for charcoal export to sediments on the northwest African margin (NWAM) (Bird and Cali, 1998; Dupont and Schefuß, 2018; Herring, 1985; Verardo and Ruddiman, 1996), however, the timing of peak burning is debated between records. Consequently, there are still number of unknowns regarding fire activity on northern Africa for which marine charcoal records are an invaluable resource.

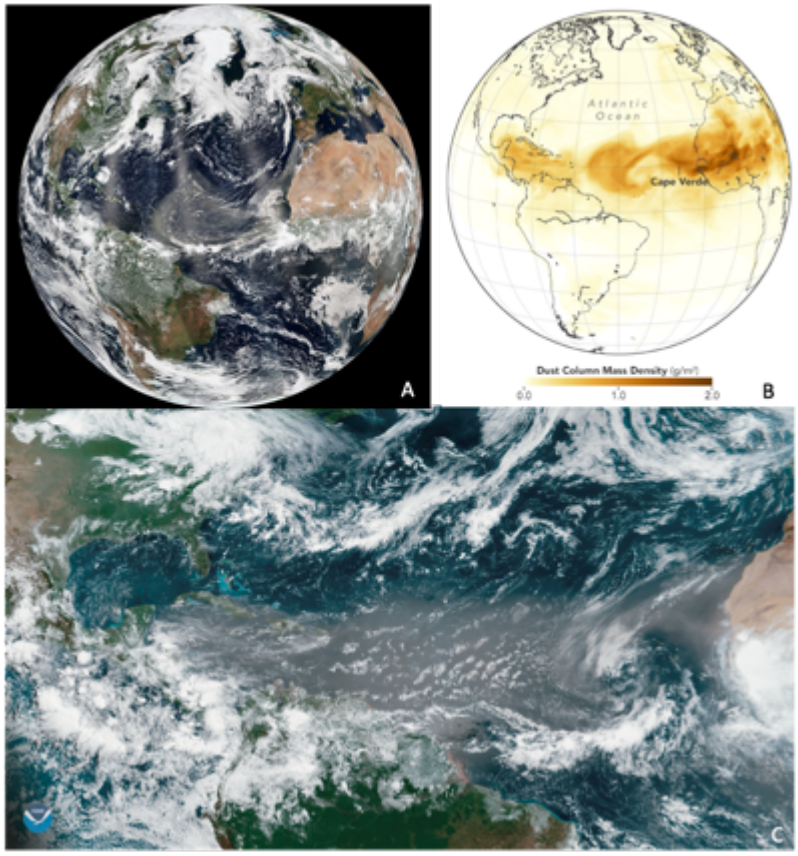

Figure 2.1: North African Dust Plume. A) This composite projection shows the dust storm using data from seven orbits of the Suomi NPP satellite on August 1, 2013. Credit: NASA's Earth Observatory. B) Dust Plume June 28, 2018. Credit NASA Earth Observatory North African. C) North African Dust Plume across the Atlantic Ocean image captured by the GOES East satellite on June 27, 2018. Credit: NOAA Environmental Visualization Laboratory.

2.1.3 Site Selection and descriptions

A total of five marine sites, all located in the tropical Atlantic Ocean offshore NWAM were examined for study and the generation of charcoal flux records (Table 2.1). These 5 sites form a north-south transect along the West African Margin which enables the spatial response of fire activity to climatic change over geological timescales to be examined. In this region today, these sites span the precipitation-driven transition from desert in the north of Africa though the grassy savanna to woody savannah at the south of the transect in equatorial Africa. All the study sites sit under major dust plumes and hence receive large amounts of terrigenous input from the African continent, with southern site (GeoB9508-5) also receiving sediment from the Senegal River. All the sites are therefore well placed to document changes on land.

Site	Latitude	Longitude	Offshore Distance	Water Depth	Sedimentation Rate
658	20°44.95'N	18°34.85'W	150 km	2300 m	24 cm/kyr
659	18°34.85'N	21°01.57'W	500 km	3100 m	11 cm/kyr
668	04°46.21'N	20°55.63'W	1000 km	2700 m	17cm/kyr
GeoB9508-5	15°29.90'N	17°56.88'W	140 km	2400 m	21.5 cm/kyr
GeoB9528-3	09°09.96'N	17°39.81'W	350 km	3000 m	7 cm/kyr

Table 2.1: Study sites location information.

Ocean Drilling Program (ODP) 658 is the most northerly of my sites, located on the continental slope offshore Mauritania. This site is situated below a high productivity upwelling site giving rise to high sedimentation rates and high 0.5-4% Total Organic Carbon (%TOC)(Stein et al., 1989). My sampling covers the intervals 1.16-139.51 ka and 303.5-447 ka which allows us to examine fire activity over multiple glacial-interglacial cycles in the Quaternary and Pliocene, including the Last Glacial Cycle (LGC) (0-140 ka) and the Mid-Brunhes interval (300-450 ka). Two additional sites located further south, GeoB9508-5 ~160 km southwest of the Senegal River mouth and GeoB9528-3 on the Guinean Plateau Margin recovered by the RV Meteor Cruise, were chosen to complement the charcoal flux generated at ODP 658 to create a latitudinal transect of sites along the NWAM (Figure 2.2)Table 2.1 which span the last 0-55 kyr.

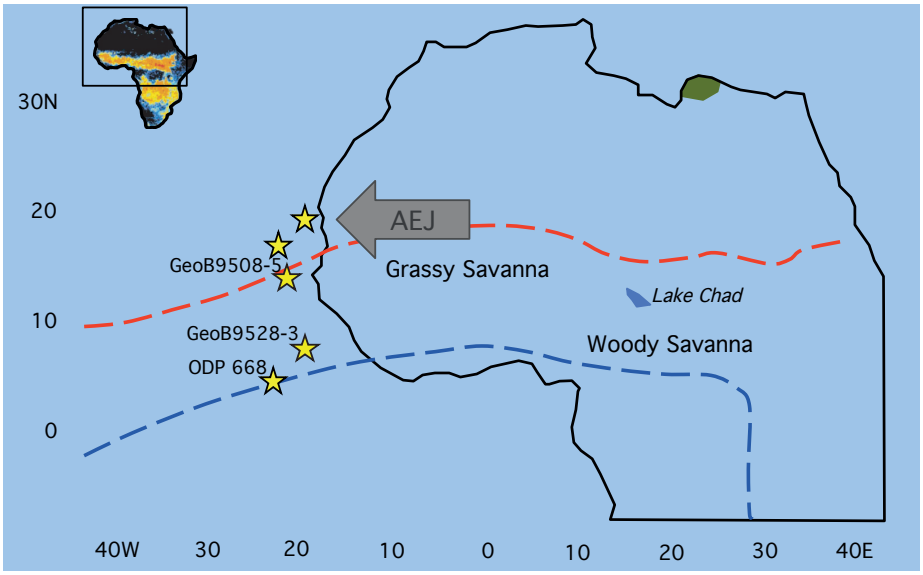

Figure 2.2: Study Sites Location Maps. Schematic map of the major North African vegetation bands, the modern summer and winter latitudinal position of the ITCZ and the African Easterly Jet (AEJ). Location of the ocean drill sites discussed in the text also shown, GeoB7920-2 not shown is a re drill of ODP 658. Adapted from (Sarnthien *et al.,* 1989; Gasse *et al.,* 1989; Vallé *et al.,* 2014). Inset: Fire Map annual average number of fires observed by satellite, Black ~0, Dark Blue 1-4, Mid-Blue 5-19, Light Blue 20-49, Green 50-99, Yellow 100-199, Orange 200-499, Red >500 (Taken from Bowman *et al.,* 2009 data from Giglio *et al.,* 2006).

In order to assess the impact of fire activity during deeper time and investigate the hypothesis that a more active fire cycle drove the C_4 grass expansion event during the Late Miocene (8-5 Ma) (Cerling, 1992; Osborne, 2008; Osborne and Beerling, 2006), I also studied ODP Site 659. This site, located close to Site 658 on the Cape Verde Plateau offshore Mauritania, recovered sediment forming a continuous Late Miocene sequence (Ruddiman et al., 1988a).

ODP 668 in the eastern Equatorial Pacific, drilled on the relatively flat crest of the Sierra Leone Rise, was previously studied by Bird and Cali (1998) who generated a record of past fire activity for Northern Africa using the Oxidation Resistant Elemental Carbon (OREC) method over the last 1 Ma. I revisit this site in order to compare optical and geochemical methods of charcoal identification to generate a fire activity record and comment on the implications for fire activity reconstructions.

2.1.4 Sources of terrigenous material

All of the sites studied here receive large dust inputs from the African continent. The summer dust plume dominates the dust inputs to ODP 658, ODP 659 and GeoB9508-5, whereas the winter dust plume delivers more material to ODP 668 and GeoB9528-3 (Figure 2.3 and Figure 2.4 respectively). Windblown terrestrial material exported to the Atlantic ocean includes dust, charcoal, diatoms, phytoliths, plant waxes and palynomorphs (Gasse et al., 1989; Kuechler et al., 2013; Tiedemann et al., 1989; Tjallingii et al., 2008; Vallé et al., 2014). This terrestrial material is transported westwards from the source areas across the Sahara, the Sahel, and Central North Africa (Bodélé depression), by the African Easterly Jet (AEJ) out across the Atlantic Ocean (Harrison et al., 2001; Hooghiemstra et al., 2006). The North East Trade Winds (NETW) are also suggested to transport material to my sites from a source north of the Sahara (Kuechler et al., 2013; Zhao et al., 2003). The latitudinal position of the AEJ is suggested to have been in a fixed position at ~21°N through the glacial termination as determined by marine pollen records for 18 ka and 9 ka timeslices, which reveal, despite latitudinal shifts of the vegetation bands, that winds trajectories remained stable (Hooghiemstra et al., 2006). This result is also by supported by Neodymium (Nd) isotopes which display very little variability since the last glacial maxima (LGM), suggestive of no change in source region and therefore a stable wind system (Cole et al., 2009). It has therefore been suggested that the AEJ has remained in the same position throughout the LGC (Castaneda et al., 2009; Cole et al., 2009; Grousset et al., 1998; Hooghiemstra et al., 2006; Sarnthein et al., 1981) meaning that, to a first approximation, there is no major change in the source regions for the windblown material transported to all of the sites examined.

Although the wind patterns over northwest Africa are thought to have remained broadly unchanged though the LGC, changes in the wind strength may have impacted the amount of terrestrially derived material delivered to all the study sites. Grain size work indicates that wind strengths were higher during glacial conditions compared to more humid and interglacial conditions across Northern Africa (Sarnthein et al., 1981). Greater fluxes of dust are therefore exported during glacial conditions, when northern Africa was arid (McGee et al., 2010). If wind strength was a driving factor behind the charcoal flux variability seen in my records, then we would expect to see increased charcoal fluxes during glacial intervals this is not the case, in fact charcoal fluxes are at minima values during glacial periods (ODP 658 : Transport to ODP 658. a) LR04 global benthic oxygen isotope stack (Lisieki and Raymo, 2005), b) Humidity Index – derived from the proportion of riverine to aeolian material (determined by grain size) reaching GeoB7920-2 (Tjalingii *et al.,* 2008),

Charcoal Flux at ODP 658 (this study), d) ln(Zr/Al) (Meckler *et al.,* Unpublished). and GeoB9508-5 Figure 2.4). Variable wind speed is discounted as a driver of charcoal flux at any of my study sites.

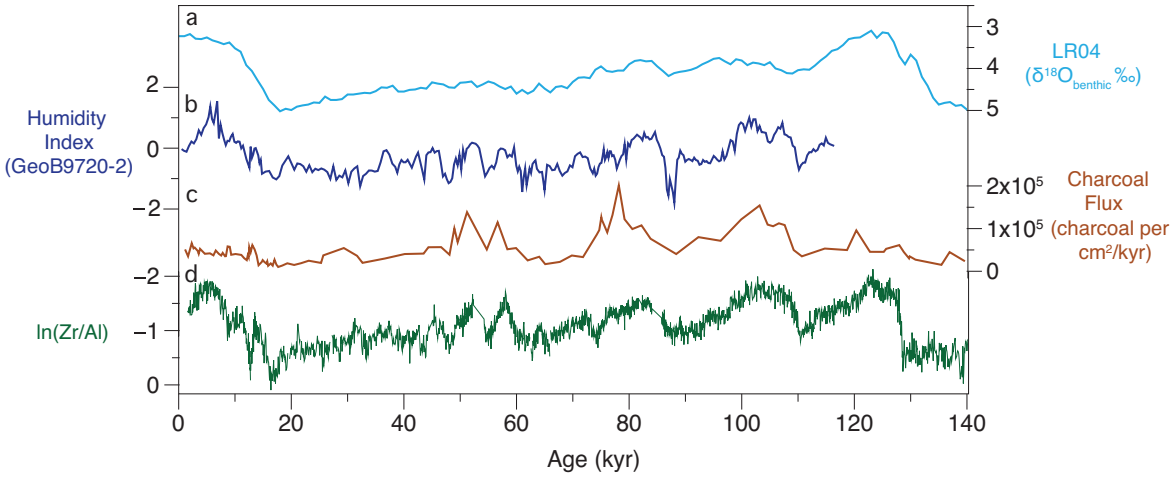

Figure 2.3: Transport to ODP 658. a) LR04 global benthic oxygen isotope stack (Lisieki and Raymo, 2005), b) Humidity Index – derived from the proportion of riverine to aeolian material (determined by grain size) reaching GeoB7920-2 (Tjalingii *et al.,* 2008), Charcoal Flux at ODP 658 (this study), d) ln(Zr/Al) (Meckler *et al.,* Unpublished).

Dust is not the only source of terrigenous inputs to the NWAM. During humid intervals, there were numerous rivers draining Western Sahara and flowing into the Tropical Atlantic (Drake et al., 2011; El-Shenawy et al., 2018; Scerri et al., 2016), including the Tamanrasset River (Skonieczny et al., 2015). At these times, the flux of riverine sediments increases, as recorded in short sediment core GeoB7920-2 recovered from a re-drill of ODP 658 (Tjallingii et al., 2008). Changes in the balance between aeolian and riverine derived sediments has the potential to cause changes in charcoal flux unrelated to fire activity if one transport pathway is much more effective at exporting charcoal than the other, for example, during humid intervals there is therefore a potential for an increased riverine flux acting to increase charcoal delivery to the sites, impacting on the charcoal flux generated. Peak riverine discharge, however, doesn't align with peak charcoal fluxes at either ODP 658 and GeoB9508-5 (Figure 2.3 and Figure 2.4) two sites where reconstructions of past humidity have been published (Mulitza et al., 2008; Tjallingii et al., 2008). Changes in the relative inputs of riverine and aeolian sediment is therefore not considered to be a controlling factor on the charcoal fluxes generated for either of these two sites.

I consider that transport processes are not the dominant control on charcoal fluxes at any of my African continental margin sites.

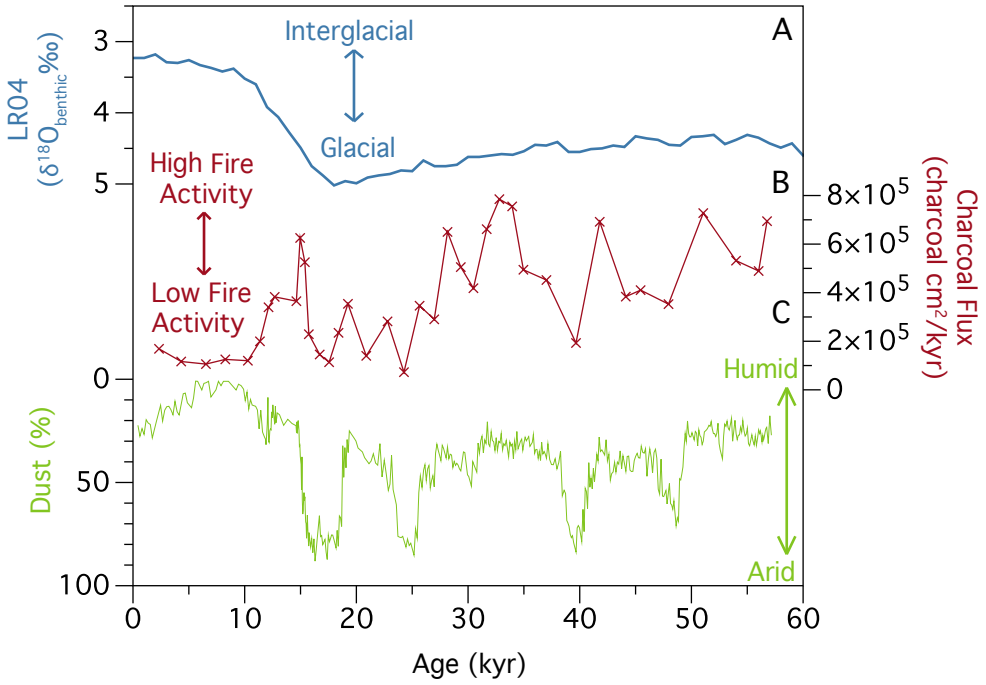

Figure 2.4: Assessing the potential effect of transport on charcoal flux. A) LR04: Global Benthic Isotope Stack (Lisieki and Raymo, 2005), B) Charcoal flux (this study). C) Dust % (Collins *et al.,* 2013).

2.2 Methods

2.2.1 Chronology

ODP 658

The age model generated for ODP 658 used was constructed using the age-depth tie-points published by Meckler *et al.*, (2013). A correlation for the sections which do not form part of the published splice was required to plot published $\delta^{18}O_{benthic}$ records for ODP 658 (Sarnthein and Tiedemann, 1989; Knaack and Sarnthien, 2005) onto the same age model as Meckler *et al.*, (2013) (Figure 2.5). This was achieved by generating RGB (Red, Green, Blue) colour profiles for ODP 658 holes A, B and C from core photographs obtained from the IODPs JANUS database using the ImageJ software. The blue component (B*) of the RGB profiles was then used to correlate between the splice (as published by Meckler *et al.*, 2013) and out-of-splice core on a hole-by-hole basis using the Linage function in AnalySeries 2.0.8 (Palliard *et al.,* 1996)(Figure 2.5). This enabled the determination of new mbsf-mcd tie-points for each hole. It was identified that 30cm of material

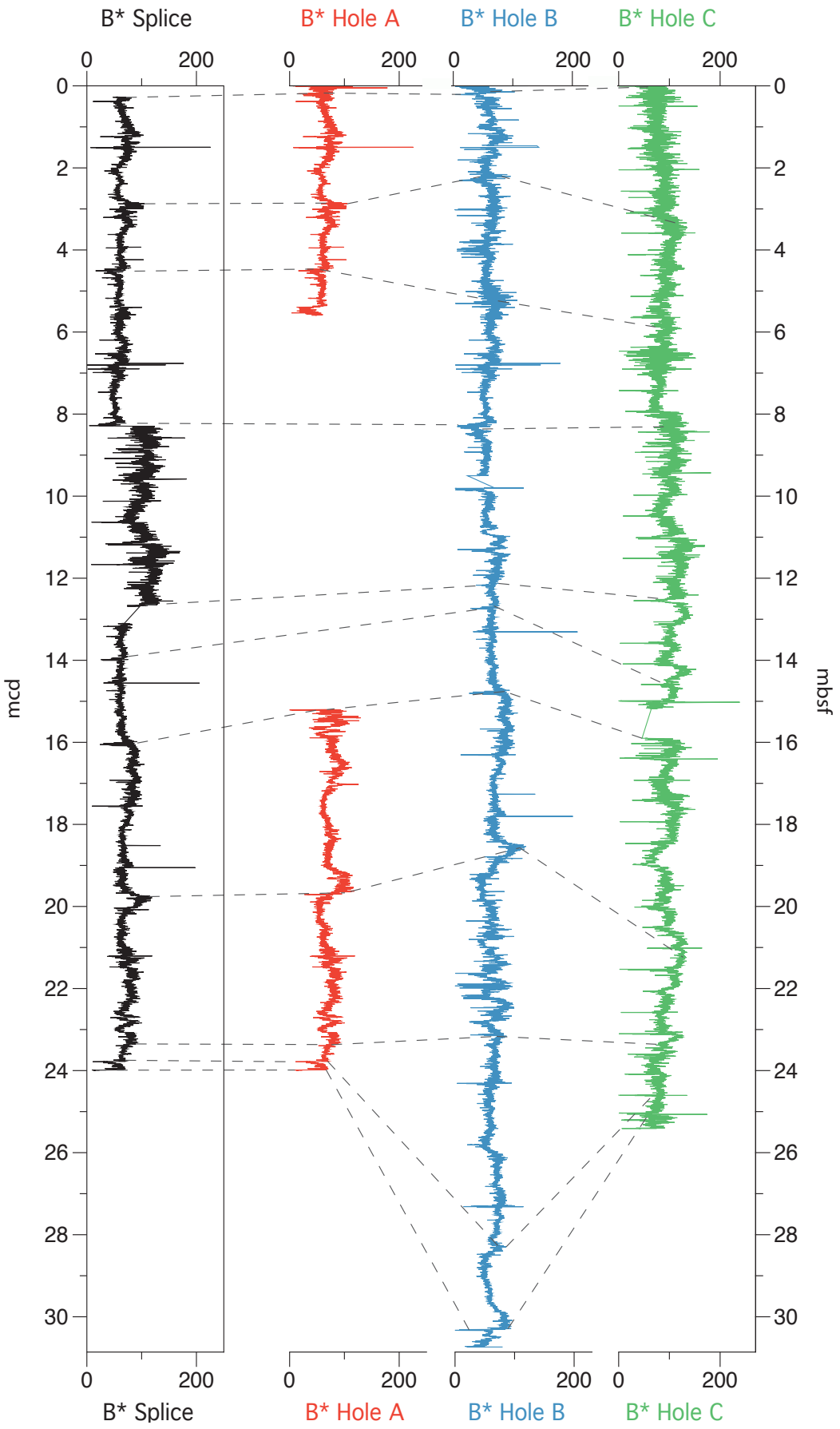

Figure 2.5: B* Correlation of Holes for ODP 658. B* correlation plots between the ODP Site 658 splice (Meckler et al., 2013) and the B* ODP Site 658 holes A, B and C from Site 658 showing tie-points

hadn't been accounted for in the Meckler *et al.*, (2013) splice in section 108-658B-2H-5, I corrected for this by adding 30cm to the mcd's below this point. These new tie-points were then used to generate new mcd-age tie-points for a new age model for the $\delta^{18}O_{benthic}$ records from the separate holes and compiled to produce a singular composite $\delta^{18}O_{benthic}$ record. All of the datasets generated from ODP 658 as part of this study are plotted on this age model. Unfortunately, the site and sample identifiers required to update the outdated age model used to plot the Zhao *et al.*, (1995) SST record for Site 658C were unavailable and therefore this record is plotted on its own published age model, hence they could not accurately be converted onto an updated age model.

GeoB7920-2

The humidity index from this site is plotted on the published age model Tjallingii *et al.*, (2008) and references therein. In brief the age model for GeoB7920-2 was generated by a visual correlation of the *C.wullerstorfi* $\delta^{18}O$ record of MD95 2042 (Tjallingii *et al.*, 2008 and references therein). AnalySeries 1.1 software package (Palliard *et al.* 2006) was used to perform a peak-to-peak correlation on 5-point-smoothed average $\delta^{18}O$ records. The MD95 2042 $\delta^{18}O$ stratigraphy was use on the GRIP ss09sea age scale. The parallel site ODP 658 and core GeoB7920 carbonate stratigraphies were used to cross checked the age scale of the last ~15 ka.

ODP 659

The ODP 659 age model was based on updates to biostratigraphy and magnetostratigraphy age points. The biostratigraphic ties were updated following Raffi *et al.*, (2006) and the magnetostratigraphy ties updated to the geomagnetic polarity timescale (GPTS), to the original shipboard data identifications (see Initial Shipboard Reports and SEDIS data). Additionally, the existing *C.wuellerstorfi* $\delta^{18}O$ (Tiedemann et al., 1994) was tuned to LR04 global benthic oxygen isotope stack (Lisiecki and Raymo, 2005) over the youngest 5 Myr and XRF Ca/Fe ratios were tuned to summer insolation at 65°N (Laskar et al., 2004).

ODP 668

An age model for ODP 668 was generated by correlating the published $\delta^{18}O$ record (Bird and Cali, 2002) to the LR04 benthic foraminifera stack (Lisiecki and Raymo, 2005) using AnalySeries software (Palliard *et al.,* 1996).

GeoB9508-5

The published age-depth tie points of (Niedermeyer *et al.*, 2010) are used to create the age model used to plot data for GeoB9508-5 was based on a combination of radio-carbon dating and $\delta^{18}O_{benthic}$ stratigraphy (Mulitza et al., 2008). 12 samples of planktonic foraminifera were run for radiocarbon ages and corrected for a reservoir age of 400 years. Generated ^{14}C ages smaller than 40 ka were converted to calendar ages (Niedermeyer *et al.*, 2010 and references therein). The alignment of the cores $\delta^{18}O_{benthic}$ record to the core MD95-2042 provided seven additional tie-points (Niedermeyer *et al.*, 2010 and references therein).

GeoB9528-3

The published tie-points of Schreuder *et al.*, (2019) were used to construct the age model for GeoB9528-3. In brief, the age model which was generated by a graphic correlation of the $\delta^{18}O_{benthic}$ *C.wuellerstorfi* record of (Castaneda et al., 2009) with Deep North Atlantic Stack (Lisiecki and Stern, 2016) and the global benthic stack (Lisiecki and Raymo, 2005) was used to produce an age model for core GeoB9528-3. Uncertainty in the down core age was modelled using the R script BACAON (version 2.2 using the 1-sigma age uncertainties assigned from the Deep North Atlantic Stack (Schreuder *et al.*, 2019 references therein). Schreuder *et al.* (2019) ran BACON using a student 't' distribution and default parameters, with shape parameter (t.a) of 10 and a scale parameter (t.b) of 11. Their estimations of the mean age and the standard deviation of the age ensemble at the sampling depth was obtained by producing 10,000 age-depth realizations (Schreuder *et al.*, 2019). Dry bulk density values used to calculate charcoal fluxes for this site Schreuder *et al.,* (personal communication).

2.2.2 Carbon and Nitrogen Isotopic Signature of Organic Matter

A 1g split of bulk sediment was freeze-dried, ground to fine powder using an agate pestle and mortar and decarbonated overnight in 10% HCl to remove inorganic carbon (carbonate). The decarbonated residue was then neutralised, oven dried at 50°C, homogenized and re-weighed to calculate the mass loss of total inorganic carbon. Approximately 10 mg of dried, decarbonated residue was weighed and sealed into tin capsules for analysis of nitrogen (%N) and organic carbon contents ($\%C_{org}$), and organic carbon ($\delta^{13}C_{org}$) and nitrogen ($\delta^{15}N_{org}$) isotopic signatures using a Vario Isotope Select Elemental Analyser coupled to an Isoprime 100 mass spectrometer at the University of Southampton National Oceanography Centre (NOCS). These data were calibrates using the

external reference standards USGS40 and USGS41a (-26.39 and 36.56 respectively) and two further standards; L-glutamic acid and peat soil (standard deviation values of 0.19 and 0.16, respectively). The percentage Total Organic Carbon (%TOC) was calculated using the bulk raw weight (g) and the decarbonated weight of the sample ($\%C_{org}$) for each sample.

2.2.3 Charcoal Extraction

I trialled two different techniques in order to find the best approach to isolate the charcoal fragments from the other sediment components so that they could more easily be counted microscopically. These approaches were: (1) oxidation using hydrogen peroxide (H_2O_2) to remove labile organic material and leave resilient charcoal (Rhodes, 1998) and (2) a modified version of standard palynological processing, where acid is used to dissolve host material to leave the organic component (after Harding *et al.*, 2011).

2.2.3.1 Oxidation by Hydrogen Peroxide

Dry sediment was macerated in 6% H_2O_2 to gently oxidize and bleach the Amorphous Organic Matter (AOM), leaving the more resilient charcoal unaffected. The samples were sieved at 10 μm to remove the clay fraction before a second H_2O_2 maceration stage was undertaken to bleach and oxidize the residual AOM. This method successfully bleached and removed some of the AOM from the samples, however, due to large siliceous and carbonaceous fractions of the sediments, it was not possible to identify charcoal. It was concluded that a method that involved the removal of the both the siliceous and carbonate fraction was required, therefore this method was discounted for charcoal extraction.

2.2.3.2 Palynological Processing

Charcoal was extracted from the sediment samples using a modified version of standard palynological processing (after Harding *et al.*, 2011) but omitting all stages involving physical damage to the samples in order to prevent charcoal fragmentation. Dry sediment (approximately 0.2-5 g) was macerated in hydrochloric acid (HCl) for 24 hours, neutralized then followed by a 48-hour hydrofluoric acid (HF) with a gentle agitation step at 24 hours. These two stages were required to remove the carbonate and silicate fraction of the sample, using HCl and HF respectively. Samples

were then boiled in HCl, ultrasonicated (20 seconds) and sieved (at 15 μm) to remove fluoride products formed during HF maceration and AOM from the samples.

The samples were then spiked (after Stockmarr, 1971) with *Lycopodium* (an exotic spore) tablets. A visual assessment of the volume of organic matter content (charcoal, cuticle, pollen and spores) following the AOM removal stage was conducted in order to determine the size of the spike required on a sample by sample basis. The aim was to achieve a ratio of about three charcoal particles to one *Lycopodium* spore per sample, however, in practice the Charcoal: *Lycopodium* (C:L) ratio in the samples was approximately 1:2. The higher ratio was achieved because at least two *Lycopodium* tablets were added to each sample, to average out discrepancies in the number of individual *Lycopodium* spores in each tablet and each tablet contained approximately 12,541 *Lycopodium* (batch number 124961). The samples were then mounted on square cover slips and dried (for 24 hours) before gluing with Elvasite.

To ensure that the ultrasonic treatment didn't contribute to fragmentation of the charcoal particles, 15 samples were checked under a microscope before they were ultrasonicated, then sieved to remove the AOM and mounted on glass slides and checked under the microscope and checked again. This technique successfully removed the AOM from the sample and caused no fragmentation of the charcoal particles, therefore the ultrasonication step was kept in the method.

Standard palynological practice is to sieve samples at 15 μm but considering distance from shore and the lack of charcoal recovery from ODP 659, the use of a smaller sieve (10 μm) to account for a very small particle size was tested. The first set of 15 samples (the pilot sample set, which sampled the entire age range of the study interval (0-140 ka) and various lithological units) that I processed I sieved at both 10 μm and 15 μm and the 10-15 μm fraction was collected, mounted and visually examined. The mounts of 10-15 μm reveal that no charcoal was lost by sieving at a larger size and given the speed benefits, 15 μm was then used as standard sieve size for the subsequent samples.

This method was adopted to produce all of the charcoal counts presented in these studies, with the exception of Site 659.

2.2.3.3 ODP 659 sample processing

The ODP 659 samples were processed at the University of Exeter using their standard palynological processing technique (after Conedera *et al.*, 2009). This protocol varies slightly from the technique used in the Palynology Laboratory at the National Oceanography Centre at the University Southampton (detailed in 2.2.3.2). Differences in the University of Exeter methodology included using a shaker table to aid in sample disaggregation, a cold HCl stage to remove calcium fluoride products, samples were not sieved due to the very low organics content and resultantly were not spiked with *Lycopodium*. An alternative, common method of mounting was also used at Exeter, a pipette of sample was mixed into warm glycerine on a hotplate, covered and left to dry, with the slide sealed using nail varnish. Due to the low organics content of these samples the entire residue of the sample was mounted. This difference in methodology is not expected to result in a difference in charcoal flux estimates, although some difference in the distribution of the material on the slide between mounting methods may have occurred. As the slides produced for ODP 659 were not used in the generation of charcoal flux for this study, this effect can be discounted.

2.2.4 Charcoal Identification

Particles were identified as charcoal if they were very dark/black in colour and fit within one of my six morphological categories. My morphologies are elongate, irregular, irregular perforated, splintery, splintery perforated and square/rectangular (Figure 2.6). The high pyrite content of some of samples hampered straightforward identification of charcoal particles because under the microscopic pyrite shares a number of visual similarities (in colour and shape) with charcoal particles. In some cases, therefore, an additional check was undertaken to test relative reflectance. The particle was viewed in low base light (microscope light) and high-top light (lamp light). Only particles that were dark or faintly reflective were classified as charcoal, whereas bright flat reflective particles were classified as pyrite. A final check was made by examining a subset of 5 samples under a reflected light microscope. Examination of the charcoal particles by this method, revealed that the cellular structure of the original biomass was preserved, ensuring that I was counting charcoal particles.

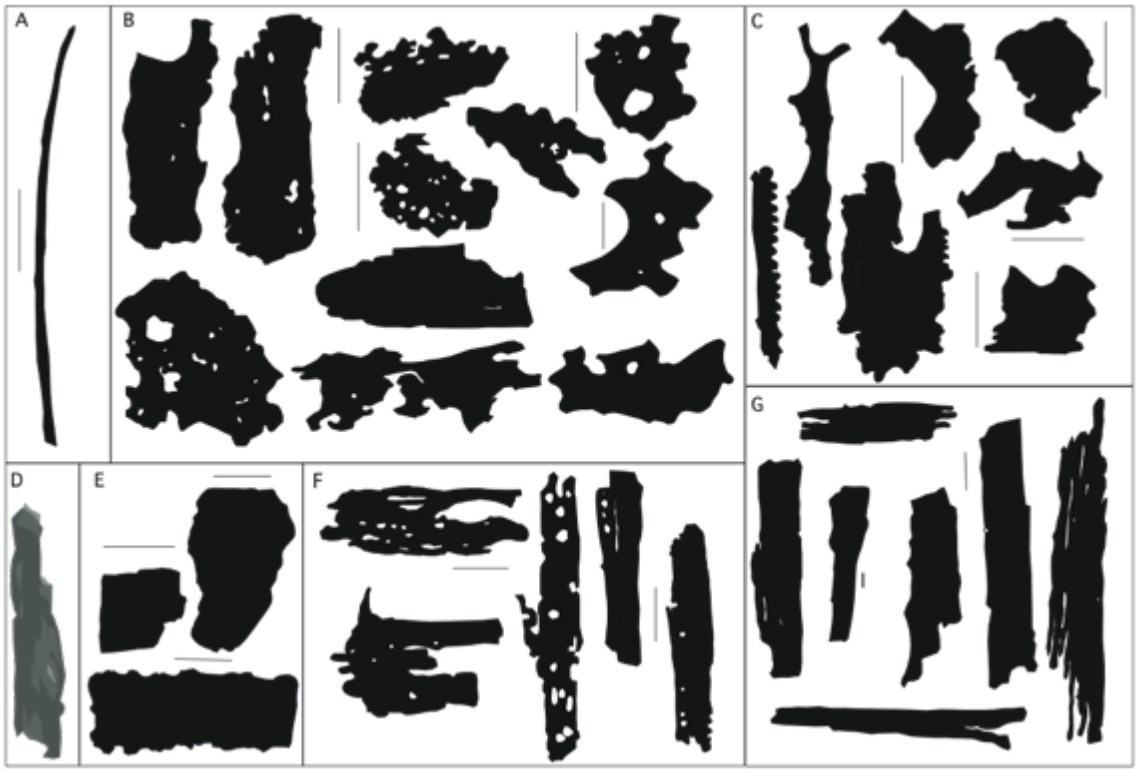

Figure 2.6: Charcoal Facies. Morphologic characteristics used to identify charcoal particles in palynological slides. A) Elongate, B) Irregular Perforated, C) Irregular, D) Grass, E) Square/Rectangular, F) Splintery Perforated, G) Splintery Perforated. Black Bars 20 μm.

The nature of the charcoal counts is somewhat subjective, even when using strict identification criteria. As a result, counting was only undertaken by me, and in blocks of time to improve the consistency of charcoal particle identification. A series of experiments to explore the reproducibility of the charcoal counting procedure are detailed in Chapter 2 section 2.2.4.1.

2.2.4.1 Method Checks

In order to quantify the reproducibility of the processing method for extracting the charcoal from the samples and to confirm that any variability in the charcoal flux record is an accurate record of changes in the sediment rather than an inherent part of the method, a clear understanding of the limitations of the method are required. To this end two checks were undertaken: 1) double spike to test the amount of *Lycopodium* in a tablet and 2) repeats to explore the reproducibility of the method.

Full *vs* Standard Counts

Following standard palynological practices charcoal particles were counted simultaneously with the exotic spore *lycopodium* until a set values of *Lycopodium* were reached, in the case of my counts 500 *Lycopodium* was used. This method means that a representative proportion of the sample was counted. To ensure that these counts were indeed representative of the sample as a whole 'Full counts' were undertaken on 6 slides. 'Full counts' quantified all of the charcoal and *Lycopodium* mounted on the cover slip, the values generated from these counts were compared against my standard counting procedure (count to 500 *Lycopodium*) to ensure that my method is representative of the sample as a whole. The error between the standard and full counts averages 10%. In an ideal scenario full counts would have been conducted on all samples, however due to time constraints it was not feasible to conduct Full counts on all samples (Full counts took >8hrs whilst Standard counts took <5hrs). I felt that a 10% error was sufficiently representative of the samples as a whole as this related to only 15 pieces of charcoal/yr difference.

	Exp	Site	Hole	Core	Core Type	Section	Section Half	Top Interval (cm)	Bottom Interval (cm)	Age (Kyr)	G - Glacial, IG - Interglacial, T - Transition, DG - Deglacial	Lycopodium	Total Charcoal Counted	Charcoal/*Lycopodium*	Charcoal Concentration	Charcoal Flux per ka
Original Mount	108	658	A	1	H	1	W	62	64	3.5114	IG	501	290	0.579	2904	43359
												2966	1876	0.633	3173	47378
	108	658	A	1	H	1	W	95	97	5.4966	IG	499	299	0.599	3131	39878
												4616	3204	0.694	3627	46195
	108	658	A	1	H	1	W	137	139	8.3919	IG	515	266	0.517	2591	35731
												4689	2598	0.554	2780	38329
Remount	108	658	A	1	H	1	W	62	64	3.5114	IG	505	344	0.681	3417	51025
												3314	2926	0.883	3321	49587
	108	658	A	1	H	1	W	95	97	5.4966	IG	505	421	0.834	4357	55483
												4420	2421	0.548	3818	48619
	108	658	A	1	H	1	W	137	139	8.3919	IG	498	337	0.677	3395	46813
												4417	2515	0.569	2857	39389

Table 2.2: Full vs Standard counts, for the original mount and the remounted sample.

Spike Check

Calculation of the charcoal flux values produced in this study relies on the ratio of charcoal to the spike, in this case, the known amount of *Lycopodium* in each sample. If an incorrect value for the number of *Lycopodium* in a sample is used, the generated charcoal flux value will be incorrect. If

the number of *Lycopodium* in a sample is overestimated, an artificially low charcoal flux values is produced, in contrast if the number of *Lycopodium* in a sample is underestimated, artificially high charcoal flux values will be produced. To confirm the correct number of *Lycopodium* were added to the samples, 4 samples were spiked for a second time following the removal of 1 aliquot of sample. The second spike was conducted using a known amount of *Lycopodium* which had been dyed pink using a saffron dye. The dyed *Lycopodium* spike was added to a processed sample from which a subset of material had already been removed and mounted onto a slide for counting. The remaining sample was then thoroughly mixed and a second aliquot of material was removed and mounted for counting. Counting of the charcoal particles was conducted in the manner as all the other samples however only pink *Lycopodium* was counted. The counts on the pink spike samples revealed that in most cases gave estimated charcoal concentrations ~25% lower than the initial counts, which is consistent with the fact that *ca.* 20 – 25% of the sample had been removed prior to addition of the dyed *Lycopodium* (approximately 4-5 mounts can be achieved from each sample and enough material for one mount had been removed). There was also approximately ~20% more of the pink *Lycopodium* visible in the slide than natural *Lycopodium*. Therefore, this test proved effective to determine that the correct number of *Lycopodium* had been added to the samples.

Exp	Site	Hole	Core	Core Type	Section	Section Half	Top Interval (cm)	Bottom Interval (cm)	Age (Kyr)	G - Glacial IG - Interglacial, T- Transition	Original (O) Remount (RM)	Charcoal Counts								Charcoal / Lycopodium	Charcoal Concentration	Charcoal Flux/ka	Percentage Differences	Overall % difference
												Splintery		Irregular		Square/ Rectangular	Elongate	Grass Char	Total Charcoal Counts					
												Unperforated	Perforated	Unperforated	Perforated									
108	658	A	1	H	1	W	62	64	3.5	IG	O	21	4	127	6	101	2	5	266	0.532	13345	39850	3.38	
108	658	A	1	H	1	W	62	64			RM	11	7	197	26	14	2	0	257	0.514	12893	38502		
108	658	A	1	H	2	W	29	31	11.1	G	O	16	4	158	32	54	6	4	274	0.548	13746	37910	4.53	
108	658	A	1	H	2	W	29	31			RM	29	7	208	38	4	1	0	287	0.574	14398	39708		
108	658	A	1	H	1	W	95	97	5.5	IG	O	8	0	187	41	67	7	0	310	0.62	15552	41263	2.21	6.2
108	658	A	1	H	1	W	95	97			RM	37	5	224	33	14	4	0	317	0.634	15903	42194		
108	658	A	1	H	1	W	137	139	8.4	IG	O	13	4	134	48	21	8	0	228	0.456	11438	31545	14.30	
108	658	A	1	H	1	W	137	139			RM	46	14	164	41	15	2	0	282	0.564	14147	36808		
108	658	A	1	H	2	W	1	3	9.4	IG	O	7	2	163	80	46	6	0	304	0.608	15251	39680	6.58	
108	658	A	1	H	2	W	1	3			RM	35	13	178	37	17	4	0	284	0.568	14248	37069		

Table 2.3: Remounts of the samples. Comparison of the counts achieved between original and remounts of the same sample material. IG - Intergalcial, G – Glacial.

Remounts and Reprocessing

To ensure that the mounted samples were representative of the sample of as a whole, a sub-set of 5 samples were mounted from the sample for a second time (remount). The Standard counts

achieved on the remount and the original were compared producing an average difference of ~6.2% (Table 2.3). Whilst the Full counts on the original and remount of 3 samples (Table 2.2) averages at 4.1%. Thereby the material removed from the sample for mounting was representative of the sample as a whole.

In order to assess the reproducibility of the processing and spiking method adopted for this study, a subset 6 of the samples were reprocessed, spiked and recounted as direct comparisons. Repeat samples followed the same method as previously detailed however, it should be noted that the repeated samples had a markedly smaller start weight (0.6-3 g dry weight) compared to the original runs and as a result were only spiked with a single *Lycopodium* tablet.

Values of these reprocessed samples differed from the original values by an average of ~12.5% (Table 2.4). This variability is much lower than the magnitude of variability in my downcore records (Chapter 4, Chapter 5 and Chapter 6)**,** indicating that the time series presented here represent real environmental changes and are not a result of the inherent variability in the method. However, in order to better understand which stages in the method introduce the observed variability between recounts, a number of tests were performed to isolate different stages of the processing procedure.

Exp Site Hole	Core Core Type	Section Section Half	Top Interval (cm)	Bottom Interval (cm)	Age 26.04.2016	G - Glacial IG - Interglacial T - Transitional	Total Lycopodium	Counted Lycopodium	Originial (O) Reprocessed (RP)	Charcoal Counts								Charcoal Flux/ka	% difference between counts	Average % difference between reprocessed counts
										Splintery		Irregular		Square/Rectangular	Elongate	Grass Char	Total Charcoal Counts			
										Unperforated	Perforated	Unperforated	Perforated							
108 658 A	1 H	1 W	62	64	3.5114	IG	25084	500	O	21	4	127	6	101	2	5	266	39850	27.69	12.5
							12542	500	RP	4	0	75	16	7	1	0	103	55110		
108 658 A	1 H	2 W	29	31	11.0680	G	25084	500	O	16	4	158	32	54	6	4	274	37910	69.71	
							12542	500	RP	6	1	149	6	2	2	0	166	38048		
108 658 A	1 H	1 W	137	139	8.3919	IG	25084	500	O	13	4	134	48	21	8	0	228	31545	18.73	
							12542	500	RP	34	10	111	21	21	5	0	202	38817		
108 658 A	1 H	2 W	1	3	9.3477	IG	25084	500	O	7	2	163	80	46	6	0	304	39680	0.93	
							12542	500	RP	18	16	130	32	18	6	0	220	40051		
108 658 A	1 H	2 W	47	49	12.215	G	25084	500	O	3	2	155	18	21	3	0	202	31666	17.68	
							12542	500	RP	6	11	120	8	4	2	0	151	38465		
108 658 A	1 H	2 W	71	73	13.438	G	25084	500	O	12	6	222	39	45	1	0	325	53228	9.85	
							12542	500	RP	25	4	143	11	16	0	0	199	47983		

Table 2.4: Reprocessing Counts. Comparison of counts achieved between the original sample and the reprocessed sample and calculated percentage difference. Original counts used 2 Lycopodium tablets, whereas the reprocessed counts used 1 Lycopodium tablet, due to the smaller starting weight. IG - Interglacial, G - Glacial.

Consistency in identification of charcoal

Multiple counts of almost exactly the same field of view across a single transect of the cover slip ('precision counts') were conducted to assess whether differences in which particles were identified as charcoal were responsible for the variability between sample repeats. This test revealed that the counts made are reproducible within 4.32% error (Table 2.5). Given the small total number of particles counted across a single transect of the slide (~100 *Lycopodium*) each difference in a charcoal counted is equivalent to approximately 1%. At least part of the difference between repeated counts of the same transect can be attributed to subtle variability in the fields of view, resulting in variability in both the numbers of *Lycopodium* and charcoal counted (Table 2.5). There is a degree of movement when setting to the microscope stage to the same axis coordinates and therefore charcoal and *Lycopodium* particles can be either added or subtracted around the margins of the field of view. However, even with these slight variations in the field of view, a reproducibility error of <4.5% suggests that consistency in identification of charcoal particles is not responsible for the majority of variability observed between recounts.

	Age (kyr)	G - Glacial, IG - Interglacial, T - Transition	Count	Transect	Count	Field of View																													Total	C/L	% Difference	Estimated Charcoal	charcoal concentration (charcoal/g)	Charcoal Flux/ka	Difference in charcoal fluxes (%)	Average % difference
						0.0	1.0	2.0	3.0	4.0	5.0	6.0	7.0	8.0	9.0	10.0	11.0	12.0	13.0	14.0	15.0	16.0	17.0	18.0	19.0	20.0	21.0	22.0	23.0	24.0	25.0													
108-65BA - 3H-4W 37-39 cm	129.63	IG	1st	0	C			0	0	3	4	2	3	2	5	1	6	3	5	4	4	6	1	5	5	3	2	0	3	0					67	0.16		4021	804	7557		
				125	L	4	7	10	7	16	22	22	28	20	23	44	25	18	25	29	20	31	20	13	18	5	7	4							418								
			2nd	0	C			0	0	3	2	3	5	2	5	3	6	3	5	5	4	7	1	4	5	2	2	0	3	0					70	0.17		4241	848	7972	5	
				125	L	5	7	10	7	16	21	22	29	19	20	43	27	20	24	30	19	30	18	13	18	5	7	4							414								
			Dif.	0	C			0	0	0	2	-1	-2	0	0	-2	0	0	0	-1	0	-1	0	1	0	1	0	0	0	0					1		8.29						
				125	L	-1	0	0	0	0	1	0	-1	1	3	1	-2	-2	1	-1	1	1	2	0	0	0	0	0	0	0					4		0.96						
108-65BA - 2H-6W 71-73 cm	13.438	G	1st	0	C			2	5	7	3	10	10	9	1	11	5	1	5	3	7	5	10	5	4	5	0	0	0	0					108	1.4		35118	6753	86600		4.32
				125	L	2	1	6	6	6	4	7	5	5	2	7	1	6	2	3	4	1	4	1	4	0	0	0							77								
			2nd	0	C			2	4	7	3	9	9	9	3	10	4	1	4	5	7	7	9	4	5	5	0	0	0	0					107	1.45		36372	6995	89693	3	
				125	L	2	1	6	6	8	3	5	5	5	2	7	1	3	2	4	5	1	4	1	3	0	0	0							74								
			Dif.	0	C			0	1	0	0	1	1	0	-2	1	1	0	1	-2	0	-2	1	1	-1	0	0	0	0	0					1		0.93						
				125	L	0	0	0	0	-2	1	2	0	0	0	0	0	3	0	-1	-1	0	0	0	1	0	0	0							3		3.90						

Table 2.5: Precision counts. Direct comparison of the charcoal (C) and lycopodium (L) counts in each field of view and the difference (Dif.) between first and second count. Numbers are green if within 1 and orange if 2 different in counts in the same field of view. Green numbers if overall average error is less then 5%. The effect of the varying counts achieved on flux and percentage difference calculated. IG - Interglacial, G – Glacial.

Recounts of the same slide

As a check to ensure that despite the counts being undertaken at different times (intervals of months between counting sample sets) charcoal identification remained consistent across all the samples, a series of sample slides were recounted using the original method. Different sections of the same microscope slide were counted each time, as no record could easily be made of exactly which parts of the slide were counted in the original analysis. The recounts showed that in almost all cases that recounts produced different Charcoal: *Lycopodium* ratios (C:L). The average percentage difference between counts was about 11%, in good agreement with the difference between independently processed parts of the same sample (Table 2.6). The most obvious reason for the disparity in the counts is the distribution of material on the cover slip, with different sections of the slide counted during each recount. If the ratio between charcoal and *Lycopodium* particles is not homogenous across the slide, counting different parts of the slide will result in different estimated charcoal concentrations. In order to assess the magnitude of this effect, a series of additional tests were devised to assess the effect of particle distribution across the slide on the charcoal fluxes.

Exp	Site	Hole	Core	Core Type	Section	Section Half	Top Interval (cm)	Bottom Interval (cm)	Age (Kyr)	G - Glacial, IG - Interglacial, T - Transition, DG - Deglacial	Original Count (O) Recount (R)	Charcoal Counts: Splintery Unperforated	Splintery Perforated	Irregular Unperforated	Irregular Perforated	Square / Rectangular	Elongate	Grass Char	Total Charcoal Counts	Charcoal / Lycopodium	Estimated Total Charcoal	Charcoal per gram sediment	Charcoal Flux per ka	Percentage Differences			Average percentage difference between counts per slide	Overall average percentage difference between counts
108	658	A	1	H	1	W	62	64	3.511	IG	O	21	4	127	6	101	2	5	266	0.532	13345	2669	39850	14.29			9.66	11.05
											R	43	13	133	18	21	0	0	228	0.456	11438	2288	34157		10.94			
											R	46	13	163	26	2	5	1	256	0.512	12843	2569	38352	3.76				
108	658	A	1	H	2	W	128	130	17.43	G	O	1	1	60	5	28	0	0	95	0.19	4766	953	10883	7.77			15.45	
											R	12	5	76	10	0	0	0	103	0.206	5167	1033	11800		29.13			
											R	15	1	49	3	5	0	0	73	0.146	3662	732	8363	23.16		24.75		
											R	9	1	73	10	4	0	0	97	0.194	4866	973	11113	2.07	5.82			
108	658	A	1	H	2	W	13	15	10.05	IG	O	13	5	190	52	32	6	0	298	0.596	14950	2875	39644	7.45			4.97	
											R	53	30	179	41	8	11	0	322	0.644	16154	3107	42837		7.45			
											R	57	22	150	46	17	6	0	298	0.596	14950	2875	39644	0.00				
108	658	A	1	H	2	W	44	46	12.02	G	O	8	0	178	21	44	0	0	251	0.502	12592	2422	33392	30.28			24.51	
											R	34	9	103	16	10	3	0	175	0.35	8779	1688	23281		14.29			
											R	20	9	95	18	6	2	0	150	0.3	7525	1447	19955	40.24		29.25		
											R	26	6	143	19	16	2	0	212	0.424	10636	2045	28203	15.54	17.45			
108	658	B	2	H	5	W	41	43	48.1	T	O	36	8	162	31	29	3	0	269	0.538	13495	2454	30386	5.95			3.99	
											R	55	18	148	14	16	2	0	253	0.506	12693	2308	28579		2.32			
											R	49	19	160	15	13	3	0	259	0.518	12994	2362	29257	3.72				
108	658	C	2	H	2	W	76	78	64.29	T	O	52	21	131	38	55	8	0	305	0.61	15301	2732	35038	1.29			2.17	
											R	61	23	169	29	21	6	0	309	0.618	15502	2768	35497		3.24			
											R	59	19	174	21	20	4	2	299	0.598	15000	2679	34348	1.97				
108	658	B	3	H	1	W	6	8	85.72	T	O	65	29	91	21	18	7	1	232	0.464	11639	2425	52816	19.16			14.61	
											R	61	21	131	51	16	7	0	287	0.574	14398	3000	65337		3.04			
											R	76	25	140	40	11	4	0	296	0.592	14850	3094	67386	21.62				
108	658	B	3	H	3	W	83	85	106.5	T	O	163	74	218	94	50	30	1	630	1.26	31606	6450	98574	19.13			13.02	
											R	204	93	318	134	23	7	0	779	1.558	39081	7976	121888		5.78			
											R	200	85	269	134	24	21	1	734	1.468	36823	7515	114847	14.17				

Table 2.6: Slide recounts. Comparison of charcoal counts achieved between recounts of the same slide and calculated percentage differences between achieved counts. IG - Interglacial, G - Glacial and T= Transitional (neither glacial or interglacial).

Slide Heterogeneities

Transects

A cursory visual inspection indicates that the slides have a higher density of material near the centre of the cover slip. Steps were taken during mounting to improve material distribution across the cover slip (material was pipetted into each corner and the centre was filled in last) however, some cover slips show slightly more clumped areas of material, noticeably the slides with a higher amount of undissolved lithics where the heaviest material instantly settles on the slide once pipetted onto the cover slip. In order to get the most representative view of the slide, all counts were begun on the edge of the centre of the cover slip and transects were covered in order sample both the least and most densely populated areas of the cover slip.

Sample	Age (Kyr)	G - Glacial IG - Interglacial T - Transitional	Transect	Charcoal	Lycopodium	C/L	Estimated Charcoal	Charcoal Concentration	Charcoal Flux/ka	Difference percentage of the Transects 1	Difference percentage of the Transects 2	Average percentage difference	Average differnce in transect
108-658A-1H-1W 62-64 cm	3.5114	IG	0,125	135	270	0.500	12542	2508	37453	5.7			11.13
			15,0	122	230	0.530	13305	2661	39733				
108-658A-1H-2W 29-31 cm	3.5114	IG	0,125	140	206	0.680	17047	3409	47014	32.0			
			15,0	97	210	0.462	11586	2317	31954				
108-658A-3H-4W 113-115 cm	135.33	IG	0,125	67	418	0.160	4021	804	7557	5.2			
			0,125	70	414	0.169	4241	848	7972				
108-658A-1H-1W 95-97 cm	5.4966	IG	0,128	138	225	0.613	15385	3205	40819	7.7			
			12,0	133	235	0.566	14196	2958	37666				
108-658A-1H-1W 137-139 cm	8.3919	IG	0,125	148	252	0.587	14732	2946	40628	7.7			
			13,0	129	238	0.542	13596	2719	37496				
108-658A-1H-1W 137-139 cm	8.3919	IG	0,125	129	253	0.510	12790	2558	35273	20.8		14.1	
			0,135	134	332	0.404	10124	2025	27921		17.9		
			12,0	108	258	0.419	10500	2100	28958	3.6			
108-658A-1H-4W 1-3 cm	32.509	T	0,125	113	189	0.598	14997	2830	39019	7.6			
			14,0	119	185	0.643	16135	3044	41980				
108-658B-2H-6W 71-73 cm	58.614	T	0,125	108	77	1.403	35183	6766	86761	3.0			
			0,125	107	74	1.446	36270	6975	89442				

Table 2.7: Transect counts comparison. Counts achieved on single full transects and calculated percentage differences. IG – Interglacial, G – Glacial and T – Transitional.

Assuming a well-mixed sample, then any counts made over different areas of the slide should produce, if not exactly the same concentrations then very similar values. However, recounting of the same slide across different areas, yielded different charcoal concentrations that on average vary by ~11% (Table 2.6). The change in distribution is most easily observed when examining individual transects of the cover slip, each transect generates a unique C:L value (see appendix of all the transect counts). The average difference between the individual transects generated from a single mount of a samples is ~11% (Table 2.7). These results would suggest that distribution of material on the cover slip and the areas in which the count was conducted across slide ultimately influences the end charcoal flux calculated and may be responsible for much of the variability between recounts of the same sample (Table 2.6).

Periodic Counts

In order to assess the representativeness of the counted areas of the slide, 'periodic counts' were conducted. At semi-regular intervals (~50 *Lycopodium*) the raw counts of charcoal and *Lycopodium* were made during counting, to see how stable or otherwise the C:L remains (Figure 2.7).

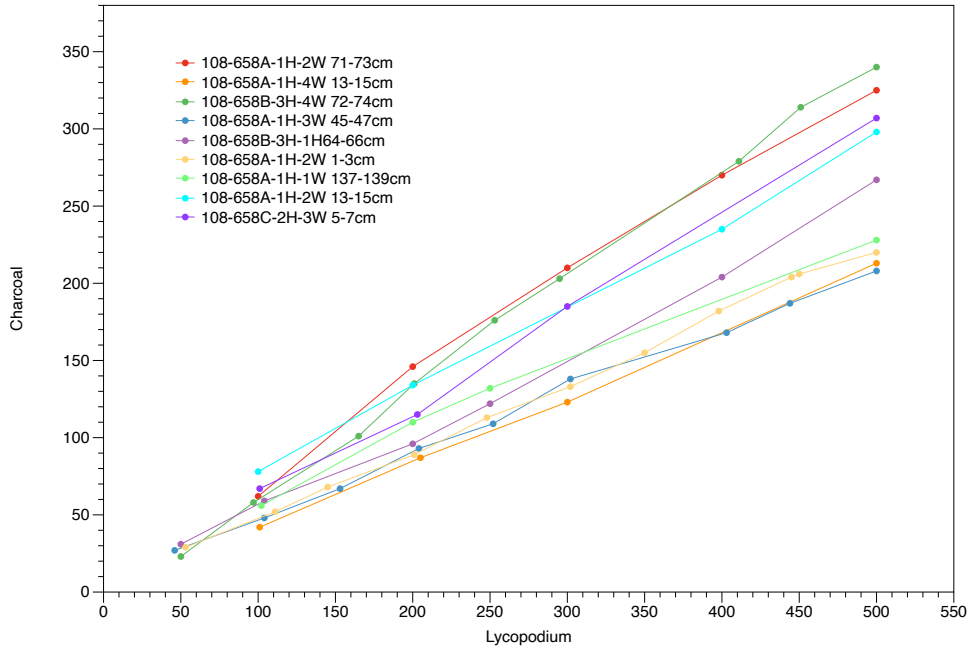

Figure 2.7: Running totals of counted charcoals against *Lycopodium.*

Examination of the periodic counts, show that smaller the number of *Lycopodium* counted the greater the discrepancy between this count and the final count achieved at 500 *Lycopodium*. In

order to get a consistent or closely reproducible C:L at least 500 *Lycopodium* needs to be reached (Figure 2.8). Comparisons between full counts values and the 500 *Lycopodium* counts (standard counts) reveal that there is only an average difference in the ratios produced of ~9.95% therefore in the interest of time counts (average count time standard counts 1-3 hours, full counts 5-8 hours per slide) 500 *Lycopodium* was deemed to be sufficiently representative of slide to produce reliable.

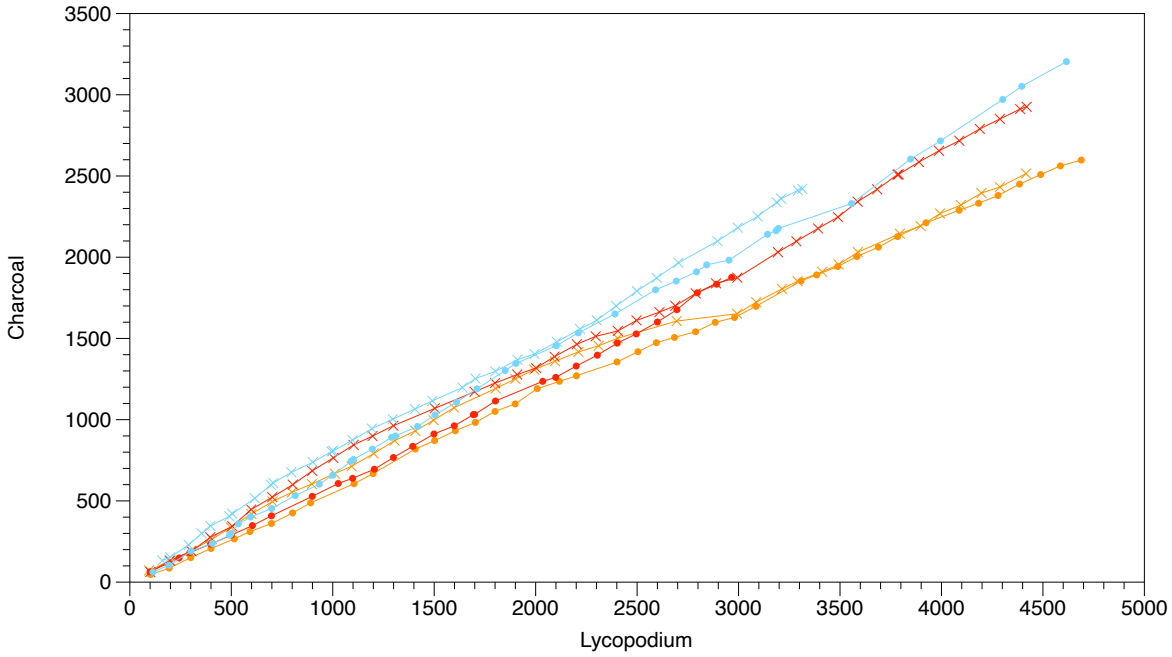

Figure 2.8: *Lycopodium* vs Charcoal on the fully counts slides, determine the stability of counts. Red Circles 108-658A-1H-1W 62-64cm Original Full Count, Red Crosses 108-658A-1H-1W 62-64cm Remount Full Count, Blue Circles 108-658A-1H-1W 95-97cm Original Count, Blue Crosses 108-658A-1H-1W 95-97cm Remount Full Count, Orange Circles 108-658A-1H-1W 137-139cm Original Count, Orange Crosses 108-658A-1H-1W 137-139cm Remount Full Count.

2.2.4.2 Summary of charcoal count reproducibility studies

Repeat measurements of charcoal concentrations from the same sediment sample give a reproducibility of approximately ±12%. Much of this variability appears attributable to an uneven distribution of both charcoal and *Lycopodium* particles across the microscope slide, giving different ratios between the two depending upon which region of the slide is counted. In order to mitigate this effect, charcoal particles should be counted until at least 500 *Lycopodium* have been recorded (Figure 2.8) to ensure a significant proportion of the slide is incorporated into the recorded concentrations. The similarity between variability in samples which have been reprocessed and

remounted (12.5%) and those where the same slide has been recounted (11%) suggests that bulk sediment samples are relatively homogenous over large scales. Errors attributable to inconsistency in the identification of charcoal particles are small (~4%). I thereby ascribe an overall reproducibility error of ~12.5% to all charcoal counts.

The error is larger than I would have liked but, but the tests I have undertaken to determine errors and by keeping the methodology consistent mitigates these errors as much as possible. An important consideration when interrogating this data is that the raw counts and therefore the charcoal fluxes although instructive, are less significant than the trends produced by the data collectively. In the following studies I am more interested in shifts between lower and higher fire activity and the variability I examined is greater than that of the error on the counts. Due to the reproducibility error, variability below 12.5% is not considered to result from natural forcing mechanisms.

Chapter 3 Validation of the Charcoal Proxy

3.1 Abstract

Charcoal is commonly used as a first order proxy for past fire, variability in charcoal fluxes enables palaeo-fire activity to be examined, as charcoal is assumed to highly resilient in the geological records. The charcoal taphonomy literature is complicated, as due to the varying methods used to extract 'charcoal', impacts on the which specific aspect of the combustion continuum (soot, ash, charcoal, partly charred biomass) is recovered and studied and separate parts of the charcoal continuum display specific chemical behaviours. Consequently, the literature is awash with different 'charcoal' terminology and inconsistencies exist surrounding the preservation of charcoal in palaeo-archives. I present a comparative analysis of charcoal fluxes generates from Ocean Drilling Program (ODP) sites 658, 659 and 668, examining factors influencing the variations in charcoal recovery. In addition, I also present a methods comparison between a geochemical and an optical method of charcoal identification to indicate the disparity in charcoal flux generated using different processing techniques. My results indicate that charcoal preservation in palaeo-archives can be modified by oxidation of the sediments, and that geochemical methodology using an oxidation stages may be comparatively less sensitive to capturing charcoal flux variability.

3.2 Introduction

Fire has been an integral mechanism within the Earth's ecosystems since the Silurian (Glasspool et al., 2004), acting as a mechanism to maintain and expand the planet's vegetation zones, most notably today in the north African Savanna by preventing woodland encroachment into the savanna grassland (Beerling and Osborne, 2006; Hoetzel et al., 2013; Osborne, 2008; Scheiter et al., 2012). Fires are ephemeral events that are not themselves preserved in geologic record, but combustion products produced during these fires can be preserved and can therefore be used as a proxy for fire. Multiple burning products encompassing a large range of particle sizes and degrees of charring are produced during fires. These can be grouped into three major groups: charcoal, ash and soot. These umbrella terms can be broken down and burning products more specifically classified using the charcoal continuum (Czimczik et al., 2002; Masiello and Druffel, 1998; Thevenon et al., 2010). Given the multitude of different products produced during burning,

it is hardly surprising that a vast terminology describing combustion products exists in the literature. Examples of terms used for combustion products include, biochar, black carbon, soot, Oxygen Resistant Elemental Carbon (OREC), and pyrogenic carbon (Bird and Ascough, 2012; Bird and Cali, 1998; Bird and Gröcke, 1997; Preston and Schmidt, 2006; Thevenon et al., 2010). A related issue is that there are multiple methods, both microscopic and geochemical, for determining past fire activity in the geological record. Direct comparisons between records generated using different methodologies are not straightforward. A further issue concerns the resilience of these combustion products to oxidation and hence aliasing of fire activity records by differential post-depositional preservation histories.

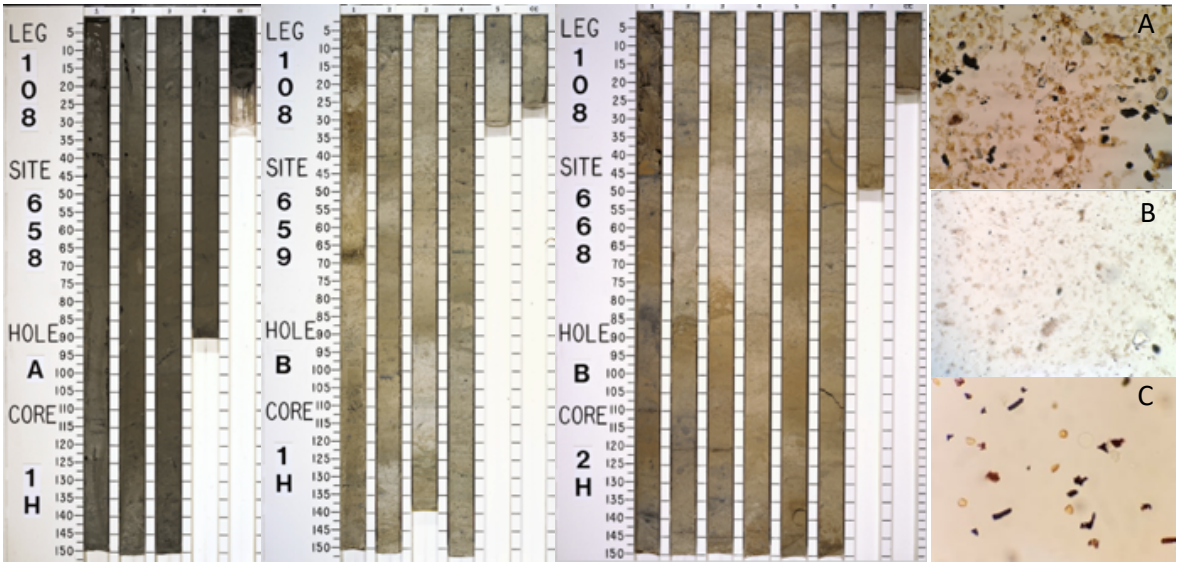

Figure 3.1: ODP Sites Core Comparison Photographs. Core images of ODP sites 658, 659 and 668 cores from the JANUS database. Palynology slides typical of samples produced from A) ODP 658, B) ODP 659 and C) ODP 668.

Here I report the results of a study to validate charcoal count-based fire activity records produced by microscopic examination of marine sediment samples. Herein, charcoal is defined as any carbon-rich terrestrially derived material produced by total combustion either by natural or anthropogenic mechanisms (Bird and Ascough, 2012; Keeley and Rundel, 2005). Traditionally, charcoal is considered one of the most refractory components of marine sediments (Herring, 1985). On the other hand, experimental studies show that charcoal is lost under highly oxidizing conditions (Bird and Gröcke, 1997; Bruun et al., 2008; Hammes et al., 2007; Masiello, 2004; Masiello and Druffel, 1998) while the colour of terrestrial sediments is widely used as an informal

indicator when prospecting for charcoal (dark sediments are strongly favoured over pale or red-coloured deposits). I find that charcoal recovery is excellent from the overall darker sediments of ODP sites 658 and 668 from all lithologies targeted (Figure 3.1). Whilst, irrespective of lithology, no or negligible amounts of charcoal were recovered from the much paler sediments and red sediments (red is indicative of the high iron oxide and hydroxide content (Vallé et al., 2014)) of site 659 (Figure 3.1). The palynology slides produced from the differing sites also mark ODP 668 as noticeable different (Figure 3.1 A-C).

3.3 Site Selection and Chronology

The study sites are located proximally and downwind of the region of highest modern fire activity in Northern Africa, the North African Savanna (Figure 3.2). Ocean Drilling Program (ODP) sites 658, 659 and 668 and GeoB9528-3 are located in the eastern equatorial Atlantic. Site 658 is located 160 km offshore Mauritania on the continental shelf (20°44.95'N, 18°34.85'W at water depth ~2200m), ODP 659 is located ~500 km offshore Senegal on the Cape Verde Plateau (18°04.63'N, 21°01.57'W at a water depth of 3100m) and ODP 668 is located on the Sierra Leone Rise ~1000 km offshore (4°46.12'N, 20°55.62'W at a water depth of ~2700m). GeoB9528-3 was recovered from Guinian Plateau Margin (09°09.96'N, 17°39.81'W) at a water depth of ~3000m, ~350km offshore Guinea. Terrestrial material including dust, charcoal, diatoms, phytoliths and palynomorphs (Gasse et al., 1989; Kuechler et al., 2013; Tiedemann et al., 1989; Tjallingii et al., 2008; Vallé et al., 2014) is transported westwards across the Atlantic Ocean by the African Easterly Jet (AEJ) from a number of source regions in the southern and central Sahara and North African Savanna to these sites by the major African dust plume (Harrison et al., 2001; Hooghiemstra et al., 2006). ODP sites 658 and 659 are located below the summer position of this dust plume whereas ODP 668 and GeoB9528-3 are located below its winter position (Figure 3.2). The position of the AEJ is inferred to have been stable across glacial and interglacial climatic fluctuations from palynological and geochemical records despite the implied latitudinal shifts in the position of the vegetation bands (Cole et al., 2009; Dupont, 2011, 1993).

ODP sites 659 and 668 have sedimentation rates typical for open ocean sites, 11 cm/kyr and 17 cm/kyr respectively, contrastingly ODP 658 experiences higher sedimentation rates 24 cm/kyr owing to its position below a high productivity upwelling cell. As a result, ODP 658 also has a very

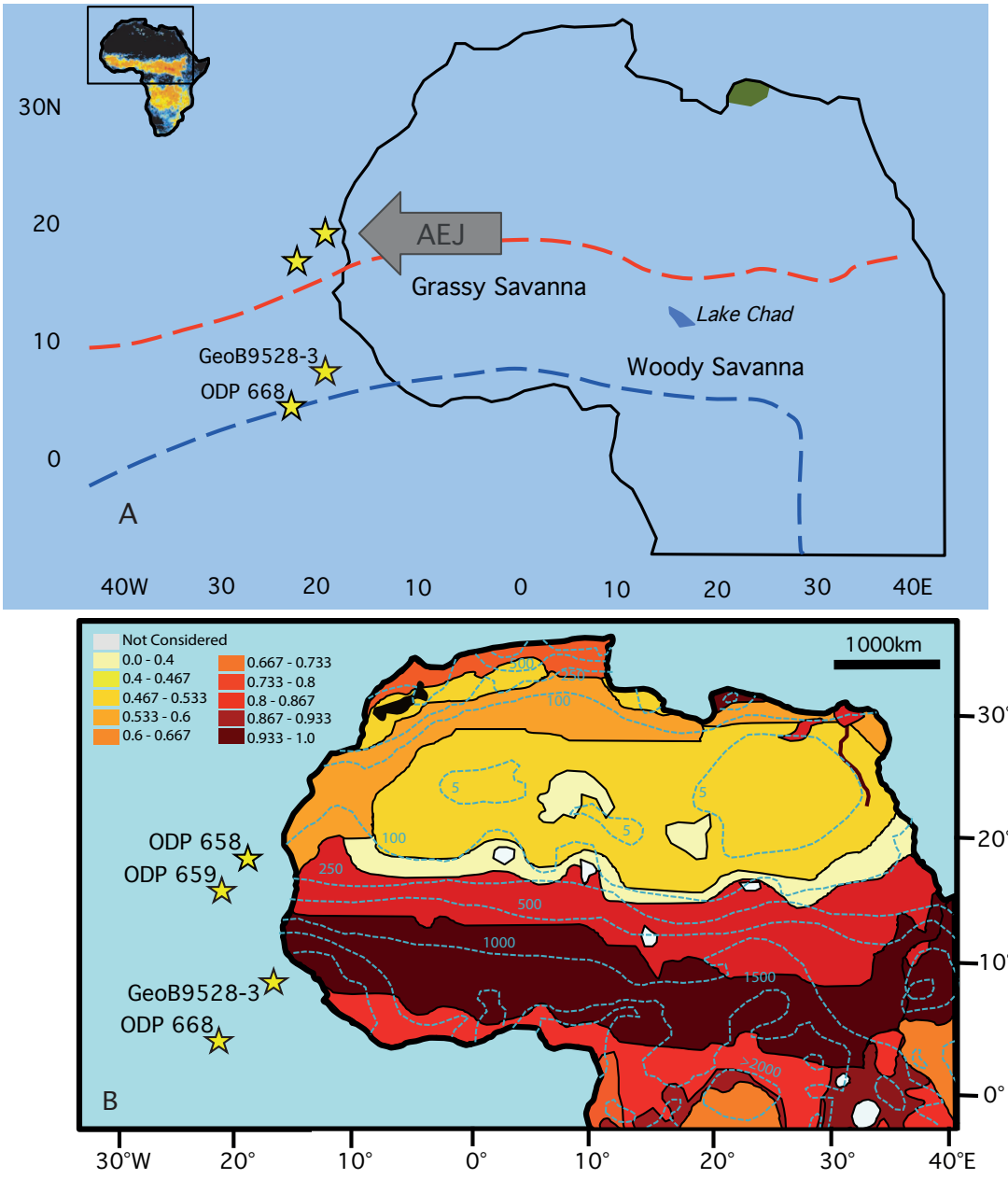

Figure 3.2: Transect of Sites Map. Schematic map of the major North African vegetation bands, the modern summer and winter latitudinal position of the ITCZ and the African Easterly Jet (AEJ). Location of the ocean drill sites discussed in the text also shown. Adapted from (Sarnthien *et al.,* 1998; Gasse *et al.,* 1989; Vallé *et al.,* 2014). Inset: Fire Map annual average number of fires observed by satellite, Black ~0, Dark Blue 1-4, Mid-Blue 5-19, Light Blue 20-49, Green 50-99, Yellow 100-199, Orange 200-499, Red >500 (Taken from Bowman *et al.,* 2009 data from Giglio *et al.,* 2006). B: Fire Activity Map (adapted from Pausas and Ribeiro, 2013), overlain by present day precipitation mean annual precipitation contours after Larrasoaña *et al.,* (2013).

high total organic carbon (TOC) 0.5-4.0%, compared to ODP 659 and 668 which have TOC values of <0.4% TOC and 0-0.33% respectively (Figure 3.3) (Ruddiman et al., 1988b; Stein et al., 1989).

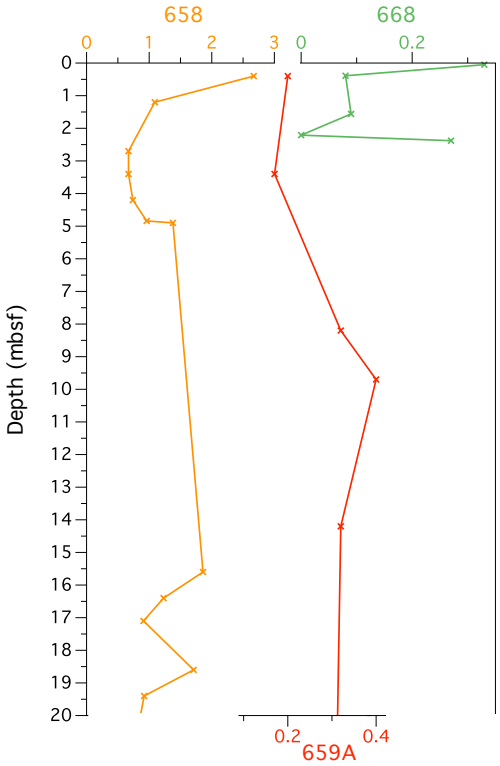

Figure 3.3: TOC comparison of ODP sites 658, 659 and 668. TOC values from Stein et al., (1989) and Ruddiman et al., (1988a,b,).

3.4 Methods

3.4.1 Site Chronologies

The age model for ODP 658 is detailed in full in Chapter 2 Section 2.2.1. In brief, the age model was constructed using a slightly modified version of the published age-depth tie points of Meckler *et al.*, (2013).

The age model for ODP 659 is detail in full in Chapter 2 Section 2.2.1. In brief, updates were made to the biostratigraphic (after Raffi *et al.*, 2006) and magneostratigraphic age points (using geomagnetic polarity timescale (GPTS) to the original shipboard data (see Initial shipboard reports

and SEDIS). Over the youngest 5 Myr the existing *C.wuellerstorfi* $\delta^{18}O$ was tuned to LR04 (Lisiecki and Raymo, 2005) and the XRF Ca/Fe ratios were tuned to summer insolation at 65°N (Laskar et al., 2004).

The age model for ODP 668 was generated from the $\delta^{18}O$ *G.ruber* values for ODP 668 (Bird and Cali, 2002) were correlated to the LR04 $\delta^{18}O_{benthic}$ foraminfera stack (Lisiecki and Raymo, 2005) using AnalySeries software (Palliard *et al.*, 1996).

3.4.2 Carbon and Nitrogen concentrations and isotopes

Bulk sediment was freeze dried and approximately ~1g was weighed and crushed into a fine powder. Decarbonisation of the sample was achieved by submerging the sample in 10% HCl until the reaction ceased. The samples were dried and weighed after neutralization following decarbonization and weight loss and Total Inorganic Carbon (TIC) calculated. ~10 mg of re-homogenized sample were run on the Vario Isotope Select Elemental Analyser coupled with an Isoprime 100 mass spectrometer at the National Oceanography Centre at the University of Southampton to generate percentage organic carbon (%C_{org}), organic $\delta^{13}C$ ($\delta^{13}C_{org}$), percentage nitrogen (%N) and organic nitrogen isotope ($\delta^{15}N_{org}$) data. Total bulk sediment dry weight was divided by decarbonated fraction for each sample to generate the percentage Total Organic Carbon (%TOC) for each sample.

3.4.3 Charcoal concentrations

A modified version of standard palynological processing using a two-step acid maceration (similar to that detailed by (Harding et al., 2011)), however steps involving physical agitation were omitted to avoid charcoal fragmentation were used to prepare the bulk sediment samples for charcoal counts for the ODP 668 samples. A treatment of HCl (for 24 hours) and HF (for 48 hours) was applied to 2-3.5g of unground oven-dried bulk sediment to remove the unwanted carbonate and silicate fractions respectively. The fluoride compounds formed during HF maceration were removed from the samples by boiling HCl and sieving at 15 μm. A short ultrasonic step (20 second) followed by sieving (15 μm) was used to remove the remaining Amorphous Organic Matter (AOM).

A known dose of the exotic spore *Lycopodium* (clubmoss) was used to spike to spike the samples (>15 μm size fraction) to enable the charcoal concentrations to be calculated (Stockmarr, 1971). Samples were mounted on glass slides for examination and counting under transmitted light, counting proceeded on charcoal and *Lycopodium* concordantly until 500 *Lycopodium* was reached. An Olympus BH-2 microscope in coordination with a freestanding light was used to optically identify charcoal using shape, colour and reflectance characteristics. Straightforward identification of the charcoal particles was hindered by the high pyrite content of some of the samples, therefore an additional check was employed to view the particle in low base light (microscope light) and high upper light (lamp light). Particles displaying very high reflectance were classified as pyrite. Only black particles with transparent edges, with low reflectance and fell within specific morphological categories: elongate, splintery perforated and splintery unperforated, irregular perforated, irregular unperforated or square/rectangular, were counted (Figure 3.4). A subset of five of the site 658 samples were examined under reflected light, to identify retained plant cellular structure in the charcoal particles (Figure 3.4).

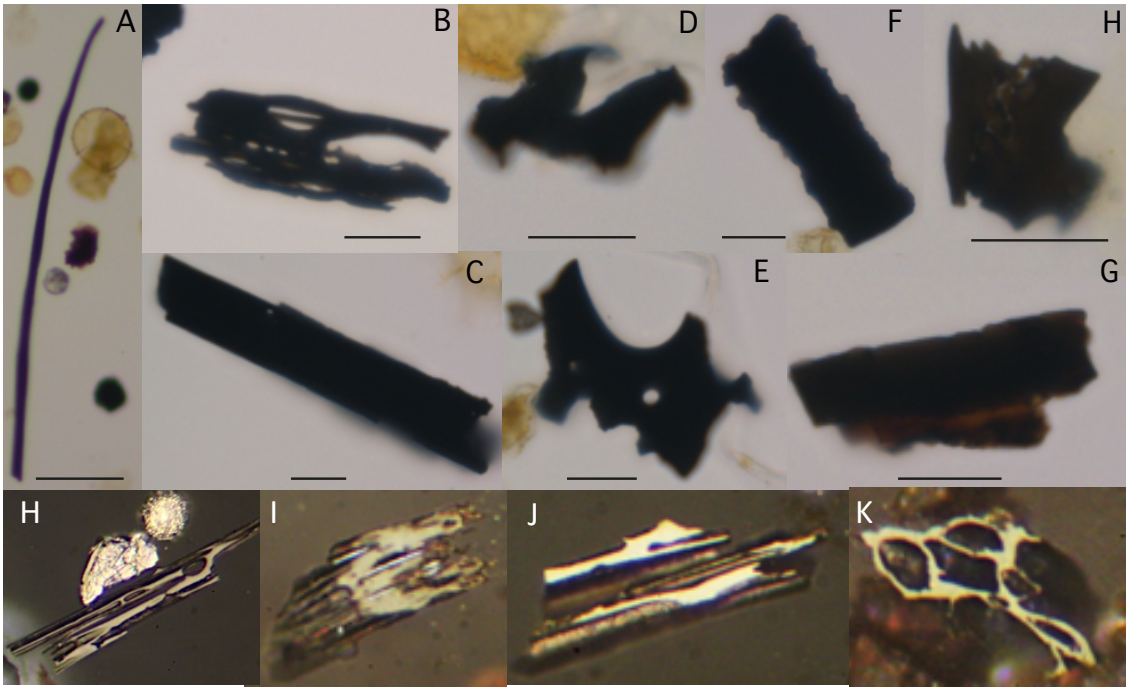

Figure 3.4: Charcoal Morphology A) Elongate, B) Splintery Perforated, C) Splintery Unperforated, D) Splintery Unperforated, E) Irregular Perforated, F) Square/Rectangular, G) Dark Terrestrial Organics, H) Grass. Black bars represent 20 μm. H-K) Reflected light Images of charcoal particles, showing original biomass structure.

The site 659 samples were processed at the University of Exeter using their standard method omitting stages where physical damage may occur. Methological differences include, the use of a shaker table to aid disaggregation, cold HCl to remove calcium fluoride products, no sieving and samples were mounted in glycerine. The low yield of organics from these samples, resulted in the entire sample residue to be used for mounting.

All samples were counted following standard palynological methodology, the charcoal slides were counted for charcoal particles using an Olympus BH-2 microscope at x20 or x40 magnification. Standard counting procedure was to concurrently count for charcoal and *Lycopodium* on multiple transects near the centre of the slide until 500 *Lycopodium* was reached. I term these as 'Standard counts'.

Charcoal concentrations were calculated using equation 1:

Eq. 1:-

$$((\text{Charcoal counted} \div \text{Lycopodium counted}) \times \text{total Lycopodium}) \div \text{dry sediment weight (g)} = \text{charcoal concentrations (charcoal/g)}$$

Fluxes of charcoal were calculated using bulk density and sedimentation rates using equation 2:

Eq. 2:-

$$(\text{charcoal concentration (charcoal/g)}) \div \text{dry bulk density (g/cm}^3) \times (\text{sedimentation rates (cm/kyr)} \times 100) = \text{charcoal flux (charcoal/cm}^2\text{/kyr)}$$

3.4.4 ODP 668 Sample Determination

The OREC/dust data presented in Bird and Cali (1998) and Bird and Cali (2002) were reconstructed from the published graphs using WebPlotDigitizer (https://automeris.io/WebPlotDigitizer/), with these depths matched to samples taken by the authors as recorded in the Bremen Core Repository Drilling Information System (DIS) (Table 3.1).

Assigned Depth	Generated Depth	OREC/Dust	Age (kyr)
0.02	0.015	1.3114	1.1
0.08	0.085	0.2330	4.35
0.13	0.133	0.1325	7.05
0.19	0.192	0.0488	10.3
0.41	0.407	0.0756	27.6
0.64	0.639	0.0053	40.4
0.81	0.805	0.3335	49.9
0.88	0.877	0.6951	54.38
0.94	0.957	0.4373	56.3
1.16	1.154	0.1057	74.2
1.39	1.386	0.0387	86.4
1.55	1.581	0.0253	94.8
1.85	1.838	0.0588	110.6
2.03	2.023	0.0186	120.22
2.24	2.233	0.0756	138.3
2.43	2.427	0.0890	165.2
2.78	2.779	0.1727	211.8

Table 3.1: ODP 668 Depth Assignment. Depth tables indicating the depth and OREC/Dust values of the Bird and Cali, (1992) sample depth generated using WebPlotDigitizer (generated depth) and the correlating sampling depth indicated by the Bremen Core Repository Drilling Information System (assigned depth).

3.5 Results

3.5.1 Charcoal Recovery

Charcoal particle abundance at ODP Site 659 is extremely low compared to sites 658 and 668, the low organic carbon content of the site 659 samples meant that the entire sample was mounted for examination and only a handful of charcoal particles were recovered from all of the samples processed. In contrast, only a fraction of the ODP sites 658 and 668 sample residues was required for examination. The sample set taken for site 659 deliberately targeted a wide range of lithologies exhibiting textural (sandy, crumbly, clay, nannofossil rich) and colour (white, red, green, purple-grey brown and grey) differences, suggestive of contrasting lithology and preservation. Amorphous Organic Material (AOM- structureless organic material formed from microbial degraded marine microorganisms) was present in all site 659 samples of varying amounts, but the samples were almost all totally barren of terrestrial organic material and only one the samples yielded any charcoal (108-659C-1H-4W 94.5-96.5cm – purple-grey brown in colour) and in insufficient amounts for study. One other sample from site 659 yielded plant cuticle (108-659B 16H-5W 24-26 – pale nanno-fossil rich lithology). In contrast, all samples from ODP site 658 yielded very abundant charcoal processed and generated an excellent charcoal flux record (charcoal flux ranges from $1.1x10^4$ to $13.4x10^4$ cm^2/kyr) (Figure 3.5). Charcoal recovery was also good (flux ranges from $2.3x10^4$ to $7.3x10^4$ cm^2/kyr) from ODP Site 668 (Figure 3.5), situated further offshore below the winter African dust plume and more distally to the NAS, than site 659 (Figure

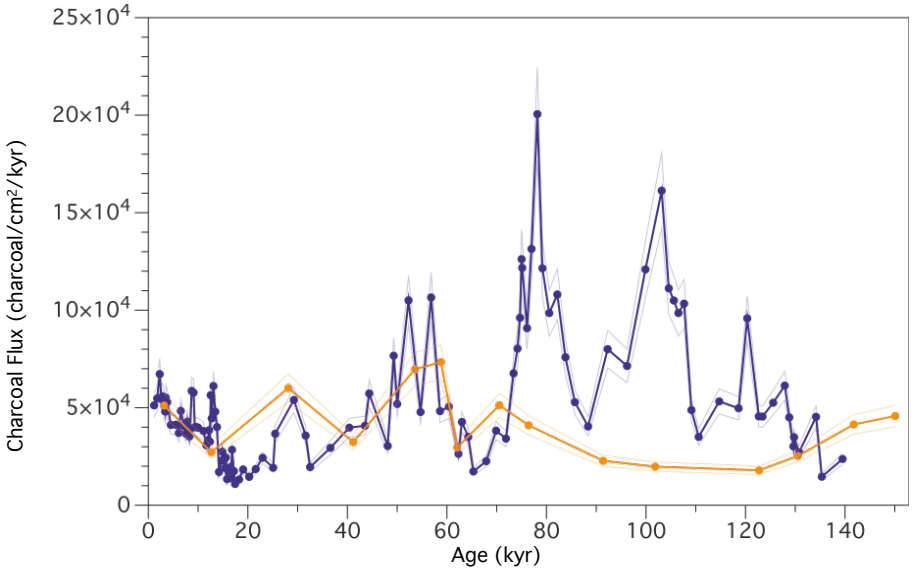

Figure 3.5: Charcoal Flux comparison between ODP site 658 (shown in blue, 12.5% error shown in light blue) and ODP site 668 (shown in orange, 12.5% error shown in light orange).

3.2), and yet the absence of charcoal at Site 659 is surprising for a number of reasons. ODP site 659 is located proximal to the modern main fire band in northern Africa (Figure 3.2), the NAS, and is situated below the major summer African offshore dust plume, and this site receives good terrestrial material delivery, which presumably included charcoal (Kuechler et al., 2013; Tjallingii et al., 2008; Vallé et al., 2014).

3.5.2 Extremely low charcoal counts at ODP Site 659

While the precise chronostratigraphic coverage of data differs between the three study sites (Figure 3.6) the great contrast in charcoal fluxes observed between Site 659 and both sites 658 and 668 rules out the possibility that the lack of charcoal recovery from ODP site 659 sediments is attributable to a lack of fire activity. Furthermore, the abundance of charcoal in the highly distal Site 668 sediments also rules out the possibility that the lack of charcoal at Site 659 is attributable to rapid decay in particle flux and/or size with distance-to-source (Figure 4.2). Next I consider the role of preservation.

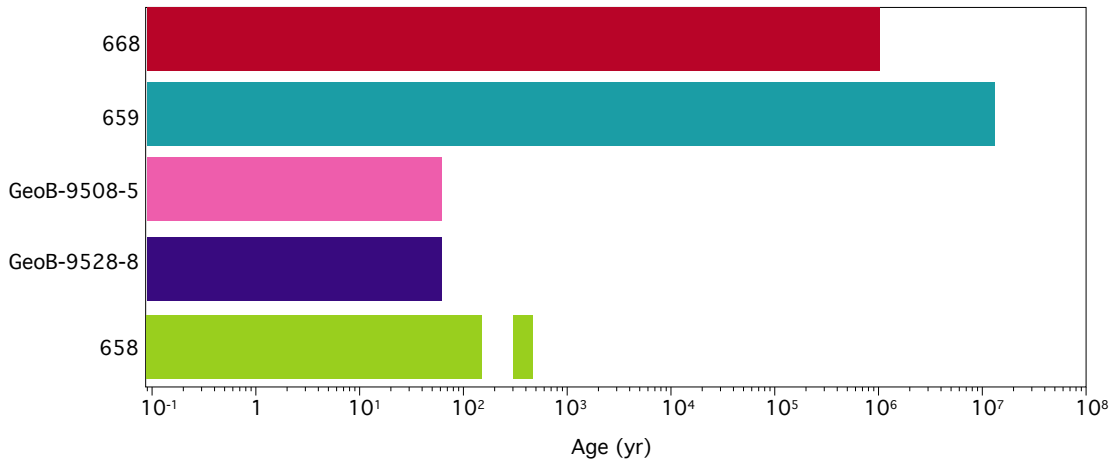

Figure 3.6: Sampling age range. Range of samples examined in this study from each of the study sites.

The total organic carbon (TOC) content of the studied sediments varies between sites: ODP 659 (<0.5%); and ODP 668 (0.1-0.3%) values are typical for open ocean sites whereas concentrations are much higher at Site 658 (0.5-4.0%) in keeping with its position below a surface ocean high productivity cell (Figure 3.3) (Shipboard Scientific Party *et al.,* 1988a,b Stein *et al.,* 1989). The variable TOC preserved in the sediments is reflected in sediment colour (Figure 3.1).

C/N and $\delta^{13}C$ values for the ODP site 658 samples are indicative of being of marine origin (i.e photosynthesising algae) (Meyers, 1994)(Figure 3.7). C/N values are consistent with nitrogen-limited conditions (Meyers, 1994) of the high productivity cell, agrees with evidence of upwelling today (Lange et al., 1998) and in past (e.g. (Meckler et al., 2013; Sicre et al., 2002). The TOC profile for ODP site 659 samples, provides no indication that this site has been situated below a high productivity cell. The TOC dataset available for ODP 668 is extremely limited, the available data suggest that the values for site 668 are more in keeping with site 659 than site 658.

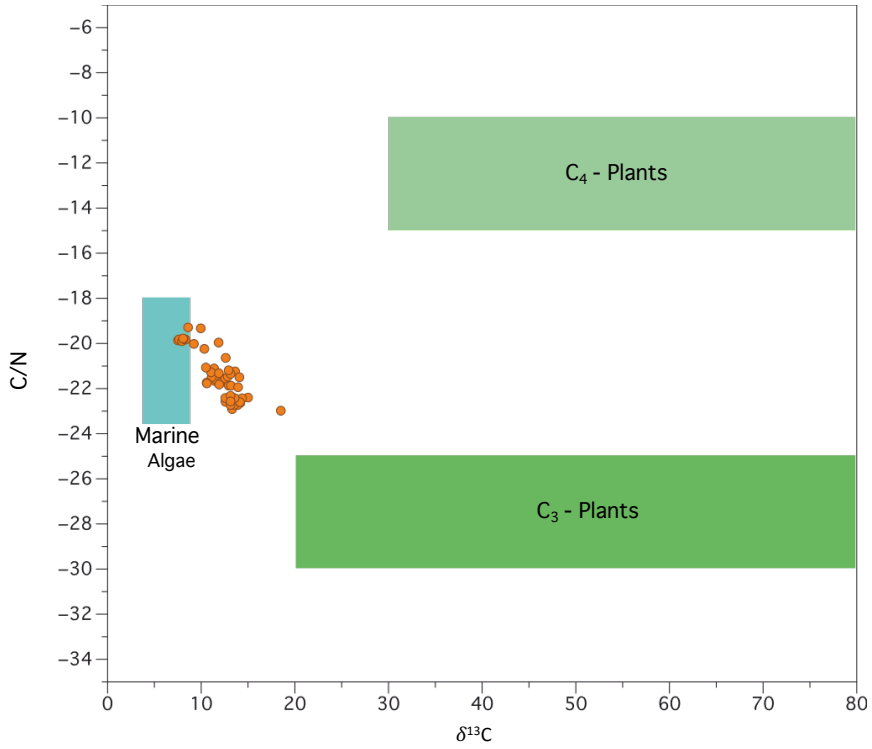

Figure 3.7: TOC Origins at ODP 658. Cross Plot of $\delta^{13}C_{org}$ (‰) and C/N for the ODP 658 samples.

Charcoal is generally considered to be chemically and biologically inert (Scott, 2010) however even a simple mass balance equation indicates that this logical is flawed (Masiello and Druffel, 1998; Masiello, 2004 and reference therein), as it is not possible to reconcile the amount of charcoal production with against the amount of charcoal that is preserved in palaeo-archives. It follow as a result that charcoal must degrade and be lost over geologic time (Bruun et al., 2008; Masiello, 2004). The stability of charcoal in palaeo-archives, however, is not well understood or constrained. The behaviour of charcoal under highly oxidizing conditions is debated. Some studies infer charcoal loss (Bird and Gröcke, 1997; Hammes et al., 2007; Masiello, 2004), others its resistance (Verardo, 1997). The strongest argument for the long-term preservation of charcoal and resilience to chemical or biological loss in marine sediments is the lack of size sorting with age

because degradation is likely to affect the smallest particles with the smallest volume to area ratio first, yet no trends towards the preservation of only larger particles in older sediments are observed (Herring 1985).

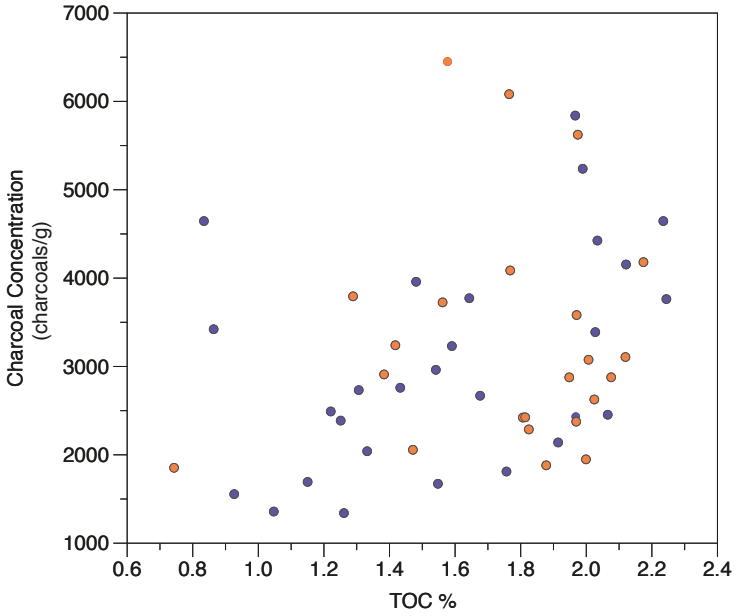

Figure 3.8: Cross Plot TOC% vs Charcoal Concentration at ODP 658. Cross plot of charcoal concentration in each sample plotted against corresponding % TOC for ODP Site 658. Purple points indicate AHP aged samples, orange points indicate non-AHP aged samples

To explore the extent to which temporal variability in organic carbon content exerts a control on charcoal preservation, I compared %TOC and charcoal fluxes during the Last Glacial Cycle (LGC) at Site 658. A cross plot of these two variables shows no relationship (Figure 3.8). Charcoal flux variability through the LGC reconstructed at site 658 is not, therefore, attributable to preservation (Chapter 4, Chapter 5 and Chapter 6). My charcoal recovery comparison between ODP sites 658 and 659 strongly suggests that the lack of charcoal at site 659 results from charcoal loss from under oxidizing conditions.

3.5.3 Method Validation: Methodological Differences in Charcoal Extraction

A comparison of methods was undertaken to test the OREC- based records of Bird and Cali (1998) using a sampling set taken from the same depth where possible or where not immediately next those used in that study (Table 3.1) and that of a levoglucosan biomarker record from a nearby Site GeoB9528-3 (Schreuder et al., 2019), both OREC and levoglucosan are proxies for fire. OREC is used as a proxy for charcoal, the samples are highly oxidized to remove the labile organic component to leave the resilient and inert 'charcoal' whereas levoglucosan is an organic biomarker for fire formed by the combustion of biomass (specifically cellulose and hemicellulose) (Hawthorne et al., 2017; Kehrwald et al., 2012; Schreuder et al., 2019).

A comparison of the down-core OREC based record with my charcoal-counts shows some broad similarities but also major discrepancies (Figure 3.9). In particular, this comparison strongly suggests that the OREC-record severely underestimates charcoal flux during MIS 3 (Figure 3.9).

The comparative lack of sensitive in the OREC/Dust compared to the charcoal flux record may highlight a serious underlying problem with oxidation as a method for generating a fire activity record. Experimental studies have shown that charcoal is lost under oxidizing conditions (Bird and Gröcke, 1997; Hammes et al., 2007; Masiello, 2004; Masiello and Druffel, 1998; Schmidt and Noack, 2000). Results derived by the OREC method could potentially remove charcoal and retain non-charcoal within the samples during the oxidizing stage, fire activity records produced by this method could therefore be flawed. The peak charcoal flux in the site 668 charcoal flux and OREC records matches peak burning in the levoglucosan record also centred at ~55 ka (Schreuder et al., 2019)(Figure 3.9). The levoglucosan records indicated that this increase in burning is associated with a floral change, however as the concentration of levoglucosan is production during burning is dependent on floral type a change in flora may result from an increased production of levoglucosan rather than a change in fire activity.

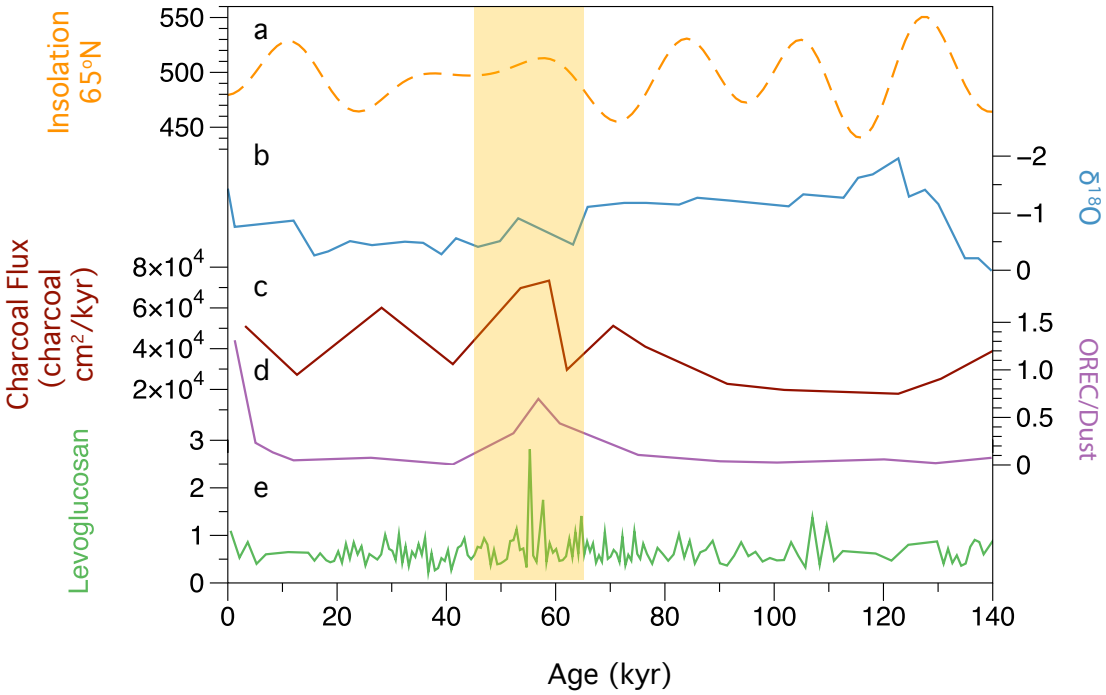

Figure 3.9: Fire activity comparison at ODP 668. A) Insolation 65°N (JJA) W/m^2(Laskar *et al.,* 2004), B) Oxygen Isotope (Bird and Cali, 2002), C) ODP 658 Charcoal Flux (this study), D) ODP 668 OREC/Dust (Bird and Cali, 1992), E) GeoB-9528-3 Levoglucosan record (Schreuder *et al.,* 2019). Yellow Bar MIS 3.

The strong correlation in timing of the charcoal peaks observed in the Site 668 and GeoB9528-3 (Figure 3.9), by three by independent proxies (charcoal flux, OREC and levoglucosan) for fire activity would suggest that northwestern Africa experience increased burning at *ca.* 55 ka.

In summary, my comparison calls into question the reliability of the geochemical methods for the identification of charcoal by the OREC method and optically. I infer that the oxidations stages used in the OREC method have the potential to induce charcoal loss and therefore under-estimate charcoal flux and therefore fire activity.

3.6 Conclusions

The lack of charcoal recovery at ODP site 659 was unexpected. Distance, delivery and age effects have been discounted as cause for the barren nature of the site 659 samples, however it is speculated that heavy oxidation at this site might have induced charcoal loss. This explanation raises questions about the resilience of charcoal in marine settings over geological time. Oxidation is suggested as a possible cause because multiple studies have identified charcoal is lost under oxidizing conditions. The argument for a potential oxidation control is strengthened by the comparatively less sensitive profile of the OREC/dust record when directly compared to the charcoal flux record generated on the same sampling sets taken from site 668. The highly oxidizing stages involved in the generation of a fire activity record using the OREC method may have induced charcoal loss, hence the less variable profile.

Chapter 4 Spatial variability of fire activity along a latitudinal transect on the Northwest African Margin for the last 50 kyr

Supporting Authors: Anya Crocker[1], Paul A Wilson[1], David Beerling[2], Colin Osborne[2]and Nele Meckler[3]

[1]University of Southampton - National Oceanography Centre, Waterfront Campus, European Way, Southampton, United Kingdom. SO14 F5D

[2]University of Sheffield - Department of Animal and Plant Sciences, Alfred Denny Building, Western Bank, Sheffield, United Kingdom. S10 2TN

[3]University of Bergen – Department of Earth Science, Postboks 7803, 5020 Bergen

4.1 Abstract

Fire is a strong driver of floral change at observational and geological timescales. Here report the findings of an examination of regional fire activity variability along a transect on the northwest African margin (NWAM) between (21 - 9°N) across North Africa in response to strong climate variance. Whilst the northern (21°N – Ocean Drilling Program (ODP) 658) and southern (9°N – GeoB9528-3) extremes of transect exhibit an opposing response in fire activity under increasing humidity. Increased moisture at the northern end of the transect is inferred to promote grassy savanna expansion and the development of a larger fuel source. Contrastingly, at the southern site elevated moisture is inferred to increase the ecosystem woody component, decreasing fuel loads by increase fuel moisture content and excluding fuel producing grasses. Fire activity response if more mixed at the central site (15°N – GeoB9508-5), fire activity decreases during wet and dry climate events. The proximal location of GeoB9508-5 to the Sahara-Sahel boundary captures inferred positional shifts in the latitude of this boundary in response to climatic forcing, by insolation and sea surface temperatures. The high sensitivity of this region to latitudinal shifts in rainfall is illustrated by clear millennial-scale variability in fire activity. I report here that temporal variability in fire activity over thousands of years largely seems to be driven by the same factors as modern spatial variability on the African continent.

4.2 Introduction

Fire has long been recognized as a major driver of ecological changes over both observational and geological time scales. Fire plays a role in both the global carbon cycle and the release and redistribution of nutrients. It also shapes ecosystems by favouring flammable grasses and grazing herbivores over trees and browsing herbivores (Archibald and Hempson, 2016). As a result, fire is largely responsible for the maintenance of wetter savanna biomes, which would transition into forest without regular disturbance (Accatino et al., 2010; Beckage et al., 2009; Bond et al., 2005; Sankaran et al., 2005). Fire also shapes ecosystems over geological timescales, for example, acting as a key positive feedback on the expansion of the C_4 savanna ecosystem since the Late Miocene (Beerling and Osborne, 2006; Cerling, 1992; Ehleringer et al., 1997; Osborne, 2008).

Ecosystem flammability is determined by a complex interplay of climatological and ecological factors, including herbivory (Archibald and Hempson, 2016), temperature (Pausas and Ribeiro, 2013), soil nutrient concentrations (Bond et al., 2005) and atmospheric carbon dioxide concentrations (Bond et al., 2003), but the balance between plant types is the key factor. The rapid regenerative capacity and high-water use efficiency of tropical grassy plants (which typically use the C_4 photosynthetic pathway) allows the generation of large amounts of highly flammable, low moisture-content fuels notably in Africa savanna systems (Figure 4.1) (Bond et al., 2003; Dupont et al., 2013; Sage, 2004). Fuels loads produced by woody plants (commonly C_3) are smaller, have a higher moisture content and ecosystems are typically less flammable (Ripley et al., 2010). Biomes dominated by C_4 grasses are therefore among the most flammable in the world. The presence of a small proportion (10–40%) of resin-rich trees in a grass-dominated savanna biome can enhance fire activity, because these trees are excellent converters of lightning strikes into successful ignitions (Beckage et al., 2009; D'Onofrio et al., 2018; Larrasoaña et al., 2013). Ultimately, the balance between grassy and woody plants is strongly affected by the amount and seasonality of precipitation, which also has a direct influence on the flammability of the biomass produced.

Modern fire activity maps (Figure 4.1) (Archibald et al., 2013; Bowman et al., 2009; Giglio et al., 2006; Pausas and Ribeiro, 2013; van der Werf et al., 2006) show that northern Africa is home to some of the highest fire activities in the world, with regions combining high temperatures (> 28 °C), intermediate annual rainfall (350–1100 mm) and prolonged dry periods (Aldersley et al., 2011). Africa is unusual in that the distribution of its biomes is rainfall- rather than temperature-dependent. The spatial extent and distribution of the biomes fall along latitudinal precipitation

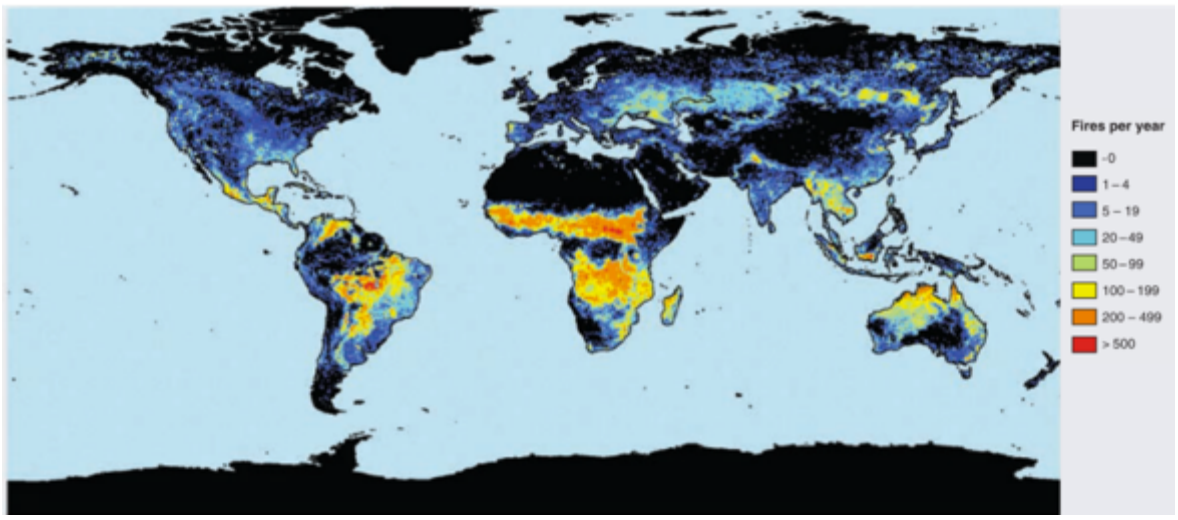

Figure 4.1: Global Fire Map. Annual average number of fires observed by satellite (taken from Bowman *et al.,* 2009, data from Giglio *et al.,* 2006).

gradients and are therefore highly sensitive to changes in the hydrological cycle (Figure 4.2) (Dupont, 1993; Dupont et al., 1989). Today, the highest fire activities occur in wet or woody savannas (woody plant coverage of between 10–40% (Larrasoaña et al., 2013)), which are currently located between about 15°N and 9°N (Figure 4.2) and thrive under intermediate precipitation regimes (500–2000 mm/yr Mean Annual Precipitation (MAP)) (Pausas and Ribeiro, 2013; Staver et al., 2011a). Fire activities decrease to the south where a semi-deciduous forest biome is dominant, and to the north where climatically maintained grassy or dry savannas with a woody plant component remaining below <10% dominate under low precipitation regimes (100–500 mm/yr MAP) (Figure 4.2) (Accatino et al., 2010; D'Onofrio et al., 2018; Larrasoaña et al., 2013; Ratnam et al., 2011; Sankaran et al., 2005).

Precipitation in northern Africa is strongly influenced by the position of the Intertropical Convergence Zone (ITCZ) (Dupont, 1993; Dupont and Hooghiemstra, 1989) (Figure 4.2). In addition to seasonal migrations between summer and winter latitudinal extremes (9°N–2°N) (Schneider et al., 2014), the position of the ITCZ over longer timescales is driven by both high and low latitude forcing mechanisms (Bouimetarhan et al., 2009; Collins et al., 2013, 2010; Dupont, 1993; Larrasoaña et al., 2013). Examples of both of these types of forcing occurred within the last 50 kyr. Increases in boreal summer insolation at low latitudes driven by variability in Earth's orbit of the Sun, particularly the precession of the equinoxes, induced more pronounced seasonal ITCZ migration to higher latitudes, bringing increased rainfall to much of northern Africa during African Humid Periods (AHPs) greening the Saharan desert (Rohling et al., 2002). In contrast, widespread cooling of sea surface temperatures in the North Atlantic Ocean associated with abundant iceberg carving at high

northern latitudes during Heinrich (H-) events resulted in a southward displacement of the ITCZ over northern Africa, resulting in a 1000 km southward shift in the boundary between the Saharan Desert and the Sahel (Heinrich, 1988; Hemming, 2004; Mulitza et al., 2008).

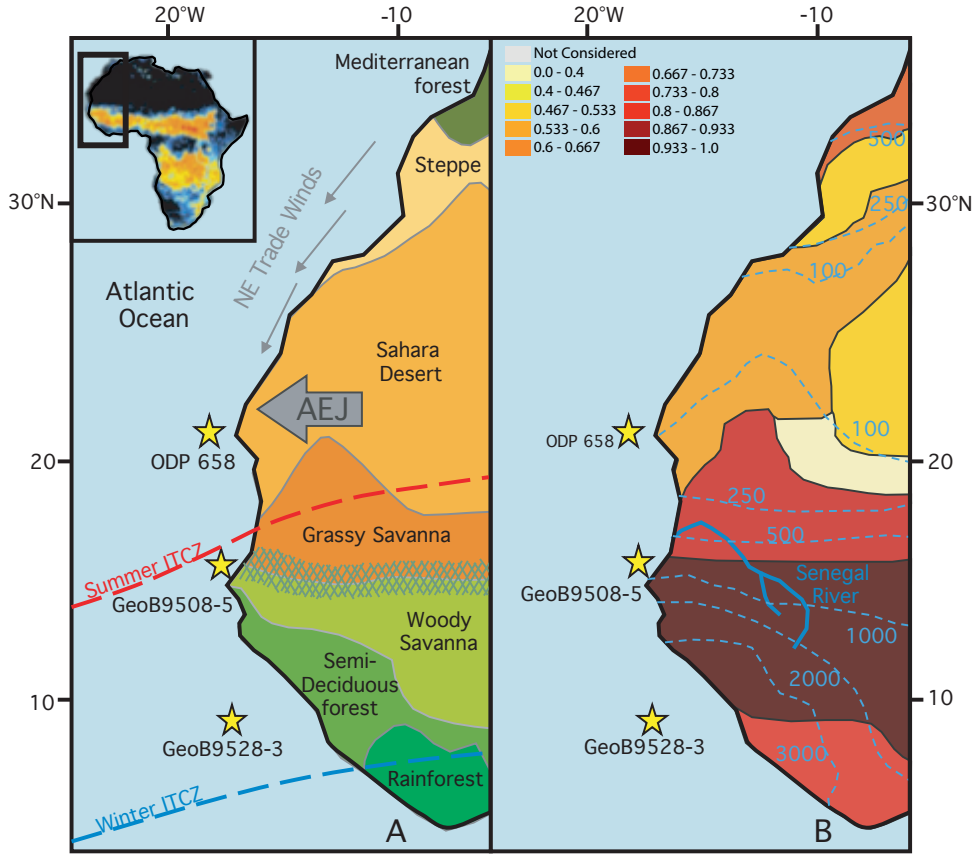

Figure 4.2: Location of transect sites. Schematic map of the major North African vegetation bands, the modern summer and winter latitudinal position of the ITCZ and the African Easterly Jet (AEJ). Location of the ocean drill sites ODP 658 at 21°N, GeoB9508-5 at 15°N and GeoB9528-3 at 9°N. Adapted from (Kuechler *et al.,* 2013). Inset Map: annual average number of fires observed by satellite, Black ~0, Dark Blue 1-4, Mid-Blue 5-19, Light Blue 20-49, Green 50-99, Yellow 100-199, Orange 200-499, Red >500 (Taken from Bowman *et al.,* 2009 data from Giglio *et al.,* 2006). B: Fire Activity Map (adapted from Pausas and Ribeiro, 2013), overlain by present day precipitation mean annual precipitation contours after Larrasoaña *et al.,* (2013).

To understand how fire activity responded to such pronounced changes in northern African rainfall climate, I studied charcoal flux over the past 50 kyr to three marine sediment cores at sites located on a latitudinal transect along the north west African margin (NWAM). I studied marine archives because of their proven potential (Bird and Cali, 1998; Daniau et al., 2007; Dupont and Schefuß, 2018; Herring, 1985; Hoetzel et al., 2013; Verardo and Ruddiman, 1996) to yield continuous largely

undisturbed sequences of exported terrestrial material with excellent age control, allowing for the examination of long, regionally integrated reconstructions of past fire activity on land.

4.3 Results and Discussion

Variations in past fire activity are recorded by the relative changes in charcoal flux to the sediments, with periods of high fire activity denoted by the greatest charcoal fluxes. Examination of multiple records of charcoal flux along the NWAM at 21°N (Ocean Drilling Program (ODP) Site 658, 15°N (GeoB9508-5, hereafter, GB-08) and 9°N (GeoB9528-3 hereafter, GB-28) reveal strong latitudinal variability in fire activity in their response to both orbital and millennial-scale climatic events incorporating conditions both more arid and more humid than today (Figure 4.3).

4.3.1 The Last Glacial Period

Northern Africa was largely arid during the last glacial period (Gasse, 2000) with high dust fluxes, attributed to both aridity and high wind speeds, reconstructed at all three of my study sites (Figure 4.3) (Collins et al., 2013; McGee et al., 2010; Straub et al., 2013). However, the response of fire activity to this cross-latitudinal aridity differs markedly between the three sites.

The two most northerly sites, ODP 658 and GB-08 both record low glacial fire activities, with an overall decrease in charcoal flux as glacial conditions intensified towards the Last Glacial Maximum (LGM) ~20 kyr ago, charcoal fluxes are at ODP 658 are at a minimum or are close to minimum values at GB-08 acived during the LGM itself (Figure 4.3). I attribute this reduction in fire activity to a decrease in the amount of fuel available to burn at the two higher latitude sites during intervals of peak aridity. Reconstructions suggest that the Saharan Desert expanded southwards to 12°N, displacing the grassy savanna (Collins et al., 2013; Dupont, 2011; Hoogakker et al., 2016) and resulting in a reduction in total vegetation biomass. Climate may also have had a direct influence over fire activity, with cold winters and dry summers invoked to explain the low LGM fire activities recorded further north in Morocco, which lead to a reduction in terrestrial biomass and therefore fuel loads (Reddad et al., 2013; Tabel et al., 2016). The Holocene profiles for two northern sites however diverge. A slight increase in fire activity is recorded at ODP 658 from the deglacial into the present, whilst at GB-08 the fire activity profile remains stable recording minima values.

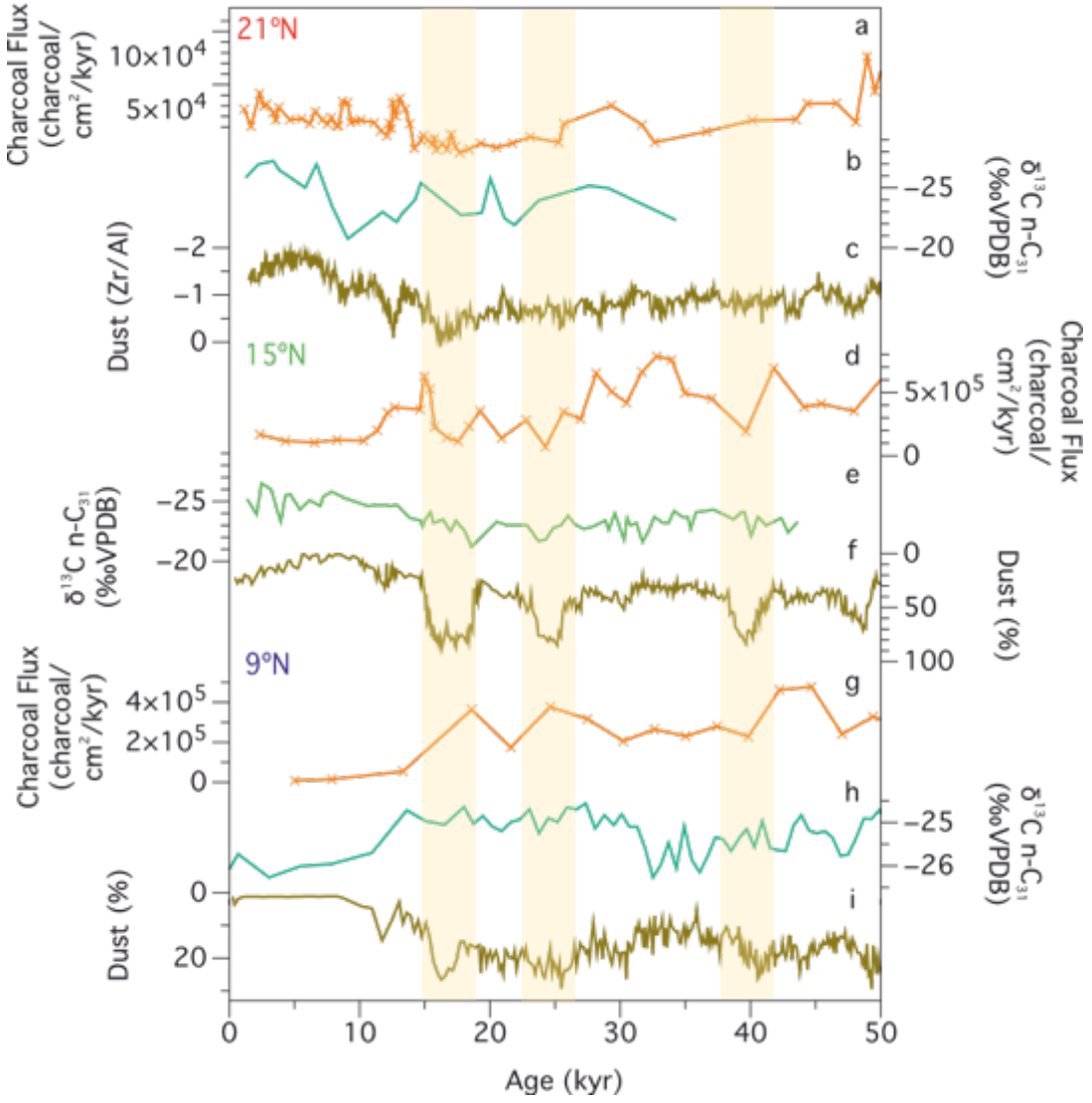

Figure 4.3: Northwest African Margin Transect. Comparison of Transect of sites along the Northwest Africa. Sites at 21°N ODP 658 records shown in red, 15°N GeoB9508-5 and 9°N records shown in green, GeoB9529-3 records shown in blue. a) Charcoal Flux at ODP 658 (This study), b) δ^{13}C n-C_{31} at ODP 658 (Zhao et al., 2003), c) Dust (Zr/Al) at ODP 658 (Meckler et al., 2013), d) Charcoal flux at GeoB9508-5 (This Study), e) δ^{13}C n-C_{31} at GeoB9508-5 (Neidermeyer et al., 2010), f) Dust Flux at GeoB9508-5 (Collins et al., 2013) g) Charcoal Flux at GeoB9528-3 (This Study), h) δ^{13}C n-C_{31} at GeoB9528-3 (Castañedana et al., 2009), i) Dust flux at GeoB9528-3 (Collins et al., 2013). Yellow bars are Heinrich Events.

Site GB-28, however, shows very different behaviour to that seen at the two more northerly sites, with charcoal fluxes between 50 ka and 18 ka much higher than the Holocene fluxes. Similarly high fire activities under glacial conditions are also recorded at equatorial sites RC27-04 (Verardo and Ruddiman, 1996) and Lake Challa, where C_4 grasses thrived (Nelson et al., 2012). Elevated glacial

fire activity compared to Holocene values contrasts, however, with decreased fire activity documented across much of the globe during the LGM (Daniau et al., 2010; Marlon et al., 2016; Power et al., 2008). Pollen data indicates that the climate on the continent close to GB-28 was more humid than my other two study sites, with a mixture of savanna and forest (Dupont, 2011). A decrease in precipitation associated with the descent into the glacial promoted a southward expansion of the flammable savanna and open woodland, at the expense of the less flammable rainforest (Dupont and Agwu, 1992; Jahns et al., 1998).

It is worth discussing the impact of lower pCO_2 on fire activity. Even during glacial periods when global carbon dioxide levels are low, pCO_2 declines to 180 ppm which is only 100 ppm lower than that of 290 ppm pCO_2 recorded for interglacials (Lüthi et al., 2008). This is not low enough to supress plant primary productivity so far as to produce a period of no burning due to lack of fuel. Plants using the C_4 PHP are at an advantage under low pCO_2 (<500 ppm) which arguably suggests that an increase in fuel production is possible under these conditions supporting increased fire activity. The lower global may impact on C_3 plants, by slowing growth rates, however there is no evidence that growth was completely halted in fact C_3 plants are clearly present in pollen records spanning the period, at the southern end of the study transect (Dupont. 2011).

4.3.2 Heinrich Events

During the last glacial interval, the climate of northern Africa was punctuated by a number of periods of extreme drought (Collins et al., 2013; Mulitza et al., 2008; Tjallingii et al., 2008) associated with cooling of the North Atlantic Ocean during H-events resulting in a strengthening of the African Easterly Jet (AEJ), reducing precipitation in West Africa (Mulitza et al., 2008; Niedermeyer et al., 2009). The Sahara-Sahel boundary shifted southwards by *ca.* 3-4° from its "background" glacial position (Mulitza et al., 2008), a much greater shift than the estimated global mean southward displacement of the ITCZ position (~0.6°) (McGee et al., 2014).

At my mid-transect site GB-08 (~15 °N), charcoal fluxes drop by a factor of at least two in-step with four pronounced aridification events marked by increased dust inputs during Heinrich Events H1–4 (Figure 4.3). Yet corresponding minima in charcoal flux are inconsistent and/or indistinct at either end of my transect (at 21°N and 9°N respectively) (Figure 4.3). At the northern end of the transect, only H1 is clearly expressed in the dust % record, but the corresponding signal in the charcoal flux

record is small. H-events are only weakly expressed in dust % at GB-28, and I find no conclusive evidence for a major response in fire activity.

I attribute the contrasting sensitivity of the three sites to hydroclimate and fire regime to their positions relative to the boundary between desert and grassland. Reconstructions suggest the Sahara-Sahel boundary shifted southwards from ~16°N to ~13°N during H-events (Collins et al., 2013; Mulitza et al., 2008), with sand dunes identified as far south as 14°N (Collins et al., 2013). Site GB-08 at 15°N would therefore be greatly influenced by the shift from flammable grassland to fuel-limited desert that occurred during H-events. Sites ODP 658 and GB-28 at 21°N and 9°N respectively are a long way from this major vegetation boundary shift and hence any ecosystem changes are likely to be more limited. Vegetation coverage is minimal at 21°N, with desert at this latitude today and even greater aridity reconstructed during the LGM, therefore further intensification of the arid baseline state would not have caused major ecosystem shifts or significant change in dust production. In this interpretation, the comparative insensitivity to H-event climate forcing in the fire regime at the southern end of my transect (GB-28) is explained by the lack of a strong influence over either the proportion of C_4 plants (Castaneda et al., 2009) or the fire activity exerted by the expansion of grassland at the expense of tropical forests, indicating a lack of drying able to drive an increase in dust production (Handiani et al., 2013)(Figure 4.3).

4.3.3 African Humid Period 1 (AHP1)

During the early Holocene, northern Africa was much wetter than the present day and was well vegetated with abundant lakes and rivers (Armitage et al., 2015; Damnati, 2000; Gasse, 2000; Jennings et al., 2015; Larrasoaña et al., 2003; Pausata et al., 2016; Rachmayani et al., 2015; Skonieczny et al., 2015; Tierney et al., 2017b; Wang et al., 2008) as a result of a northward shift in the position of the major rainbelt at a time of increased solar insolation (Laskar et al., 2004). This period is known as the African Humid Period 1 (AHP1) and the contemporaneous rainfall increase drove a greening of the Sahara (Claussen and Gayler, 1997; DeMenocal et al., 2000; Hély et al., 2014; Ritchie et al., 1985), documented by vegetation reconstructions, fossil evidence and human rock art and engraving in the central Sahara (Barnett, 2002; di Lernia and Gallinaro, 2010; Dumont, 2017; Gallinaro, 2013). Pollen reconstructions suggest that the vegetation assemblage that developed between 19–29°N was unlike anything found today, with coexisting savanna and tropical taxa (Hély et al., 2014; Lézine, 2009; Watrin et al., 2009).

All three of my studied sites cover this interval of humidity in the early Holocene, indicated in the marine realm by reduced dust fluxes and pollen records (Dupont, 2011; Meckler et al., 2013; Tjallingii et al., 2008)(Figure 4.3), however, the associated response in fire activity is strongly divergent between sites. AHP1 is associated with low fire activity in both my southern (where the decline is most precipitous) and mid-transect sites while at the northern end of the transect I see increased fire activity compared to the preceding glacial. I attribute this pattern in fire activity to differing ecosystems response to rainfall climate forcing. At the lower latitude sites, I infer that increased precipitation suppressed fire activity due to a combination of factors including promotion of the growth of more fire resistant vegetation and/or reduced desiccation of biomass (Beckage et al., 2009; Bistinas et al., 2014; Ratnam et al., 2011; Sankaran et al., 2005), while at higher latitudes, a more humid climate permitted the expansion of flammable plant material into previously desert regions, as reconstructed from palynological elements (Larrasoaña, Roberts and Rohling, 2013 and references therein). It should be noted here it is impossible therefore to avoid a degree of circularity when using palaeoprecipitation estimates to reconstruct floral assemblage. The generation of palaeoprecipitation estimates often incorporates pollen and plant wax proxy records amongst other precipitation proxies including rainfall records extracted from speleotherms, lake level records and sedimentary sequences to inform the model parameters.

Reconstructed rainfall values, were determined using vegetation and physiographic elements (Larrasoaña, Roberts and Rohling, 2013 and references therein), at 15°N during AHP1 are ~500-1000 mm/yr MAP (Larrasoaña et al., 2013), close to the threshold at which fire activity becomes suppressed in modern day Africa (Archibald et al., 2009; Hély et al., 2014; Sankaran et al., 2005; Staver et al., 2011b, 2011a). This threshold typically occurs at a woody canopy cover of *ca.* 40%, as determined by modern remote sensing studies, above which fuel-producing grasses are excluded (Archibald et al., 2009; Archibald and Hempson, 2016; Bond et al., 2005). Increased woody cover during AHP1 is evidenced as far north as 20°N by floral reconstructions using pollen records (Hély et al., 2014; Larrasoaña et al., 2013; Lézine, 2009; Watrin et al., 2009). Both of my two most southerly study sites show a more negative δ^{13}C plant wax values indicative of a higher proportion of C_3 plants within the floral assemblage, supporting an increase in the proportion of woody C_3 plants during the early Holocene (Castaneda et al., 2009; Niedermeyer et al., 2010)(Figure 4.3). A dominance of evergreen broadleaf trees during AHP1 is also suggested by vegetation model reconstructions, indicating a high woody cover without a significant grass fraction at latitudes <14°N (Lu et al., 2018), a result suggestive of small fuel loads with a high moisture-content. This interpretation is consistent with palaeo-precipitation estimates of >2000 mm/yr MAP (Larrasoaña et al., 2013; Tierney et al., 2017a; Wang et al., 2014), which lie above the threshold for near-outright

fire suppression observed in modern environments (Accatino et al., 2010; Lasslop et al., 2018; Staver et al., 2011b; Stott, 2000). Thus, I attribute decreased charcoal fluxes during AHP1 between at least 15°N and 9°N to rainfall amounts that exceed the than optimum for ecosystems flammability, or a "too-wet to burn" scenario.

Northward expansion of the northernmost limit of the ITCZ and hence also the savanna grasslands during AHP1 shifted the Sahara-Sahel boundary position to ~20°N (Collins et al., 2013). This is very close to the latitude of ODP 658 where increased precipitation promoted desert greening with increased proportions of *Cyperaceae* and *Poaceae* pollen evidencing a northward migration of a diverse woody savanna biome into the desert region (Dupont, 2011; Dupont and Schefuß, 2018). I therefore infer precipitation-led increased fuel loads for burning in a fuel-limited environment (Claussen and Gayler, 1997; DeMenocal et al., 2000; Hély et al., 2014; Ritchie et al., 1985) to explain increased charcoal flux at the northern end of my transect including C_4 grasses (as evidenced by plant wax $\delta^{13}C$ signatures (ratio of C^{13} to C^{12} contained within the plant waxes)) (Kuechler et al., 2013; Zhao et al., 2000)(Figure 4.3).

4.3.4 "Goldilocks" fire activity

Each of my three studied sites along a latitudinal transect of the northwestern African coast shows a different relationship between aridification and fire activity. I attribute this result to a strongly inflected relationship between fire activity and rainfall climate whereby burning is greatest at intermediate humidity levels. Such a relationship is observed in modern ecosystems, where peak fire activity is documented at precipitation levels of 1000–2000 mm/yr MAP (Archibald and Hempson, 2016; Pausas and Ribeiro, 2013; Van Der Werf et al., 2008) (Figure 4.3), with decreasing fire activity where rainfall either increases or decreases outside this range (Pausas and Ribeiro, 2013) (Figure 4.2). My results signal the first evidence of such a relationship from the palaeo-record over multi-millennial timescales, and that this relationship holds across boundary conditions.

At my southernmost site (Figure 4.3), I report low fire activity at times when low dust fluxes indicate a more humid climate, and high fire activities at times of aridity. This positive correlation between fire activity and aridity has also been observed over a range of timescales at other near-equatorial localities such as the Niger Delta (Morley and Richards, 1993), Tropical Atlantic (Daniau et al., 2013; Verardo and Ruddiman, 1996), Uganda (Colombaroli et al., 2014), Mount Kenya (Rucina et al., 2009)

and northeast Nigeria, where fire activity is greatest at times of low water levels (Waller et al., 2007). Very high fire activities are found around 9°N today (Figure 4.2)(Archibald et al., 2013; Pausas and Ribeiro, 2013)), where a mixture of tropical grasslands, shrublands and broadleaf forests are found today (Olson et al., 2001). Modern precipitation values vary from approximately 1000 mm/yr (inland) to >2500mm/yr (coastal regions), spanning the range associated with a peak burned fraction of vegetation to an environment with very limited burning (Archibald and Hempson, 2016). I therefore suggest that fire activity become suppressed inland during AHP1 and Eemian if rainfall exceeded modern levels where outright suppression is observed (>2000 mm/yr)(Accatino et al., 2010; Larrasoaña et al., 2013; Lasslop et al., 2018; Staver et al., 2011b; Stott, 2000). Increased precipitation supported a higher proportion of C_3 woody plants, as observed in both the pollen and δ^{13}C n-alkane records (Castaneda et al., 2009; Dupont, 2011; Kuechler et al., 2013). During drier intervals, such as the LGM, fire activity increased at GB-28. This suggests that conditions at ~9°N were not dry enough at any point during the last 50 kyr to transition to a fuel-limited environment.

ODP 658, my northernmost site, exhibits the opposite relationship between fire activity and precipitation to GB-28, with increased charcoal fluxes occurring at times of relative humidity and very low charcoal fluxes when the climate is arid. Decreasing fire activity with increasing aridity is recorded in arid/semi-arid regions of Africa over a range of timescales, including southern Algeria (Lécuyer et al., 2016), Mali (Neumann et al., 2009), Morocco (Reddad et al., 2013; Tabel et al., 2016), Lake Malawi (Cohen et al., 2007) and southern Africa (Daniau et al., 2013). In these environments, broadly speaking, increased precipitation promotes an increase in total biomass, resulting in a larger potential fuel source and increasing fire activity (Van Der Werf et al., 2008). ODP 658 lies just to the north of the modern Sahara-Sahel boundary, with minimal vegetation occurring in the desert to the north transitioning to grassland and savanna further south where precipitation exceeds *ca.* 200 mm/yr MAP. During times when precipitation increased above modern levels, such as the AHP1, vegetation reconstructions and modelling results indicate a northward expansion of the highly flammable grassy savanna biome (Dupont, 2011; Hoogakker et al., 2016; Jolly et al., 1998; Larrasoaña et al., 2013), and increased charcoal fluxes are recorded. In contrast, when precipitation decreased below current levels, such as during the LGM, much of northern Africa became a highly inhospitable as the Sahara Desert expanded.

GB-08, the mid-transect site, exhibits the most striking relationship between precipitation and fire activity. Here, charcoal fluxes are low both during the wettest (AHP1) and driest (H1–4) intervals of the last 50 kyr. Given the proximity of this site to the latitude of the modern grassy savanna-

woody savanna boundary (where fire activity is extremely high today (Figure 4.2), my records suggest that even small changes in precipitation outside the optimum rainfall window for fire activity of approx. 800–1400mm/yr MAP (Archibald and Hempson, 2016; Van Der Werf et al., 2008) promote major variations in the floral assemblage and burning. Major shifts in the latitude of the Sahara-Sahel boundary are identified through my studied interval, both to north and to south (Figure 4.4)(Collins et al., 2013). During times of high humidity, pollen records indicate an increase in less flammable sedges concordant with a shift towards more negative *n*-alkane values indicative of an increase in C_3 plants (Dupont, 2011; Niedermeyer et al., 2010) which typically produce more moisture-rich fuels (Dupont, 2011; Niedermeyer et al., 2010; Ripley et al., 2010). Palaeoprecipitation reconstructions estimate MAP values of *ca.* 1000 mm/yr MAP at 15°N during AHP1 (Larrasoaña, Roberts and Rohling, 2013), close to values at which modern fire activities start to decrease with increased precipitation as the system becomes limited by humidity rather than fuel availability (Archibald and Hempson, 2016; Van Der Werf et al., 2008). A similar scenario is recorded in Late Naivasha, in currently fuel-limited semi-arid Kenya, where marked variation in forest and woodland plants versus *Poaceae* over the past 1200 years indicates fire suppression when climates became sub-humid (Colombaroli et al., 2014). However, sites exhibiting this "Goldilocks" behaviour between precipitation and fire activity are very rare, and this behaviour has not previously been documented over millennial timescales on Africa.

4.4 Conclusions

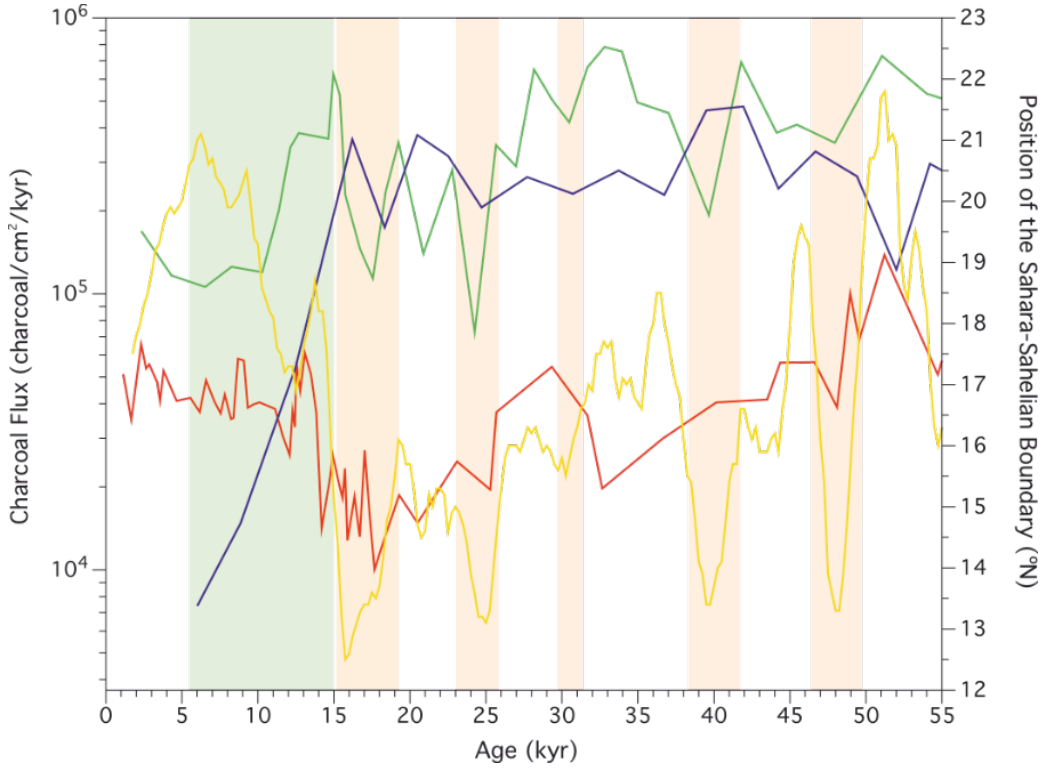

Figure 4.4: Relationship between the location of the Sahara-Grassy Savanna Boundary and Charcoal Flux. Sahara-Sahel Boundary reconstruction (Collins *et al.,* 2013). ODP 658 shown in Red, GB-08 shown in Green and GB-28 shown in Blue. Green Bar AHP1, orange bars Heinrich Events.

I report clear latitudinal variability in the response of fire activity to hydroclimatic shifts through the last 50 kyr along the NWAM. At my most northerly site (ODP 658, 21°N), fire activity is highest during more humid conditions, such as AHP1, while the most southerly site (GB-28, 9°N) has the opposite response, with peak burning at times of aridity (e.g. the last glacial period). I attribute these drastically different responses in fire activity at the two sites to very different biomes. At ODP 658, increased precipitation allows the expansion of flammable grassy savanna into desert regions, potentially with lower percentages (10-40%) of woody cover acting to increase ignition likelihood if precipitation levels were high enough, as observed at the end of AHP1 when ~1000 mm/yr MAP supported an increase in C_3 vegetation (Kuechler et al., 2013; Larrasoaña et al., 2013; Niedermeyer et al., 2010; Wang et al., 2006). In contrast, increased precipitation at GB-28 likely increased the proportion of woody plants to high values at the expense of more flammable grass biomass, as well as increasing the moisture content of the fuel, hence suppressing fire activity. The intermediate latitude site (GB-08, 15°N) exhibits reduced charcoal fluxes during both the wettest (e.g. AHP1) and driest (e.g. H1–4) intervals, with maximal fire activity occurring at moderate humidity levels. GB-08

is located close to the Sahara-Sahel boundary, which reconstructions suggest shifted both north and south of the site over the last 50 kyr, resulting in major biome shifts as a response to forcing both by insolation and sea surface temperatures. The high sensitivity of this region to latitudinal shifts in rainfall is illustrated by clear millennial-scale variability in fire activity. I therefore find that temporal variability in fire activity over thousands of years largely seems to be driven by the same factors as modern spatial variability on the African continent.

4.4.1 Materials

ODP 658 was drilled at 20°44.95'N, 18°34.85'W ~150km offshore Mauritania on the Mauritanian Margin at a water depth of ~2300m beneath a high productivity upwelling zone. This site was selected to capture fire activity variability in response to changes at the Sahara Desert – grassy savanna boundary.

GeoB9508-5 was drilled ~160km offshore Senegal 15°29.90'N, 17°56.88'W at a water depth of 2384m. This was specifically chosen to capture shifts in the position or the grassy savanna – woody savanna boundary and therefore fire activity.

GeoB9528-3 was drilled on the Guinian Plateau Margin at a water depth of 3057m ~350km offshore Guinea. This site was selected to be sensitive to changes at the woody savanna – semi-deciduous forest boundary.

4.4.2 Methods

4.4.2.1 Processing

Charcoal here is defined as any carbon-rich terrestrially derived material produced by either natural (lightning strikes) or anthropogenic mechanism (Bird and Ascough, 2012; Keeley and Rundel, 2005). The magnitude of charcoal production is a direct indicator of fire activity, larger charcoal flux reflects increased fire activity.

Standard palynological methods (after Harding *et al.*, 2011) was modified to avoid charcoal fragmentation by removing physical agitation stages to produce slides for charcoal counts. Oven dried bulk sediment was treated with HCl and HF to remove carbonate and silicate material respectively. A combination of boiling HCl, ultrasonic treatment and sieving at 15 μm was used to remove fluoride compounds and Amorphous Organic Material (AOM) from the sample.

Mounts of the >15 μm fraction spiked with a known dose of exotic *Lycopodium* (Stockmarr, 1971) were examined under transmitted light. Optical charcoal identification was achieved using an Olympus BH-2 microscopic in conjunction with a freestanding lamp using shape, colour and reflectance characteristics.

Concurrent counting of charcoal particles and *Lycopodium* spores until 500 spores were reached. Charcoal identification occurred if particle was completely black and fitted into one of the following morphological categories; elongate, splintery perforated, splintery unperforated, irregular perforated or square/rectangular. High top light and low bottom light was used to separate charcoal particles from pyrite on the basis on reflectance level, non or faintly reflectively particles were classified as charcoal whilst highly reflectively particles were classified as pyrite. The charcoal particle to *Lycopodium* spore ratio was used to calculate charcoal concentrations.

Due to the difficulties in exactly reproducing the counts due to heterogeneities between sample mounts and material distribution across the palynological slide a reproducibility error of 12.% is given to these counts (full testing methodology to determine these errors are detailed in Chapter 2 section 2.2.4.1). However, for identifying changes in fire activity the overall trends in the data are more instructive than the exact numbers, caution must be applied not to over interpret the data as any variability <12.5 should not be considered to be driven by natural forcing mechanisms.

4.4.2.2 Chronology

Data from ODP 658 is presented on a modified version of Meckler *et al.*, (2013) published age-depth model, which was produced by tuning $\delta^{18}O_{benthic}$ data from Site 658 on a revised composite depth scale to the LR04 stack (Lisiecki and Raymo, 2005) using AnalySeries software package (Palliard *et al*., 1996). The last 120 kyr, age was refined by 1) matching XRF-derived Ca from Hole 658A

to %$CaCO_3$ in radiocarbon-dated Hole 658C (deMenocal et al., 2000) and 2) tuning ln(Zr/Al) data from ODP 658 (a proxy for grain size) to the grain size-based humidity index from nearby core GeoB7920-2 (Meckler et al., 2013; Tjallingii et al., 2008).

An age model was generated from the published age-depth tie points of (Niedermeyer et al., 2010) for GeoB9508-5 for full details see section Chapter 2 Section 2.2.1. In brief this age model based on C^{14} dates and $\delta^{18}O_{benthic}$ and correlated to core MD95-2042 (Niedermeyer *et al.*, 2010 and references therein).

The age-depth tie points of Schreuder *et al.*, (2019) was used to generate the age model for GeoB9528-3, for full detailed refer to Chapter 3 section Chapter 2 Section 2.2.1. In brief, the $\delta^{18}O_{benthic}$ was correlated Deep North Atlantic and global benthic oxygen stacks (Lisiecki and Raymo, 2005; Lisiecki and Stern, 2016), down core uncertainty was modelled using the R script BACON (Schreuder *et al.*, 2019 and references therein).

4.5 Supplementary Material

Increased river drainage either from ephemeral rivers on the North West African Margin near 21°N (Skonieczny et al., 2015) and the sustained activity of the Senegal River proximal to 15°N presents a potential riverine transport of charcoal mechanism. The lack of alignment between peaks in riverine sediment flux and elevated charcoal flux, however is not indicative of major riverine transport mechanism to either site (Collins et al., 2013; Niedermeyer et al., 2009; Tjallingii et al., 2008). Transport to the study sites is therefore dominated by aeolian processes. Thermal buoyancy generated during fires lofts microscopic charcoal (<1mm) into the air (Clark, 1988; Crawford and Belcher, 2014; Masiello, 2004; Scott and Damblon, 2010; Verardo, 1997), transported westwards along with terrigenous material including dust and plants waxes (n-alkanes) by the African Easterly Jet (Kuechler et al., 2013; Tjallingii et al., 2008; Vallé et al., 2014). The AEJ transports its entrained material westwards across the Atlantic Ocean from consistent source locations across the Last Glacial Maximum (LGM), despite latitudinal shifts in the position of the vegetation bands (Castaneda et al., 2009; Harrison et al., 2001; Hooghiemstra et al., 2006).

Trajectories generated by back modelling studies suggest similar source regions for the sites at 21°N and 15°N (ODP 658 and GeoB9508-5)(Schefuß et al., 2003), however the dissimilarity in charcoal flux trends and the magnitude of the charcoal fluxes between the sites argues against this scenario. A source location of 15°N is implied by back modelling studies for the site at 9°N however, the lack of similarity between the charcoal flux trends for GeoB9508-5 at 15°N and GeoB9528-3 at 9°N is again not indicative of similar source region. Separate source regions are further indicated by core top samples for the site at 9°N (GeoB9528-3) suggestive of a source region between 12-9°N, which is consistent with n-alkane record (Castaneda et al., 2009).

An absence of a relationship between organic carbon and the calculated charcoal concentration at my site at 21°N argues against the low charcoal flux values resulting from a preservation control. The observed changes in the charcoal flux record seen at all of my sites is therefore attributed to natural variability in fire activity.

Chapter 5 A strong, non-linear relationship between fire activity and hydroclimate in northern Africa over the last glacial cycle

Supporting Authors: Anya Crocker[1], Paul A Wilson[1], David Beerling[2], Colin Osborne[2]and Nele Meckler[3]

[1]University of Southampton - National Oceanography Centre, Waterfront Campus, European Way, Southampton, United Kingdom. SO14 F5D

[2]University of Sheffield - Department of Animal and Plant Sciences, Alfred Denny Building, Western Bank, Sheffield, United Kingdom. S10 2TN

[3]University of Bergen – Department of Earth Science, Postboks 7803, 5020 Bergen

5.1 Abstract

Fire is a major driver of ecological and evolutionary change but detailed records of fire activity variability over geological timescales are scarce. I studied changes in fire activity over the last glacial cycle in the Northern African Savanna (NAS), the most frequently burnt ecosystem on Earth. I present a new record of charcoal accumulation rates in deep sea sediments from the North African margin at Ocean Drilling Program Site (ODP) 658. My record shows a distinctive pattern of change over the last 150 kyr, with multiple high amplitude peaks that correspond remarkably well, especially between 40 and 140 ka, to the African Humid Periods (AHPs) of increased rainfall over northern Africa, implying a strong link between fire activity and insolation-driven changes in northern African hydroclimate. The sign of this relationship is consistent with modern Earth Observation for Africa (Archibald and Hempson, 2016). Fires require fuel to burn and, over the last 150 kyr, there were major expansions of vegetation over northern Africa in response to orbitally paced insolation maxima that drove poleward migration of the Intertropical Convergence Zone (ITCZ) during boreal summers, bringing increased precipitation to northern Africa. In detail, however, my data suggest an inflected relationship between rainfall climate and fire activity: increasing rainfall promotes increasing fire activity only up to a point. The very wettest intervals in northern Africa over the last glacial cycle (AHPs -5 and -1) show modest peaks in fire activity compared to AHPs -3 and -4, the cause of which requires further exploration. Fire activity also shows a clear response to millennial-scale variability in hydroclimate during the last deglaciation,

although the variability is more muted at my study site than that driven by precessional forcing, especially during hyper-arid events superimposed on dry baseline glacial conditions (H1).

5.2 Introduction

Fire has been a major driver of ecological change since the Silurian (Glasspool et al., 2004). Tropical ecosystems that experience frequent fires become progressively more predisposed to burning because fire feedbacks selectively promote the growth of more flammable, fire-adapted, and often C_4, arid-adapted plant species (Beerling and Osborne, 2006; Bobe, 2006; Furley et al., 2008; Hoetzel et al., 2013; Keeley and Rundel, 2005). A notable example of fire driven-ecological change is suggested to have occurred in the Late Miocene when it is hypothesized that enhanced fire activity contributed to a decrease in C_3 woodland cover and the expansion of C_4 grasslands (Bond et al., 2005; Furley et al., 2008; Hoetzel et al., 2013; Keeley and Rundel, 2005; Osborne and Beerling, 2006). Located between the hyper-arid Sahara Desert to the north and the more humid C_3 woodland environments to the south, the resulting C_4 grassland-dominated Northern African Savanna (NAS) is the most frequently burnt ecosystem on Earth today (Cincotta et al., 2000; De Rouw, 2004; Oweis and Hachum, 2006) (Figure 5.1). Naturally occurring fires ignited by lightning strikes are commonplace and preserve the open high-light C_4 tropical grassland environments that characterise the savanna, preventing C_3 forest encroachment by removing dead material and killing saplings (Beerling and Osborne, 2006; Bobe, 2006; Furley et al., 2008; Hoetzel et al., 2013; Keeley and Rundel, 2005; Osborne and Beerling, 2006). Anthropogenic burning of the NAS is also common, where fire is employed as a management system to maintain or produce areas of agricultural land in a region where a large human population relies on subsistence farming and pastoralism (Cincotta et al., 2000; Laris and Wardell, 2006; Vierich and Stoop, 1990).

On inter-annual timescales, the fire reoccurrence interval in the African savanna is rapid at one to five years, supported by the fast regeneration of the grasslands (Bond et al., 2005; Keeley and Rundel, 2005). Annually, burning in the NAS is strongly linked to rainfall climate. Burning begins in the northern fringes of the savanna (17°N) early during the dry season (October-November) following a short “drying out” period or “climatic curing” and progresses southwards as the dry season advances (Carmona-Moreno et al., 2005; Cooke et al., 1996; Harrison and Sanchez Goñi, 2010; Stott, 2000). Yet, while the NAS is prone to extreme rainfall climate variability on human to geological timescales (Mulitza et al., 2008; Giannini et al., 2003; Tiedemann et al., 1994; Larrasoaña

et al., 2003; Nikolova et al., 2013; Sjolte and Hoffmann, 2014), little is known about the pattern of past fire activity in the region, even for the Last Glacial Cycle (LGC).

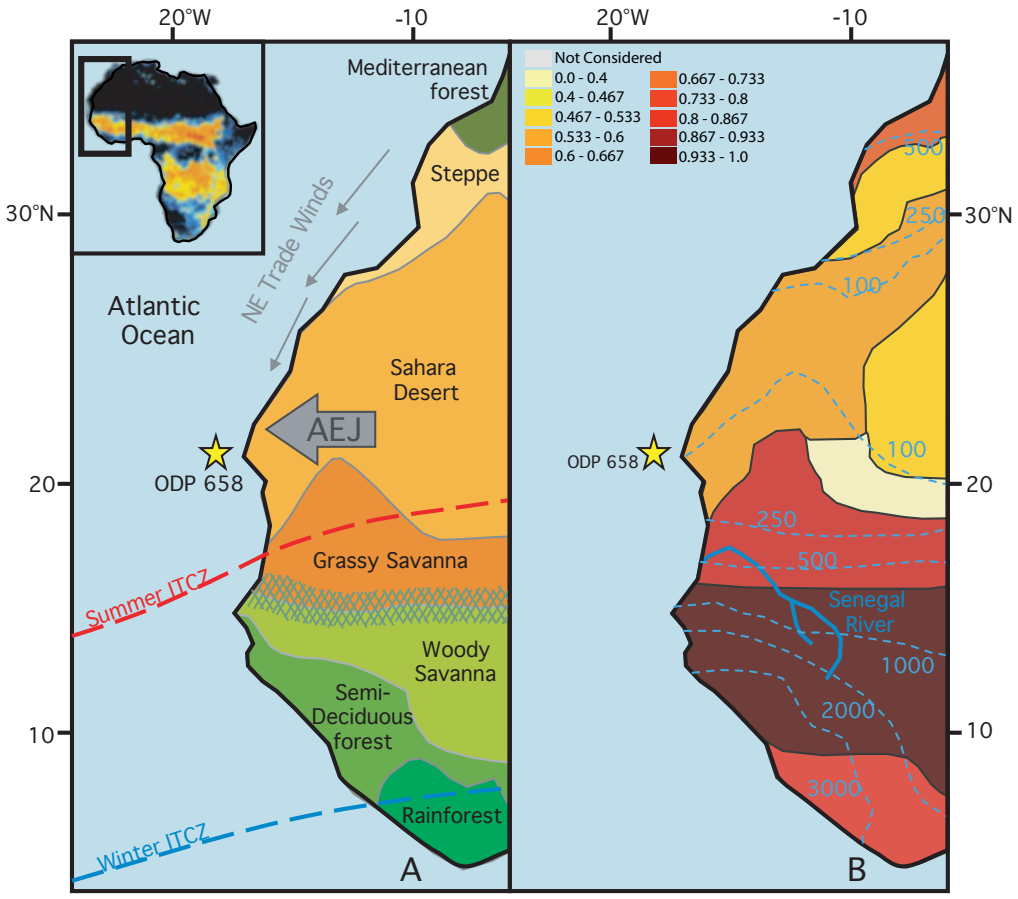

Figure 5.1: Site Map for ODP 658. Schematic map of the major North African vegetation bands, the modern summer and winter latitudinal position of the ITCZ and the African Easterly Jet (AEJ). Location of the ocean drill sites ODP 658 at 21°N, GeoB7920-2 is a re-drill of ODP 658. Inset Map: Fire Map annual average number of fires observed by satellite, Black ~0, Dark Blue 1-4, Mid-Blue 5-19, Light Blue 20-49, Green 50-99, Yellow 100-199, Orange 200-499, Red >500 (Taken from Bowman *et al.,* 2009 data from Giglio *et al.,* 2006). B: Fire Activity Map (adapted from Pausas and Ribeiro, 2013), overlain by present day precipitation mean annual precipitation contours after Larrasoaña *et al.,* (2013).

Here, I report the results of an investigation into fire activity variability in northern Africa associated with the pronounced shifts in regional hydroclimate during the Last Glacial Cycle (LGC, 0–150 ka). Typically, records of past burning are generated using terrestrial or lacustrine archives. I take a different approach, using marine sediments collected from the Northwest African margin (NWAM)

from Ocean Drilling Program (ODP) Site 658 to generate a record of the flux of charcoal exported from the continent through the LGC. My approach exploits longer, more continuous archives that benefit from tighter age control than those typically available on land. I compare my new charcoal records with terrestrial and marine proxy records to better understand the role of fire in the Earth system. I report strong variability in fire activity associated with changes in hydroclimate across northern Africa driven by changes in the latitudinal extent of seasonal migration of the Intertropical Convergence Zone (ITCZ) in response to low-latitude insolation forcing paced by the precession of Earth's axis of rotation. Changes in fire activity at the millennial-scale arising from the response of northern African hydroclimate to high latitude climate forcing are less pronounced at my site. My results indicate that, over these geological timescales, the influence of rainfall climate on vegetation is the main control on fire activity.

5.2.1 ODP Site 658: location and potential as a climate archive

ODP site 658 was drilled on the continental slope ~150 km offshore Mauritania in the tropical North Atlantic Ocean (20°44.95'N 18°34.85'W, water depth 2300 m)(Figure 5.1). Site 658 is located below a surface ocean high productivity cell which gives rise to high sedimentation rates (10–25 cm/kyr) (Meckler et al., 2013) and high total organic carbon contents (%TOC) of 0.5–4% in the sea floor sediments of Late Pleistocene age, helping to preserve organic carbon of terrestrial origin (Stein et al., 1989). The site is also located proximal to- and downwind of- the modern NAS, the region of highest fire activity in the world (Figure 5.1).

Vegetation in northern Africa shows strong latitudinal banding (Dupont, 1993) along precipitation gradients, whose position is strongly influenced by ITCZ-controlled rainfall. The latitude of Site 658 is close to the modern northern limit of migration of the boreal summer position of the Intertropical Convergence Zone (ITCZ) along the African continental margin (*ca.* 21°N) roughly corresponding to the 250 mm mean annual precipitation (MAP) contour (Figure 5.1)(Larrasoaña et al., 2013; Ruddiman et al., 1988a; Schneider et al., 2014). On geological timescales, the magnitude of migration of the ITCZ varies in response to a high- or low- latitude forcing mechanism (Collins et al., 2013, 2010). At the orbital scale, high insolation forcing at low latitudes in boreal summer during precession minima results in northward penetration of the rainbelt to higher latitudes than today giving rise to more humid conditions across northern Africa, evidenced by a ~3° northward shift in the position of the Sahara-Sahelian boundary compared to its modern location at 19°N (Collins et al., 2013). During precession maxima (boreal summer insolation minima), seasonal latitudinal

migration of the ITCZ is less pronounced and northern Africa dries out as precipitation becomes more concentrated at lower latitudes (Collins et al., 2010; Singarayer et al., 2017). At millennial timescales, rapid North Atlantic cooling events are suggested to trigger even more dramatic southwards ITCZ migration (Mulitza et al., 2008; Stager et al., 2011) resulting in a 6° southward shift from 19-13°N (from modern) in the position of the Saharan-Sahelian Boundary during Heinrich Events (Collins et al., 2013). This migration in the mean position of the ITCZ is suggested to result from the pronounced interhemispheric thermal asymmetry brought about by cooling of the surface North Atlantic Ocean in a manner analogous to the seasonal pattern (Arbuszewski et al., 2013; Braconnot et al., 2007; McGee et al., 2014; Merlis et al., 2013; Otto-Bliesner et al., 2014; Singarayer et al., 2017; Wang et al., 2014).

Grain size data from Site GeoB7920-2, a near-reoccupation of ODP site 658, provide a record of riverine and aeolian transport of terrigenous material and hence northern African hydroclimate (Tjallingii et al., 2008). These records reveal intervals of high contributions of fine-grained riverine material when northern Africa was much wetter than present, implying increased freshwater run-off from the (western) Sahara for example through palaeo-river channels on the currently hyper-arid Mauritanian margin (Skonieczny et al., 2015). These intervals of increased precipitation over northern Africa, termed African Humid Periods (AHPs), are also associated with greater vegetation coverage the so called Green Sahara Periods (Claussen and Gayler, 1997; DeMenocal et al., 2000; Ritchie et al., 1985).

Aeolian material is transported to site 658 from multiple locations across northern Africa. The major summer dust plume is driven by the African Easterly Jet (AEJ) and travels westwards across the Atlantic Ocean (Harrison et al., 2001; Hooghiemstra et al., 2006), transporting dust, charcoal, freshwater diatoms, phytoliths and palynomorphs to site 658 from a source region in the Southwestern Sahara and Sahel, with material also likely transported to site 658 from the north by the northeast trade winds (Harrison et al., 2001; Hooghiemstra et al., 2006; Kuechler et al., 2013; Tiedemann et al., 1989; Tjallingii et al., 2008; Vallé et al., 2014). Palynological and geochemical studies, however, suggest that the position of the AEJ remained stable (21°N) across the glacial termination despite latitudinal shifts in the vegetation bands (Cole et al., 2009; Grousset et al., 1998; Hooghiemstra et al., 2006; Sarnthein et al., 1981), implying that the source region of aeolian material transported offshore to the NWAM largely remained constant throughout the LGC. As determined by the distribution of the pollen records southern-boarder of the Sahara reflected by

the changing ratio of *Chenopodiacaea-Amaranthacaea* from desert and *Gramineae* pollen from the Sahara belt (Hooghiemstra et al., 2006).

5.3 Material and Methods

5.3.1 Charcoal Preparation and Identification

Charcoal is often used as 'catch-all' term for all material produced during combustion, encompassing everything from microscopic black carbon to large chunks of charred biomass. Here, charcoal is defined more specifically as any carbon-rich terrestrially derived material produced by total combustion either by natural or anthropogenic mechanisms (Bird and Ascough, 2012; Keeley and Rundel, 2005). The term fire activity is used here when discussing the changes in charcoal flux to avoid assumptions about the frequency, size contributions and fire proximity to the site, because of the uncertainty in source and the number of individual fire events associated with using palaeo-archives (Crawford and Belcher, 2014; Marlon et al., 2009). Charcoal fluxes are used as a proxy for fire activity, with higher charcoal fluxes indicating higher fire activity.

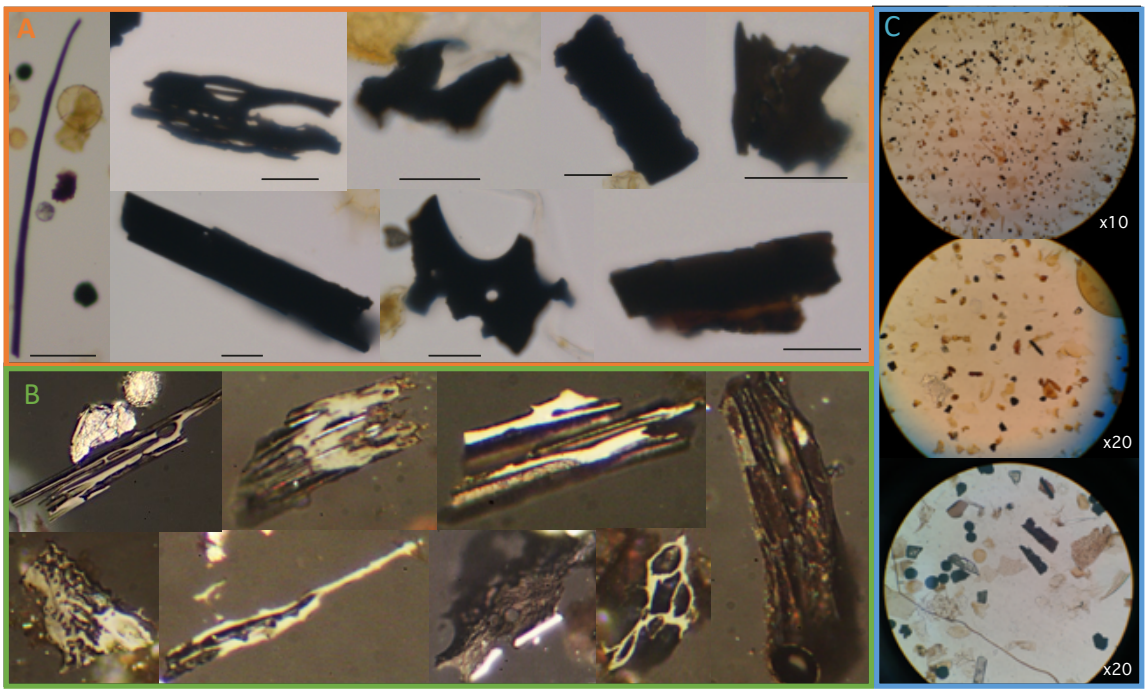

Figure 5.2: A selection of charcoal images from various samples from ODP Site 658. A) A selection of charcoal particles viewed in transmitted light, the black scale bar indicates 20µm. B) A selection of charcoal particles view in reflected light. C) A series of typical viewa of the processed samples in reflected light at the stated magnifications.

Bulk sediment samples were prepared for charcoal counts using a modified version of the standard two-step acid maceration method following standard palynological processing techniques (similar to that detailed by Harding *et al.*, 2011), but omitting steps that involve physical agitation to avoid charcoal fragmentation. The carbonate and silicate fractions were removed from unground oven-dried bulk sediment weighing 2–8 g by treatment in HCl (for 24 hours) and HF (for 48 hours) respectively. The removal of fluoride compounds (formed during HF maceration) was achieved by boiling samples in HCl and then sieving at 15 µm. Amorphous organic matter (AOM) was removed using a short (20 second) ultrasonication step followed by sieving at 15 µm.

To calculate charcoal concentrations, samples (>15 µm size fraction) were spiked with a known dose of the exotic spore *Lycopodium* (Stockmarr, 1971) and mounted onto glass slides for examination under transmitted light. Charcoal particles and *Lycopodium* spores were counted until 500 *Lycopodium* spores was reached. Optical identification of charcoal was achieved using an Olympus BH-2 microscope and a freestanding lamp using shape, colour and reflectance characteristics. Particles were classified as charcoal if they were completely black, the particle edges were transparent or slightly blue and could be fitted in one of the following morphological categories: elongate, splintery perforated and splintery unperforated, irregular perforated, irregular unperforated or square/rectangular (Figure 5.2). The high pyrite content of the ODP 658 sediments hindered straightforward charcoal identification in some cases, so an additional check was undertaken to view the particle in low base light (microscope light) and high upper light (lamp light). Only particles that were dark or faintly reflective were classified as charcoal, whereas bright flat reflective particles were classified as pyrite. A final check was made by examining a subset of samples in reflected light to ensure that preserved cellular structure of the original biomass was visible. The ratio of charcoal to *Lycopodium* spores counted was used to calculate charcoal concentrations. Several sub-sets of samples were recounted (multiple counts of the same slide, counts of a remounted sample and reprocessing of raw material; for additional details see supplementary information) to indicate a mean uncertainty in calculated concentration of 7.3%. Charcoal fluxes were then calculated using the shipboard measurements of dry sediment bulk density and sedimentation rates from Meckler *et al.*, (2013)(see supplementary information).

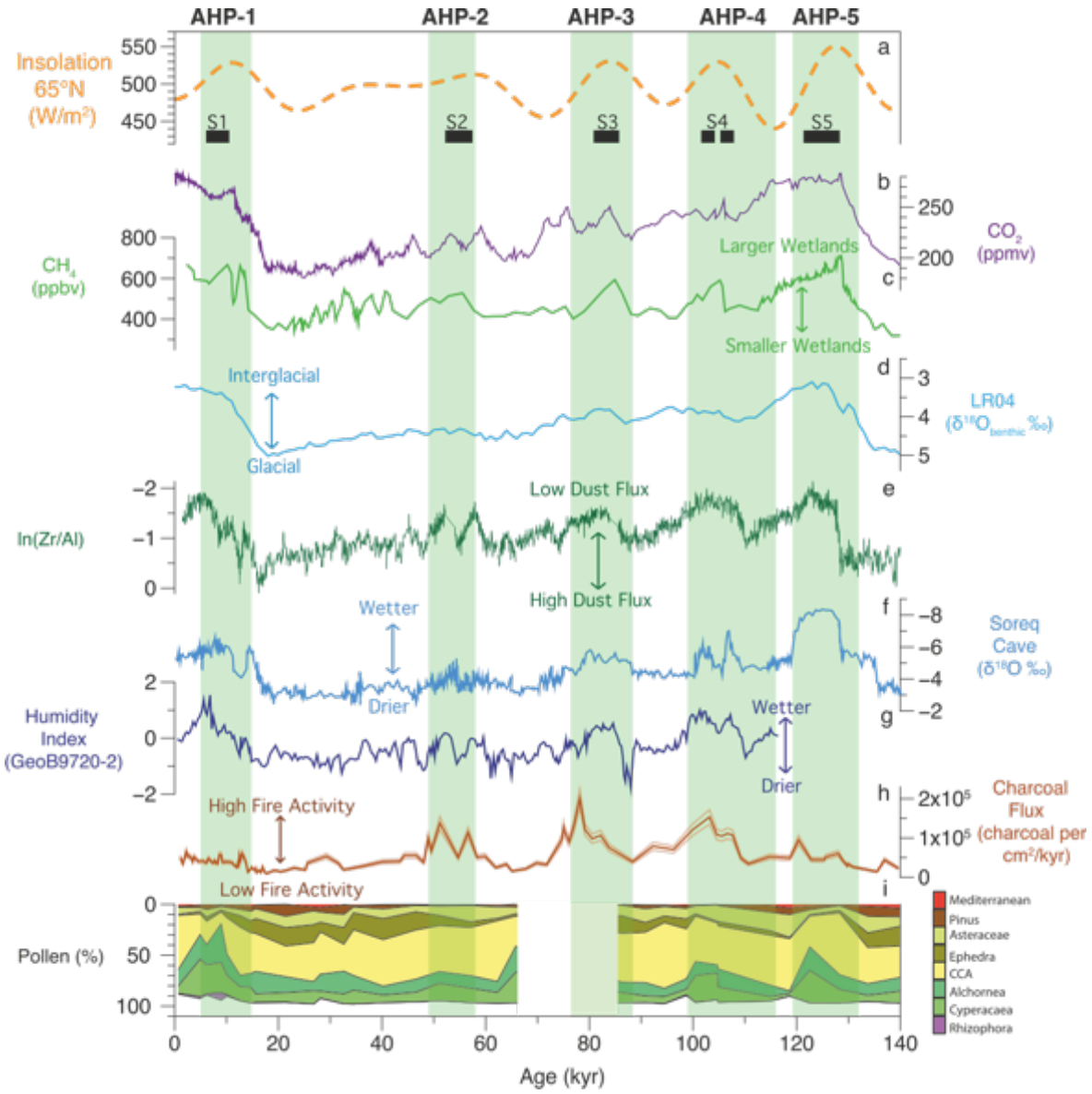

Figure 5.3: Last Glacial Cycle ODP 658. Green shaded bars wet periods. AHP: African Humid Periods. Black bars Sapropel events. a) Insolation (JJA) 65°N W/m^2 (Laskar *et al.,* 2011), b) Composite Ice Core CO_2 (Berieter *et al.,* 2014), c) Vostock Ice Core CH_4 Record (Petit *et al.,* 2001), larger and smaller wetland refers to area coverage. d) LR04 δ^{18}O‰ Benthic Foraminifera Stack (Lisiecki and Raymo, 2005). e) Soreq Cave Speleotherm δ^{18}O (Bar-Matthews *et al.,* 2003). f) Humidity Index derived from the proportion of the aeolian to riverine material delivered to Site GeoB9720-2 (Tjallingii *et al.,* 2008). g) XRF scanned ln(Zr/Al) proxy for Dust Flux (Meckler *et al.,* Unpublished). h) Charcoal flux ODP 658 charcoal per cm^2/kyr (this study), error of 12.5% is shown in lighter brown. i) Pollen % of total (CCA = *Caryophyllaceae Chenopodiaceae & Amaranthaeceae*) (Dupont *et al.,* 1989).

A reproducability error of 12.5% is given to the values dervied from these counts due to the difficulties in excatly replicating the counts due to sample mount heterogeneties, and uneven material distribution across the slide (full details of counting testing Chapter 2 Section 2.2.4.1). Despite the error, it is important to note that the raw counts produced in this study are arguably less important than the over trend in fire activity between high and low burning which has been shown to be robust. Caution must be applied not to over interpret the data as any variability <12.5 should not be considered to be driven by natural forcing mechanisms.

5.3.2 Bulk sediment carbon and nitrogen contents

Approximately 1 g of bulk sediment was freeze-dried, ground to fine powder using an agate pestle and mortar and decarbonated overnight in 10% HCl to remove inorganic carbon (carbonate). The decarbonated residue was then neutralised, oven dried at 50°C, homogenized and re-weighed to calculate the mass loss of total inorganic carbon. Approximately 10 mg of dried, decarbonated residue was weighed and sealed into tin capsules for analysis of organic carbon contents ($\%C_{org}$) using a Vario Isotope Select Elemental Analyser coupled to an Isoprime 100 mass spectrometer at the University of Southampton National Oceanography Centre (NOCS). These data are reported against external reference material (L-glutamic acid and peat soil and USGS40 and USGS41a

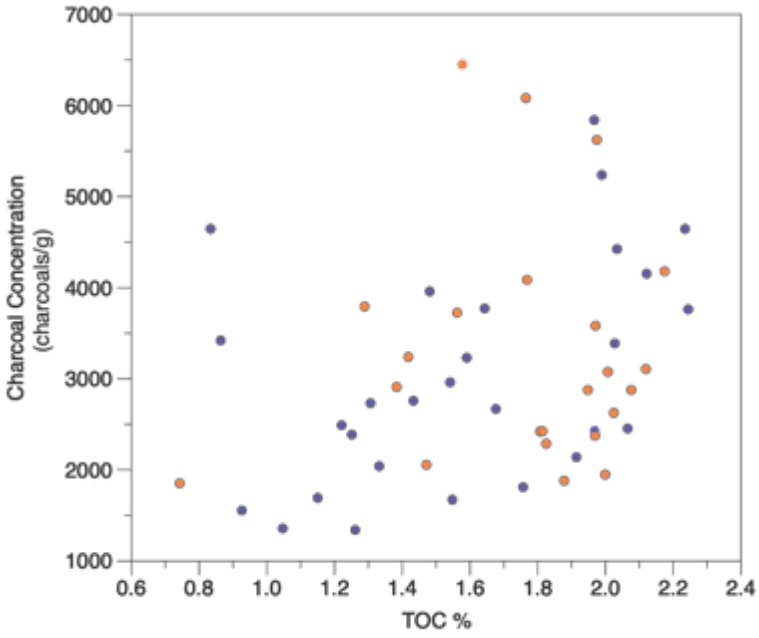

Figure 5.4: Charcoal concentration vs TOC %. No relationship is observed between these parameters indicating that charcoal recovery is not influenced by TOC%. Oranges samples date to AHPs, whereas the purple data points are non-AHP in age.

respectively) (see supplementary information). The percentage Total Organic Carbon (%TOC) was then calculated by dividing the total bulk sample dry weight (g) by the decarbonated fraction for each sample and those data are compared to charcoal concentration in (Figure 5.4). The decarbonated weight was used, so that the influence of marine carbonate production was removed from the TOC value.

5.3.3 Chronology

All data from ODP site 658 is presented on a slightly modified version of the published age-depth model of Meckler *et al.*, (2013), which was produced by tuning $\delta^{18}O_{benthic}$ data from Site 658 on a revised composite depth scale to the LR04 stack (Lisiecki and Raymo, 2005), using AnalySeries software (Palliard *et al.,* 1996). For the last 120 kyr, age was refined by 1) matching XRF-derived Ca from Hole 658A to $\%CaCO_3$ in radiocarbon-dated Hole 658C (DeMenocal et al., 2000) and 2) tuning ln(Zr/Al) data from site 658 (a proxy for grain size) to the grain size-based humidity index from nearby core GeoB7920-2 (Meckler et al., 2013; Tjallingii et al., 2008).

5.4 Results and Discussion

My record of charcoal flux to ODP site 658 shows a distinctive pattern of change over the last 150 kyr, with multiple high amplitude peaks (Figure 5.3). These maxima in charcoal flux correspond remarkably well, especially between 40 and 140 ka, to the African Humid Periods (AHPs) of increased rainfall over northern Africa that are well documented by the run-off-induced Mediterranean sapropel events (Figure 5.3). These AHPs were triggered by maxima in regional insolation forcing and paced by minima in the precession of Earth's axis of rotation as it orbits the Sun.

I interpret the strong relationship between rainfall in northern Africa and charcoal flux to site 658 as an indicator of fire activity because the absence of a relationship between the concentration of charcoal and organic carbon in my samples indicates that my record cannot be explained by changes in charcoal preservation at my study site (Figure 5.4). The possibility that the structure of my record is determined by changes in the efficiency of charcoal transport to site 658 can also be discounted based on two main lines of evidence. First, while ephemeral palaeo-rivers on the

Northwest African margin (Skonieczny et al., 2015) were presumably active during the AHPs of the Last Glacial Cycle, it is unlikely that they played a primary role in driving increased charcoal flux to site 658 because the peaks in charcoal flux in my record do not align with peaks in the proportion of riverine-derived sediments at this site (Figure 5.3). Second, the absence of a strong glacial-interglacial structure in my record argues strongly against a primary control on charcoal flux from changes in the strength and/or direction of the regional wind field (Verardo and Ruddiman, 1996). On the contrary, the distinct imprint of cyclicity in my record (precession) that has been shown to influence African precipitation, vegetation and moisture balance implies that the main factors controlling charcoal fluxes at my study site are source-area moisture and biomass changes (not temporal changes in transport mechanism). In other words, charcoal flux to Site 658 can be used as a first order proxy for fire activity in northern Africa.

Variable residence times is discount as a cause of variability as charcoal exhibits similar behaviour to pollen which is considered to be one of the most resilient organic materials and thereby are considered to have comparable residence times.

5.4.1 Fire activity in Northern Africa over the last 150 kyr

The similarity between my charcoal flux record and precessional forcing implies a strong link between fire activity and insolation-driven changes in northern African hydroclimate, the sign of the relationship is consistent from the perspective of the seasonal cycle. Annually, fires burn in northern Africa during the dry season when lightning strikes are most likely to promote ignition (Carmona-Moreno et al., 2005; Cooke et al., 1996; Harrison and Sanchez Goñi, 2010). My record shows that, over the last glacial cycle, fire activity in the region is lowest during arid intervals and distinctly higher during humid intervals (AHPs) (Figure 5.3). To a first order, this apparent contradiction has a very simple explanation. Fires require fuel to burn and, over the last 150 kyr, there were major expansions and contractions of vegetation over northern Africa in response to orbitally paced changes in insolation that drove change in the latitudinal extent of poleward ITCZ-migration during boreal summers. When insolation was highest (during precession minima), the ITCZ penetrated to latitudes well to the north of those occupied during boreal summer today (~19°N) bringing rainfall to latitudes that are now hyper-arid (Larrasoaña et al., 2013). This migration of ITCZ rainfall stimulated the northward expansion of C_4 savanna grassland and, further south, the C_3 rainforest biome (Dupont and Hooghiemstra, 1989; Kuechler et al., 2013; Singarayer et al., 2017; Zhao et al., 2003). Thus, my data strongly suggest that expansion of the highly

flammable, rapidly regenerating NAS ecosystem ~4° northward of its present latitudinal limit of ~19°N (Collins et al., 2013; Dupont et al., 1989) drove major increases in net primary productivity (NPP) (particularly C_4 grasses) in previously moisture-limited ecosystems, generating larger fuel sources capable of supporting higher fire activity (Daniau et al., 2010; Hoetzel et al., 2013; Keeley and Rundel, 2005; Lehmann et al., 2014; Moritz et al., 2012; Turner et al., 2008).

5.4.2 An inflected relationship between fire activity and rainfall/vegetation during AHPs -5 and -1

While much of the structure in my charcoal flux record can be explained by a model in which fire activity increases with increasing rainfall amounts and vegetative biomass (fuel), closer inspection suggests that this relationship is more nuanced (Figure 5.3). The highest insolation values of the past 150 kyr occurred around 130 ka and caused widespread humidity across northern Africa during AHP5 (Dupont, 2011; Larrasoaña et al., 2013; Meckler et al., 2013)(Figure 5.3). Yet, the charcoal flux peak in my records during this interval is approximately half that recorded during AHPs -4 and -3, which are dated at approximately 116–99 ka and 89–77 ka, respectively (Ehrmann et al., 2016). AHPs -4 and -3 occur during times of weaker insolation forcing leading to a more muted rainfall and vegetation response than during AHP5 (Bar-Matthews et al., 2003; Dupont et al., 1989; Tjallingii et al., 2008)(Figure 5.3). Furthermore, my record documents only a minor increase in charcoal flux documented during AHP1, which has similar insolation forcing to the much higher fire activities documented during AHPs -4 and -3. Thus, fire activity in northern Africa through the last glacial cycle is not linearly dependent upon the strength of insolation forcing driving the hydrological cycle.

Instead, one or more additional factors must exert an additional control, resulting in relatively suppressed fire activity during AHPs -5 and -1. I consider three scenarios to account for these observations: (1) High-latitude climate forcing exerted a secondary control on vegetation through remnant effects of the glacial (2) Changes in atmospheric pCO_2 exert a secondary control on fire activity by promoting forest growth at the expense of grasslands (3) The most extreme insolation peaks triggered conditions that were sufficiently humid to encourage the expansion of wetter-adapted less flammable ecosystems with higher fuel moisture contents.

My first hypothesis for the inflected relationship between fire activity and rainfall/vegetation is motivated by the observation that the modest peaks in fire activity for AHPs -5 and -1 occur shortly

after major glaciations (the Penultimate Glacial Maximum (PGM) and Last Glacial Maximum (LGM) respectively). In this explanation, widespread burning is supressed during AHPs -5 and -1 because of a remnant effect from the highly arid conditions that developed during the preceding glacial intervals. As an example, pedogenesis is almost halted under arid conditions which, coupled with an increase in dust deflation, results in very poor quality soils which would then take time to recover under higher humidity (Zerboni et al., 2011). However, even though the resolution of many pollen reconstructions is limited, there is no evidence to support a delay in vegetation recovery occurring over timescales of 5,000–10,000 years (Hély et al., 2014; Watrin et al., 2009) as would be expected if an unfavourable flora was responsible for dampened fire activity, with the pollen assemblage recorded at Site 658 during AHPs -5 and -1 comparable to AHPs -4 and -3 (Dupont, 2011). Therefore, a delayed impact from the previous glacial maxima suppressing fire activity that persists throughout the following humid interval seems unlikely.

My second hypothesis for the modest fire activity recorded during AHPs -5 and -1 draws on the observation that these two intervals occur when global atmospheric pCO_2 values are at their highest levels of the LGC (pCO_2 concentrations during AHPs -5 and -1 are ~20 to 35 ppmv higher than during AHPs -4 and -3 (Bereiter et al., 2014; Lüthi et al., 2008))(Figure 5.3). Elevated pCO_2 promotes C_3 tree growth, allowing saplings to more rapidly attain a size which allows them to survive fires (escape height) (Bond et al., 2003). As a result, small frequent grass fires are less likely to kill the saplings, facilitating woodland establishment (Bond et al., 2003). If tree establishment exceeds a specific threshold of 40–50% tree cover (Staver et al., 2011a), this can lead to a suppression of fire activity (Bond and Midgley, 2000; Bond, 2008), which could explain the muted charcoal fluxes I record during AHPs -5 and -1. However, the carbon isotopic signature of plant wax alkanes and pollen assemblages do not support an increased dominance of C_3 plants over C_4 grasslands during AHPs -5 and -1 (Dupont, 2011; Hoogakker et al., 2016; Kuechler et al., 2013; Niedermeyer et al., 2009; Zhao et al., 2003). Therefore, the promotion of tree growth by elevated pCO_2 cannot simply explain the suppressed fire activity during AHPs -5 and -1.

My third hypothesis to explain the observed reduction in fire activity at high rainfall is rooted in the observation that fire activity in northern Africa is greatest in the highly precipitation-sensitive savanna ecosystem, with fire activity decreasing if rainfall shifts outside an optimum range (1000–1500 mm/yr MAP) (Dupont and Schefuß, 2018). Fire activity decreases at higher humidity levels because biomass desiccation is inhibited and high fuel moisture contents reduce ignitability, intensity of combustion and the sustainability of a fire (Higgins et al., 2000; Simpson et al., 2016;

Stott, 2000). Therefore, the modest peaks in fire activity during AHPs -5 and -1 (14.8–5.5 ka) (Ehrmann et al., 2016) could be explained by the fact that these two intervals are the wettest events of the LGC in northern Africa, in which the ITCZ extended up to ~21°N (Rohling et al., 2002; Skonieczny et al., 2015), resulting in high lake levels across northern Africa (Armitage et al., 2015; Damnati, 2000), activation of ephemeral river systems draining the Sahara (Skonieczny et al., 2015) and the deposition of thick sapropels in the Mediterranean Sea (Ehrmann et al., 2016; Grant et al., 2016; Rohling et al., 2002).

The modern NAS is comprised of a mixture of savanna types, with higher fire activities found in savannas of intermediate humidity (600–1100 mm/yr MAP, savanna vegetation is climatically and disturbance-maintained) than either dry (100–600 mm/yr MAP, climatically maintained) or wet (>1100 mm/yr MAP, disturbance-maintained) savannas (Accatino et al., 2010; D'Onofrio et al., 2018; Jeltsch et al., 2000; Ratnam et al., 2011; Sankaran et al., 2005). Reconstructions of precipitation levels during AHPs -5 and -1 are higher than today but there are considerable discrepancies among studies as to the amplitude of this signal. Modelled rainfall estimates proximal to Site 658 at 21°N on the African continent during AHP5 range from ~180 to 825 mm/yr MAP (Herold and Lohmann, 2009; Larrasoaña et al., 2003; Nikolova et al., 2013; Sjolte and Hoffmann, 2014), with geomorphological-based estimates of 400–700 mm/yr in good agreement (Larrasoaña, Roberts and Rohling, 2013 and references therein). These estimates fall below the modern precipitation values at which fire activity starts to become significantly suppressed (1100–2000 mm/yr MAP) (Accatino et al., 2010; Lasslop et al., 2018; Staver et al., 2011a; Stott, 2000). Yet model-simulated rainfall anomalies for the best-studied humid period, AHP1, are consistently too low to account for the pollen-based reconstructions of vegetation change (e.g. Hopcroft *et al.*, 2017). Furthermore, data from leaf wax biomarker δD records suggest much larger rainfall anomalies (absolute values of 1200 mm/yr^{-1} at 31°N, Tierney, Pausata and De Menocal, 2017)) than the pollen-based estimates. These wetter reconstructions are sufficient to (i) promote the development of wet savanna (Accatino et al., 2010; Bucini and Hanan, 2007; D'Onofrio et al., 2018; Sankaran et al., 2005), (ii) exceed the threshold at which forest encroachment and grass exclusion limit fuel loads and supress burning (Archibald et al., 2009; Hoffmann et al., 2012; Sankaran et al., 2005; Staver et al., 2011a) and (iii) imply even higher levels of precipitation for AHP5.

However, if these levels of elevated humidity are to account for fire suppression during AHPs -1 and -5 relative to -3 and -4, the vegetation/fire response to increased precipitation is unlikely to have been achieved largely by simple northward migration of modern vegetation and fire activity belts.

Today, the belt of peak fire activity lies approximately 5 to 10 degrees south of my study site, roughly corresponding to a zone of mean annual precipitation between 1000 and 1500 mm/yr MAP (Figure 5.1). Working from this modern distribution, therefore, I might reasonably predict the peak fire activity belt to have migrated closer to my study site during the AHPs. A key question therefore, in addition to the amplitude of increased rainfall, concerns the extent to which northward migration of the rainbelt elicited northward migration of the modern vegetation bands or instead, the establishment of a "Green Sahara" biome with no modern analogue (Lezine, 1989; Watrin et al., 2009). During AHP1, tropical plants have been shown to migrate as far northwards as 24°N, north of the core of the tropical rainbelt (15–20°N) (Hély et al., 2014), co-occurring with persisting Saharan plants throughout the humid interval (Watrin et al., 2009). The consequences of such a mixed biome for fire activity are not known.

5.4.3 Millennial-scale variability in the charcoal flux record through the last deglaciation

The trend in fire activity from the LGM through to the Holocene revealed by my ODP site 658 records is one of an overall increase in charcoal flux values, overprinted by millennial-scale climate variability which is also visible in both vegetation and dust flux records (Figure 5.5)(Kuechler et al., 2013; Straub et al., 2013; Zhao et al., 2003). This millennial-scale variability in charcoal flux largely shows a relationship to rainfall that is of the same sign as the orbital signal: higher fire activity during more humid intervals. However, the amplitude of millennial-scale charcoal flux variability is much smaller than orbital-scale variability (Figure 5.5). Changes in northern African hydroclimate in response to millennial climate oscillations are more abrupt than insolation-forced variability (Bouimetarhan et al., 2012; McGee et al., 2014; Mulitza et al., 2008; Shanahan et al., 2015), with a greater displacement of the Sahara-Sahel boundary relative to its modern-day location owing to the migration of the ITCZ during millennial events (e.g H1, 6° southward shift) and the AHPs (AHP1, 3° northward shift) (Collins et al., 2013). The strong variability in northern African hydroclimate observed over millennial timescales is widely suggested to be controlled by changes in North Atlantic meridional surface ocean temperature gradients associated with oscillations in the vigour of the Atlantic Meridional Overturning Circulation (AMOC) (Mulitza et al., 2008). During H1 and the Younger Dryas (YD), AMOC shoaled and weakened, reducing heat supply to the high latitude North Atlantic and dragging the thermal equator and therefore the ITCZ southward (Garcin et al., 2007; Marshall et al., 2011; McGee et al., 2014; Mulitza et al., 2008; Shanahan et al., 2015; Verschuren et

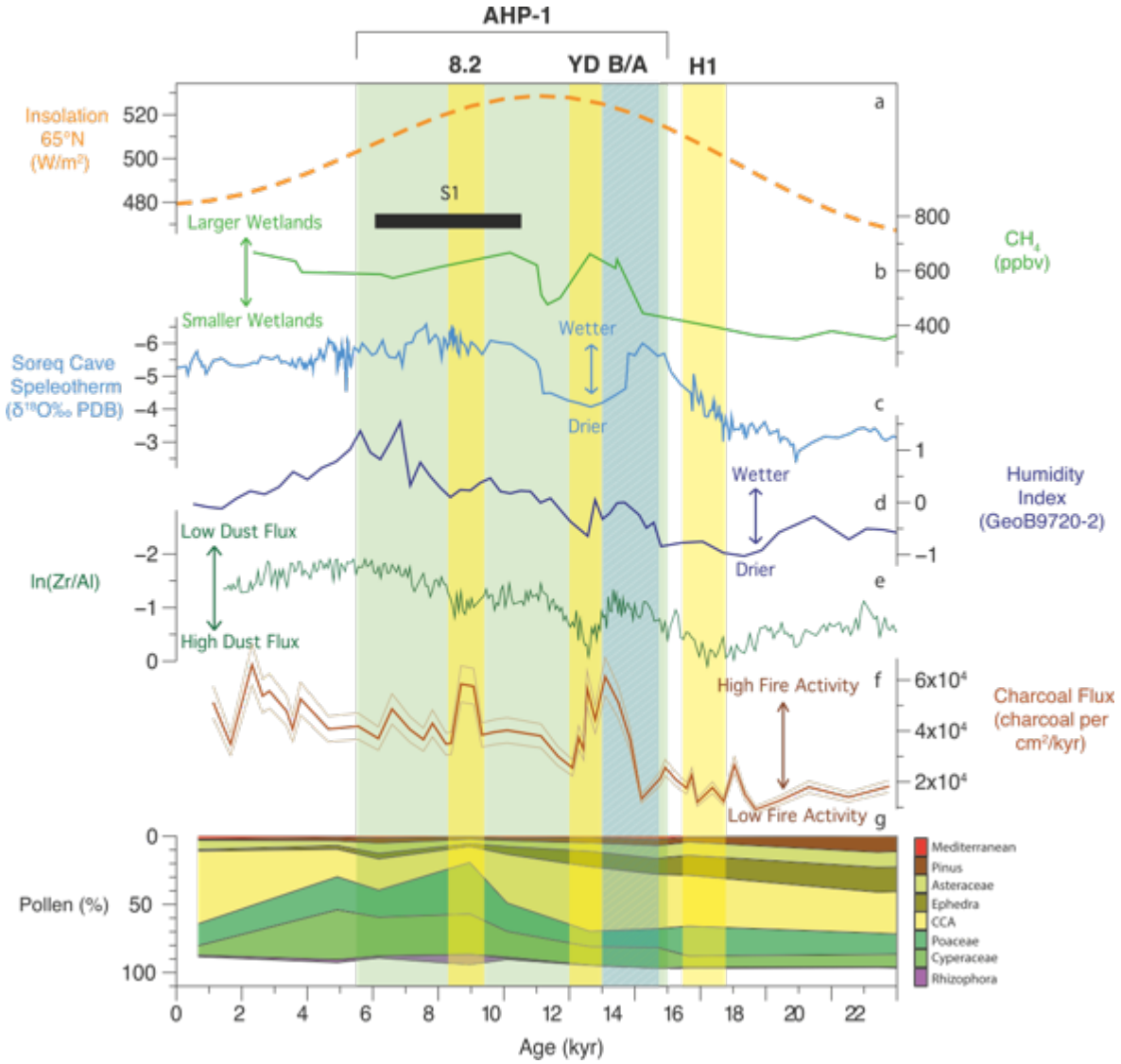

Figure 5.5: Deglacial and Holocene ODP 658. Green shaded bar wet periods, Yellow shaded bars arid periods AHP-1: African Humid Period 1. H1: Heinrich Event 1, B/A: Bølling-Allerød, YD: Younger Dryas, 8.2: 8.2 ka, S1: Sapropel 1. a) Insolation (JJA) 65°N (Laskar *et al.,* 2004), b) Vostock Ice Core CH4 Record (Petit *et al.,* 2001) c) Soreq Cave Speleotherm δ^{18}O PDB (Bar-Matthews *et al.,* 2003) d) Humidity Index, proportion of aeolian to riverine material delivered to Site GeoB9720-2 (Tjallingii *et al.,* 2008). e) XRF scanned ln(Zr/Al) proxy for Dust Flux (Meckler *et al.,* Unpublished). f) Charcoal flux ODP 658 charcoal per cm^2/kyr (this study) error of 12.5% is shown in lighter brown. g) Pollen % of total. (CCA = *Caryophyllaceae, Chenopodiaceae & Amaranthaeceae*) (Dupont *et al.,* 1989).

al., 2009). This resulted in a significant decrease in MAP at 19°N to values <100 mm/yr during H1 and to 250 mm/yr during the YD (Tierney et al., 2017b). The opposite occurred during the Bølling-Allerød (B/A) interstadial, when a reinvigorated AMOC warmed the North Atlantic, dragging the ITCZ northward, bringing more humid conditions to northern Africa, with an increase to >2000

mm/yr MAP reconstructed at 19°N, with values remaining below 500 mm/yr MAP further north (Tierney et al., 2017b).

Peak aridity in the region over the LGC is widely documented occurring during Heinrich Event 1 (H1), when the Sahara-Sahel boundary is inferred to be at its most southerly position of 13°N (Collins et al., 2013) and very high dust transport from northern Africa to site 658 is reported based on ln(Zr/Al) values (Straub et al., 2013)(Figure 5.5). Yet my charcoal record documents no major reduction in charcoal production during this event, as might be expected as a response to aridity-driven reduction in the vegetative fuel source i.e. limiting charcoal production and therefore supply to potential palaeo-archives. The lack of a strong reduction in fire activity during H1 probably arises because of the combination of the arid baseline state at the LGM and the location of Site 658 (~21°N) close to the modern Sahara-Sahel boundary (Figure 5.1). This location is ideal to record deviation from the modern baseline of fire activity but perhaps too far north to be highly sensitive to further intensification of the arid glacial state. Glacial vegetation was dominated by desert and dry grasslands (Dupont, 2011; Hoogakker et al., 2016), with very low tree cover (Sankaran et al., 2005), hence fuel levels were already very low before the further increase in aridity.

There is a clear increase in fire activity in the NAS during the B/A (at ~21°N), with charcoal fluxes reaching more than double LGM values, although total flux values are modest in comparison to those associated with the preceding insolation-driven AHPs (Figure 5.5). The increase in charcoal flux is delayed (500–1000 years) compared to the decrease in dust supply to Site 658 as recorded by ln(Zr/Al)(Figure 5.5), suggesting that vegetation takes time to recover from the aridity of H, although the existing pollen record is not sufficiently well resolved to test this interpretation (Figure 5.5). In fact, charcoal flux peaks at the B/A /YD transition possibly signifying the initial desiccation of an expanded fuel load during the well-documented aridity of the YD (Bar-Matthews et al., 2003; Gasse, 2000; Shanahan et al., 2015; Stager et al., 2002; Tierney et al., 2017b; Tjallingii et al., 2008). In this context, it is perhaps significant that I also document a modest short-lived increase in charcoal production (with maximum values of ~$6x10^4$ charcoal/cm^2 kyr) close to the 8.2 ka cold event (Alley et al., 1997; Gasse, 2000; Mayewski et al., 2004), a further brief arid interruption to AHP1 (Figure 5.5). A similar charcoal peak is documented at nearby site GeoB7920-2 (Dupont and Schefuß, 2018) and a period of increased burning is also recorded in Spain 8–8.8 ka (Davis and Stevenson, 2007).

5.5 Summary and Conclusions

I document a strong relationship between fire activity and rainfall climate in northern Africa over the last glacial cycle. The overall pattern is one of high fire activities during times of high humidity when conditions across northern Africa were sufficiently wet in response to northwards expansion of the ITCZ to sustain large fuel loads. In detail, however, my data suggest an inflected relationship between rainfall climate and fire activity: increasing rainfall promotes increasing fire activity only up to a point. The very wettest intervals in northern Africa over the LGC (AHPs -5 and -1) show modest peaks in fire activity compared to AHP -3 and -4, the cause of which requires further exploration.

Fire activity also shows a clear response to millennial-scale variability in hydroclimate during the last deglaciation, although the variability is more muted at my study site than that driven by precessional forcing. During these more rapid climate events, the preceding hydrological regime appears to strongly influence the fire activity of northern Africa. For example, there is little change in charcoal flux during the dramatic aridification documented during H1, which I attribute to the lack of a fuel source following the expansive desert conditions of the LGM as fuel supply remains relatively unchanged and consequently so does fire activity. Fire activity is greater during the more humid conditions of the B/A and AHP1, with a further short-lived increase in fire activity also recorded coincident with a minor dust flux increase likely associated with the 8.2 ka event, likely resulting from a desiccation of the abundant biomass that developed during AHP1.

5.6 Supplementary Information

5.6.1 Standards

The quality assurance standards and quality control standards used for the generation of the isotope data are detailed in Table 5.1 and Table 5.2 below:-

Quality Assurance – external reference material	Reported absolute value	Standard Deviation
USGS40	-26.39	0.04
USGS41a	36.56	0.08

Table 5.1: Quality Assurance Standards and values used for isotope calibration.

5.6.2 Charcoal counts tests

To assess the reproducibility of the charcoal counts produced by my methods of charcoal extraction are indicative of a record of change in sediment and not an inherent part of the methods a series of tests were conducted. Detailed here in brief, for full details see Chapter 2 Section 2.2.4.1.

Quality Control Standard	Internal Standard Values	Standard Deviation
L-glutamic Acid	-13.56	0.08
Peat Soil Standard	-27.80	0.07

Table 5.2: Quality Control Standards and values used for isotope calibration.

Calculation of the charcoal fluxes rely on Charcoal:*Lycopodium* ratio of the sample. An incorrect spike value will generate an incorrect charcoal flux value, an artificially low or over-estimated if the *Lycopodium* value is too high or too low respectively. 4 samples were re-spiked with pink dyed *Lycopodium,* counts on these slides produced a value ~25% lower, consistently 20-25% of sample being removed prior to the addition of pink spike, hence ~20% less natural to pink *Lycopodium* is visible in the slide. This method allows us to effectively determine the correct *Lycopodium* dosage was added to the samples.

Standard practices for counts was to concordantly count charcoal and *Lycopodium* along a transect of slides until 500 *Lycopodium* was reached, following standard palynological practices. To ensure these "standard counts" were representative of the entire sample, a sub-set of sample were fully counted on the original and remount the average difference in the counts achieved varied by 9.95% (Table 5.1 and Table 5.2).

As the nature of charcoal identification for counts are subjective thereby to ensure consistency, all charcoal were undertaken by one person in blocks of time (weeks) to improve consistency of charcoal identification.

To determine counting consistency, the same fields of view were counted along a transect multiple times to determine the similarity of the number of charcoal *Lycopodium* achieved. Slight discrepancies occurred in the counts $\pm$4.5% occurred, due to subtle changes in the field of view on re-visitation (adding or removing charcoal and/or *Lycopodium* around margins)(Chapter 2 section 2.2.4.1).

Multiple counts were conducted on different sections of the same slide, average variability between these counts ~11% (Chapter 2 section 2.2.4.1). A sub-set of 5 samples were mounted for a second time (remounted) and counted to compare counts achieved to determine each mount was representative of the sample as a whole, average variation was ~6.2% from original counts achieved (Chapter 2 section 2.2.4.1), and therefore each mount was considered representative of the sample as a whole. A final test was a sub-set of samples re-run from raw sediment (i.e. re-processed, mounted and counted) which produced an average difference in counts of ~12.5% (Chapter 2 section 2.2.4.1).

5.6.3 Flux calculations

Charcoal fluxes were generated using equations 1 and 2:-

Eq. 1:-

$$((\text{Charcoal counted} \div \text{Lycopodium counted}) \times \text{total Lycopodium}) \div \text{dry sediment weight (g)} = \text{charcoal concentrations (charcoal/g)}$$

Fluxes of charcoal were calculated using bulk density (Ruddiman *et al.,* 1989) and sedimentation rates using equation 2:

Eq. 2:-

$$(\text{charcoal concentration (charcoal/g)}) \div \text{dry bulk density (g/cm}^3) \times (\text{sedimentation rates (cm/kyr)} \times 100) = \text{charcoal flux (charcoal/cm}^2\text{/kyr)}$$

5.6.4 Bulk Density and Sedimentation Rates

Dry bulk density values used average calculated from (Ruddiman *et al.* 1989). The sedimentation rates were calculated using the XRF and tie-points of Meckler *et al.,* (2013).

Chapter 6 Comparing and contrasting trends in fire activity on North Africa across two orbitally similar glacial cycles: The Last Glacial Cycle (MIS 1-5) and Mid-Brunhes (MIS 9-11)

Supporting Authors: Anya Crocker[1], Paul A Wilson[1], David Beerling[2], Colin Osborne[2]and Nele Meckler[3]

[1]University of Southampton - National Oceanography Centre, Waterfront Campus, European Way, Southampton, United Kingdom. SO14 F5D

[2]University of Sheffield - Department of Animal and Plant Sciences, Alfred Denny Building, Western Bank, Sheffield, United Kingdom. S10 2TN

[3]University of Bergen – Department of Earth Science, Postboks 7803, 5020 Bergen

6.1 Abstract

Fire activity exhibits a strong relationship with rainfall climate across northern Africa during the Last Glacial Cycle (LGC) at Ocean Drilling Program (ODP) Site 658. New fire activity records at Site 658 presented here indicate that this relationship was also present during the Mid-Brunhes (MIS 9-11, 310-450 ka), with both time intervals broadly displaying an increase in fire activity with increasing humidity. This is attributed to precession-forced northward penetrations of the Intertropical Convergence Zone (ITCZ) bringing greater precipitation to northern Africa, allowing larger fuel loads to develop (particularly C_4 grasses) and, if precipitation levels are high enough, an increase in (C_3) woody plants giving a higher ignition success. However, only minor increases in fire activity are observed during the high humidity conditions of the interglacials in the Mid-Brunhes (MIS -9 and -11), consistent with the two most recent major interglacial intervals (MIS -5 and -1). Much larger peaks in fire activity are instead recorded associated with the precessional maxima occurring during times of intermediate glaciation as illustrated by much lower charcoal fluxes during major glacial MIS 11 than minor interglacial MIS 3, despite the two intervals occurring at times of similar insolation forcing. The cause of supressed burning during peak interglacials is unclear but may be at least in part due to the occurrence of a vegetation assemblage where further increases in precipitation suppress, rather than promote, burning. In addition, the similarities in the charcoal

flux trends and absolute values reported during the LGC and the Mid-Brunhes suggests that there is no major anthropogenic influence on North African fire activity during the LGC.

6.2 Introduction

Fire is an important driver of ecological change, particularly in northern Africa, where a strong relationship between fire activity and the hydrological cycle is observed at annual, millennial and orbital scales (Chapter 4 and Chapter 5). Hydrological variations in North Africa are strongly influenced by the extent of seasonal migration of the Intertropical Convergence Zone (ITCZ). Annually this low pressure band of intense rainfall migrates between a summer and winter position (today ~9-2°N respectively)(Schneider et al., 2014)(Figure 6.1) and is ultimately responsible for a strongly seasonal cycle of burning. Burning begins after a brief period of climatic curing early in the dry season (Oct-Nov) at the southern fringes of the Sahara (17°N) and progresses southwards as the ITCZ retreats equatorward (Carmona-Moreno et al., 2005; Cooke et al., 1996; Harrison and Sanchez Goñi, 2010; Stott, 2000). Over longer time scales, interhemispheric temperature asymmetries influence the latitudinal extent of this seasonal migration. During insolation maxima, northwards ITCZ migration during boreal summer is pronounced resulting in the generation of African Humid Periods (AHP), associated with Green Sahara (GS) intervals, when a richly vegetated landscape persisted across the latitudes of the modern Sahara Desert (DeMenocal et al., 2000; Jolly et al., 1998; Ritchie et al., 1985) Collins. During insolation minima, northwards ITCZ migration during summer is less pronounced resulting in aridification over northern African and Sahara expansion southwards (Mulitza et al., 2008; Singarayer et al., 2017). Because North African biomes are unusually precipitation-dependent, these biomes are spatially arranged along latitudinal gradients (Dupont, 2011). Strong temporal change in fire activity is predicted in response to pronounced hydroclimate variability and latitudinal redistribution of flora (Chapter 4 and Chapter 5).

In Northern African biomes, flammability is strongly influenced by the proportion of the grassy (C_4) to woody (C_3) plants, which, in turn, is strongly influenced by both precipitation (Figure 6.1) and fire activity (Chapter 4 and Chapter 5). The combination of rapid regeneration and high-water use-efficiency of grassy (C_4) plants enables them to generate large dry flammable fuel loads (Bond et al., 2005). Woody (C_3) plants have a higher water requirement and produce wetter, less flammable fuels in much smaller amounts (Dupont, 2011; Niedermeyer et al., 2010; Ripley et al., 2010). Frequent burning induces a positive feedback of increasingly arid conditions by promoting the

growth of grassy over woody plants (Beerling and Osborne, 2006; Keeley and Rundel, 2005), therefore dry dominantly grassy ecosystems (<10%) are the most flammable globally but are not the most frequently burnt (Figure 6.1). The addition of a small proportion of woody cover (10-40%)

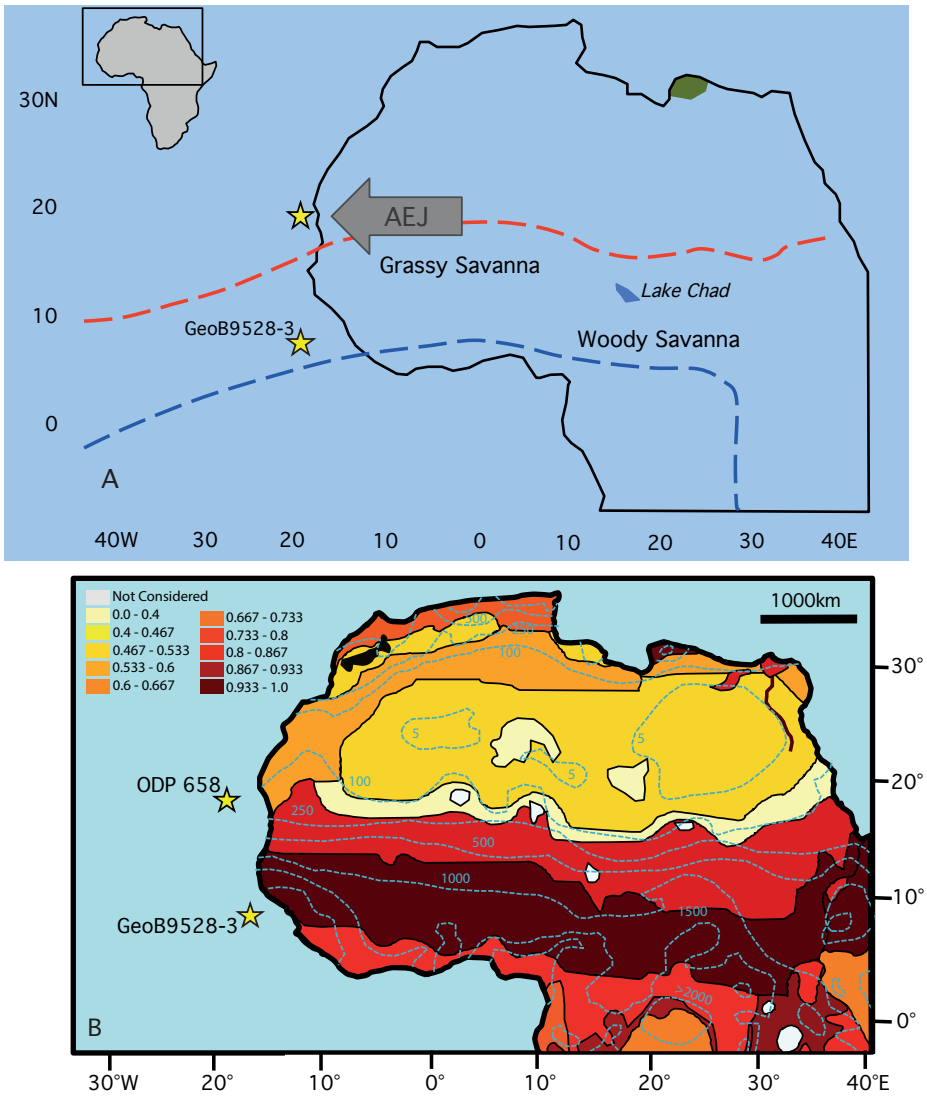

Figure 6.1: ODP Site 658 Map. Position of the African vegetation bands and dominant photosynthetic pathway of each. The modern summer and winter latitudinal position of the ITCZ. Dashed lines show precipitation contours (Larrasoaña *et al.,* 2013). Location of main dust sources and wind direction AEJ: African Easterly Jet. Location of the marine sites, ODP 658 this site was re-drilled by GeoB7920-2. Adapted from (Sarnthien *et al.,* 1998; Gasse *et al.,* 1989; Vallé *et al.,* 2014). Inset: Fire Map annual average number of fires observed by satellite, Black ~0, Dark Blue 1-4, Mid-Blue 5-19, Light Blue 20-49, Green 50-99, Yellow 100-199, Orange 200-499, Red >500 (Taken from Bowman *et al.,* 2009 data from Giglio *et al.,* 2006). B: Fire Activity Map (adapted from Pausas and Ribeiro, 2013) precipitation contours (Larrasoaña *et al.,* 2013).

increases fire activity because the resin-rich bolts associated with woody plants are better converters of lighting into successful ignitions (Beckage and Ellingwood, 2008; D'Onofrio et al., 2018). Infrequent burning in response to greater rainfall promotes the development of moister ecosystems, forest encroachment and potential canopy closure (Bond et al., 2005). Peak fire activity occurs in the wetter or woody savanna (10-40% woody coverage) located in northwestern Africa (15-9°N), which without these regular disturbances would otherwise transition into fully developed forests (Accatino et al., 2010; Sankaran et al., 2005)(Figure 6.2). Anthropogenic burning is also common practice in the savanna region where large human populations rely on subsistence farming and pastoralism and regular burns are employed as a management strategy to produce or maintain agricultural land (Cincotta et al., 2000; Laris and Wardell, 2006; Vierich and Stoop, 1990).

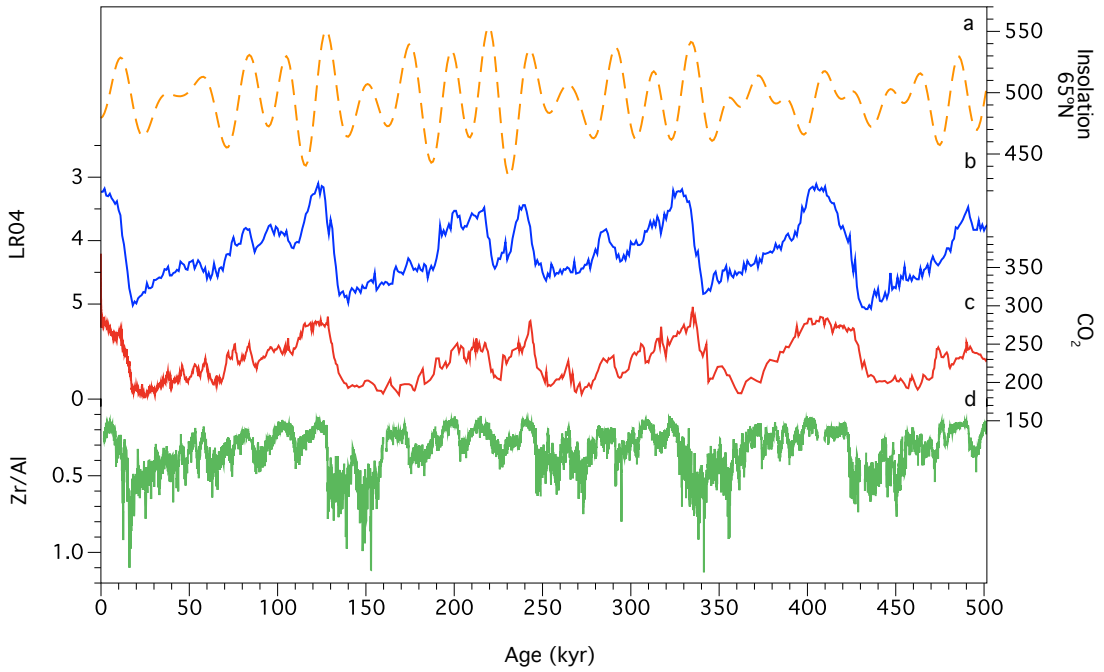

Figure 6.2: Environmental Context for the Last Glacial Cycle and the Mid-Brunhes. a) Insolation 65°N JJA (W/m^2) (Laskar *et al.,* 2004), b) Benthic Oxygen Isotope Stack (Lisiecki and Raymo 2005), c) Composite Ice Core CO_2 (Berieter *et al.,* 2014) and d) Zr/Al (Meckler *et al.,* 2013).

On geological timescales, the flammability of ecosystems at 21°N in northwestern Africa has been shown to have a strong precession signal, linked to the behaviour of the ITCZ (see the fire activity record for the Last Glacial Cycle (LGC)(Chapter 5.Figure 5.3). Periods of elevated fire activity are coupled to intervals of increased precipitation (Chapter 5. Figure 5.3) when the ITCZ penetrated furthest north during African Humid Periods (AHP) and GS intervals (Claussen and Gayler, 1997; DeMenocal et al., 2000; Ritchie et al., 1985). Intervals of fire activity minima at this latitude are associated with arid glacial periods (Chapter 5. Figure 5.3) when the Sahara Desert expanded

southwards associated with dampened seasonal latitudinal migration of the ITCZ (Dupont and Hooghiemstra, 1989; Lézine et al., 2011).

The aim of the investigation presented in this chapter is to examine the relationship between fire activity and hydroclimate at Ocean Drilling Program (ODP) Site 658 (Figure 6.1) during the Mid-Brunhes time interval (300-450 kyrs). Marine sediment cores provide an opportunity to examine palaeo-archives that have the advantage of being longer, more continuous and have good age control suffering from only minimal disturbance than is typically available on land. Correlation of terrestrial and marine proxy records with my new charcoal records enable us to better understand the role of fire within the Earth system.

The Mid-Brunhes was targeted because it presents an opportunity to investigate fire activity during the longest and warmest interval of the last 500 kyrs (Marine Isotope Stage, MIS, 11) that predates any proposed anthropogenic influence (Figure 6.2).

6.3 Materials and Methods

ODP site 658 is situated proximal and downwind of the North African Savanna (NAS) which experience the highest global fire activity (Figure 6.1) in the tropical North Atlantic Ocean ~160 km offshore Mauritania on the continental shelf (Figure 6.1)(20°44.95'N, 18°34.85'W at water depth 2200m). The site location, below a high productivity cell gives rise to high sedimentation rates (10-24 cm/kyr) and high Total Organic Carbon (TOC) values (0.5-4%)(Stein et al., 1989), promoting charcoal preservation owing to the rapid burial reduced exposure to biota and oxic conditions

Samples from ODP site 658 were processed using the same methodology detailed in Chapter 3 section 2.2.3.2. Briefly, a modified version standard palynological which omitted physical agitation steps were omitted to prevent charcoal fragmentation. A two-step acid treatment to remove the silicate (HF) and carbonate (HCl) fraction was conducted on oven dried sediment. Residual fluoride products and Amorphous Organic Matter (AOM) was removed by boiling in HCl and a combination of ultrasonic treatment and sieving at 15 μm respectively. The >15 μm fraction was spiked with a known dose of the exotic spore *Lycopodium* (Stockmarr, 1971) before mounting and examined under transmitted light. Charcoal particle colour, reflectance and morphological characteristics

(Figure 6.3) were identified using an Olympus BH-2 microscope in conjunction with free standing lamp to distinguish between charcoal and pyrite particles. Concurrent counting of charcoal and *Lycopodium* spores was undertaken until 500 spores was reached, the ratio of charcoal to *Lycopodium* (C:L) was used to calculate charcoal concentrations and fluxes.

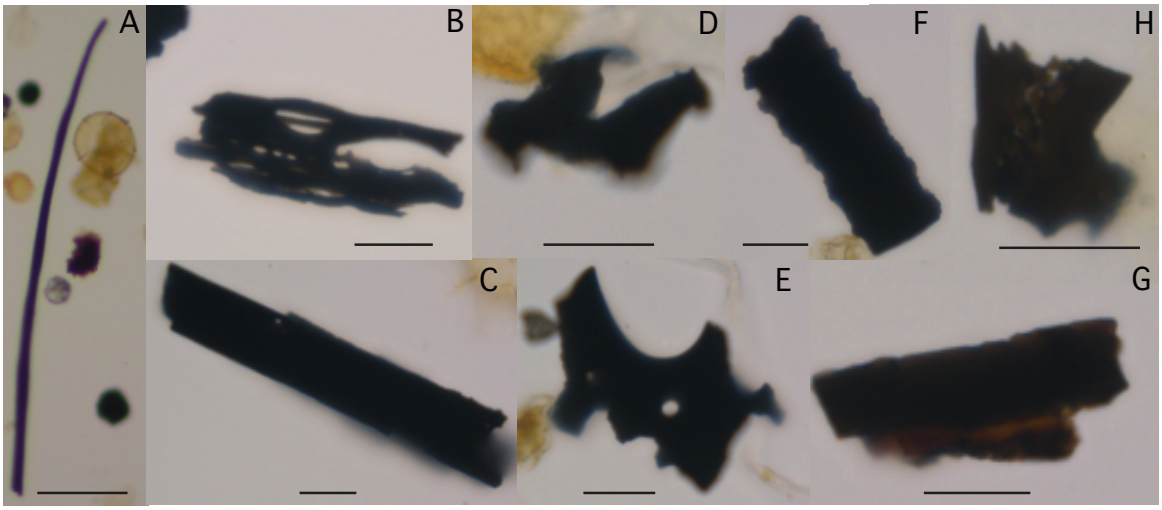

Figure 6.3: Charcoal Morphology. A) Elongate, B) Splintery Perforated, C) Splintery, D) Irregular, E) Irregular Perforated, F) Square/Rectangular, G) Dark Organic Matter, H) Grass. Black bar 20 μm.

To account for variability in the charcoal counts produced between different mounts or varying areas of the slide a reproducibility error of 12.5% is applied to all charcoal flux values (full details Chapter 2 Section 2.2.4.1.). However, the overall trends in the data are more instructive than the exact numbers, examination of variability greater than the error associated with the counts is indicative of natural forcing mechanisms.

6.3.1 Chronology

The chronology used is a slightly modified version of the published age-depth model of Meckler *et al.*, (2013), which was generated by tuning $\delta^{18}O_{benthic}$ data from ODP 658 on a revised composite depth scale to the LR04 stack (Lisiecki and Raymo, 2005). For the last 120 kyr, age was refined by i) matching XRF-derived Ca from Hole 658A to $\%CaCO_3$ in radiocarbon-dated Hole 658C (DeMenocal et al., 2000) and ii) tuning ln(Zr/Al) data from ODP 658 (grain size proxy) to the grain size-based humidity index from nearby core GeoB7920-2 (Tjallingii *et al.*, 2008; Meckler *et al.*, Unpublished).

6.4 Results and Discussion

The record of charcoal flux presented in this chapter shows a number of similarities to the pattern reported from the same site for the last glacial cycle (LGC)(Figure 6.4). Also captured is a potentially interesting feature during MIS 11 where a strong peak in burning at the interglacial termination is resolved (Figure 6.4). Fire activity is highest during precession-paced peaks in insolation that fall within intervals of intermediate glaciation, particularly between 40 and 110 ka and between 350-400 ka in the Mid-Brunhes (Figure 6.4). Intervals of muted fire activity consistently coincide with the wettest and driest intervals recorded in these records. Glacial maxima (MIS -2, -6, -10 & -12) are consistently associated with minima in charcoal flux $2x10^4$ (charcoal cm^2/kyr). Peak interglacials (MIS -1, -5, -9 & -11) trends in charcoal flux are also remarkably similar, fire activity only reaches modest peaks compared to the fire activity observed in the intermediately glaciated states which are twice as large (Figure 6.4). These observations suggest that the inflected relationship between North African fire activity and rainfall climate inferred at ODP site 658 is not peculiar to the LGC (Chapter 4). It also suggests that fire activity is most sensitive to rainfall climate during period of intermediate glaciation.

The influence of precession-paced insolation forcing on vegetation, dust and charcoal flux records for site 658 differs between the LGC and the Mid-Brunhes (Figure 6.4). The LGC displays a clear dominant set of precession cycles in both the dust and charcoal flux records and to a lesser extent the vegetation records (Figure 6.4). Whereas, the relationship between charcoal and dust flux to precession-paced insolation forcing is less consistent during the mid-Brunhes (Figure 6.4).

6.4.1 Low fire activity during peak glacial conditions

Fire activity consistently reaches low values during the glacial maxima of the LGC and the Mid-Brunhes. During glacials the North African aridity increases and the Sahara Desert expands southwards (Dupont, 2011). High dust flux, loss of woody taxa and an increase in desert specific pollen taxa (*Caryphyllaceae, Chenopodiaceae, Amaranthaceae,* CCA) combined with an overall reduction in pollen influx to ODP site 658 (Dupont, 2011)(Figure 6.4), suggests a retraction in vegetation cover and fuel for fires.

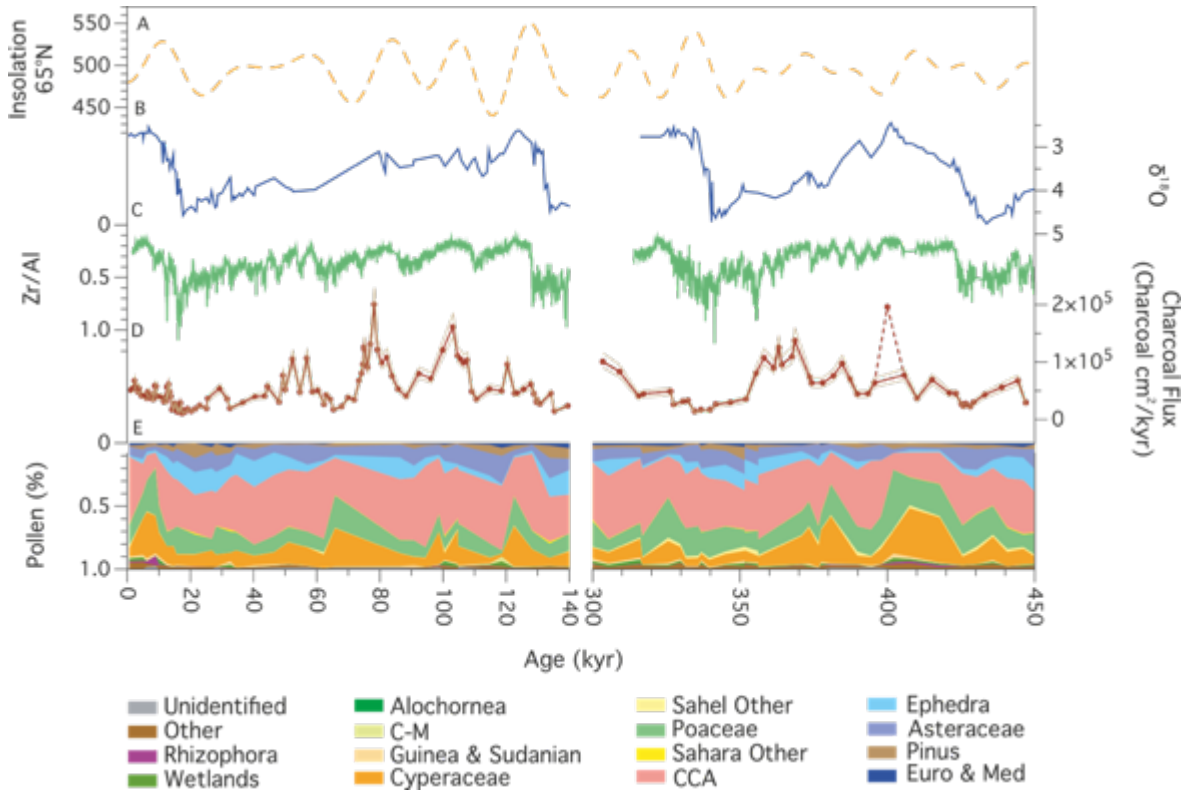

Figure 6.4: Comparison plot between the Last Glacial Cycle and the Mid-Brunhes. A) Insolation 65°N (JJA) (Laskar *et al.,* 2004), B) Oxygen isotope (LGC: Knaack and Sarnthein, 2005; Sarnthein *et al.,* 1989, Mid-Brunhes: Bird and Cali, 2002), C) Zr/Al, D) Charcoal Flux (this study)(error of 12.5% shown in light brown), E) Pollen % of sample (Dupont *et al.,* 1989). C-M *Combretaceae-Melastomataceae.* CCA = *Caryophyllaceae, Chenopodiaceae & Amaranthaeceae*). Dotted line shows the trend of the fire activity taking into account one outlier data point at ~400ka (further testing of this sample is required to ensure its validity).

6.4.2 Variability in the strength of the precession-paced hydroclimate forcing of fire activity

An intriguing result to emerge from the data presented herein is the observed peak in fire sensitivity to precession-paced insolation forcing under intermediate glacial boundary conditions (Figure 6.4). During these intervals, it is inferred that, the elevated humidity during insolation peaks drove increases in Net Primary Productivity (NPP) and the generation of large fuel sources capable of supporting higher fire activity (Daniau et al., 2010; Hoetzel et al., 2013; Keeley and Rundel, 2005; Lehmann et al., 2014; Moritz et al., 2012; Turner et al., 2008). During major interglacials, fire activity is far less responsive to insolation forcing. This observation strongly implies a non-linear relationship between fire activity and rainfall climate.

The moisture-driven increase in fire activity hypothesis is rooted in two observations from modern north African biomes/ecosystems. The first is that elevated fire activity occurs following years of increased rainfall (Archibald et al., 2009), and secondly the highest modern fire activity occurs in the woody savanna in north west Africa within an optimum precipitation range (1000-1500 mm/yr Mean Annual Precipitation (MAP)). The NAS is a mixture of two savanna types, the highest fire activities are associated with the woody savanna (600->1000 mm/yr MAP, climate and disturbance-maintained) and grassy savanna (100-600 mm/yr MAP)(Accatino et al., 2010; Sankaran et al., 2005). The hyper-arid, vegetation sparse Sahara Desert is the dominant biome at 21°N (latitude of ODP site 658), however, under AHP conditions an environment similar to the modern woody savannas is assumed to develop at this latitude. An environment similar to the modern woody savanna is hypothesized in terms of relative proportions of grassy to woody plants, because the African woody savanna exhibits the highest modern fire activity (Figure 6.1).

The periods of highest fire activity observed in the records presented herein are closely associated with peaks in northern hemisphere insolation (Figure 6.5) and can, to a first order, be understood as a response to displacement of the ITCZ northward leading to the development of an African Humid Period (AHP) (Kleinen et al., 2014; Larrasoaña et al., 2013; Rohling et al., 2015). Precipitation delivery to the Sahara region is significantly increased activating ephemeral river systems draining the Sahara (Drake et al., 2011; El-Shenawy et al., 2018; Scerri et al., 2016; Skonieczny et al., 2015) and increasing freshwater run-off and sapropel deposition in the Mediterranean (Rohling et al., 2015). The higher availability of water supported major increases in NPP in this region and the development of a richly vegetated mosaic landscape capable of supporting megafauna including elephant, giraffe, crocodiles and fish (Barnett, 2002; di Lernia and Gallinaro, 2010; Dumont, 2017; Gallinaro, 2013) and during the most recent GSP during MIS 1 human settlements, as detailed by rock art and carvings in the central Sahara dating to ca 10 ka (Barnett, 2002; di Lernia and Gallinaro, 2010; Gallinaro, 2013). Yet a straightforward northward migration of the biomes is now considered to be an oversimplification of the GSP vegetation response during AHP because the migration rates of individual plant taxa vary widely (150-740 m/yr) meaning that plant species respond uniquely to climate change rather than as a community (Hély et al., 2009; Watrin et al., 2009). Humid woody taxa are identified 4-9° north of their modern position to co-exist with arid and desert taxa typically entering as gallery forests around permanent water bodies (Hély et al., 2014), producing a non-analogous floral assemblage (Hély et al., 2009; Watrin et al., 2009) presumably capable of generating large flammable fuel source. Vegetation modelling of MIS 11 also indicates that

xerophytic shrubland increases at the expense of desert, particularly in the CLIMBER2-biome at 410 ka, although the specific floral assemblage is not described (Kleinen et al., 2014).

This more nuanced understanding of the vegetation response to rainfall climate change may go some way to explaining why it is not always the case that an implied increase in fuel loading results in elevated fire activity. This hypothesis is not straightforward to test using the available pollen records because they are of modest temporal resolution and arboreal pollen is typically severely under-represented in marine records because tropical trees are entomorphilous (low pollen producers) and the pollen produced are sticky and resist aeolian transport (Dupont, 1993), whilst *Poaceae* is high pollen producer which is well transported (Julier *et al.,* 2018). Nevertheless, the data sets available indicate a significant loss of Sahara-indicative taxa during MIS 11 while more humid taxa, including grasses and shrubs undergo a rapid expansion suggestive of a smaller Sahara and greater vegetation coverage (425-400 kyr)(Figure 6.4)(Dupont, 2011).

6.4.3 Muted fire activity during peak interglacials

A number of hypotheses were examined in Chapter 5 to explain the muted charcoal response for MIS -1 and -5 during LCG, the same set of hypothesis were considered to identify the cause of the muted fire activity observed for MIS -9 and -11 during the Mid-Brunhes. A lagged vegetation response was ruled as an unlikely cause of low fire activity in MIS 5 and 1 (Chapter 5), and also supported for the Mid-Brunhes as comparisons of modelled biomes distribution and changes in tree cover during MIS 11 (Kleinen et al., 2014) as well as vegetation reconstructions generated by pollen records (Dupont et al., 1989; Dupont and Hooghiemstra, 1989) as no lagged vegetation response is identified. The impact of higher interglacial pCO_2 (20-35 ppmv) (Bereiter et al., 2014; Lüthi et al., 2008) on plant growth, specifically boosting the rates at which "escape height" is reached by C_3 woody plants, resulting in forest encroachment (Bond et al., 2005) and more limited fuel source was also hypothesized to explain the low fire activity during the MIS -5 and -1. Like MIS -5 and -1 however an increase in C_3 plants is not observed in pollen records, or modelled vegetation assemblages across MIS -11 or -9 (Dupont, 2011, 1993; Kleinen et al., 2014).

Finally, a "too-wet-to-burn" scenario was hypothesized for MIS -5 and -1, implying this scenario for MIS -11 and -9 however is difficult because of larger uncertainty in precipitation estimates. The ITCZ is suggested to have penetrated to at least 21°N, and the Sahara-Sahel boundary migrates to

~24°N during both MIS -11 and -9 directly comparable to MIS -5 and -1. Like the LGC modelled precipitation estimates for the Mid-Brunhes display considerable discrepancies, an increase of 50-600 mm/yr above pre-industrial levels (model dependent – average 180mm/yr), rainfall values are therefore also comparable to the LGC interglacial precipitation values (Herold and Lohmann, 2009; Larrasoaña, Roberts and Rohling, 2013 and references therein; Nikolova *et al.*, 2013; Kleinen *et al.*, 2014). Precipitation estimates for the Mid-Brunhes are lower than threshold values (1100-2000 mm/yr MAP) of rainfall observed in modern systems at which fire is initially significantly supressed (Accatino et al., 2010; Staver et al., 2011a; Stott, 2000). Model estimates of rainfall however, are currently inconsistent with vegetation reconstructions (e.g Hopcroft *et al.*, 2017), there is therefore potential for rainfall to have been higher than currently estimated during AHPs. Additionally, pollen records for site 658 across MIS -11 and -9 are far from conclusive to support a "too-wet-to-burn" scenario (Dupont, 2011; Dupont et al., 1989; Dupont and Hooghiemstra, 1989), however biases in the pollen record means that a "too-wet-to-burn" vegetation assemblage can't be discounted.

6.4.4 MIS 11: an unusual interglacial

MIS 11 is a complex multi-stage interglacial (Candy et al., 2014) that is unusually warm for the Late Pleistocene, but associated with only modest insolation peaks, more akin to those associated with MIS 3 (Figure 6.5)(Capotondi et al., 2014; Kleinen et al., 2014; Laskar et al., 2004). Thus, a comparison of records for MIS -1, -3, -5e, -9 and -11 provides a way to explore the relative importance of glacial state versus insolation forcing on the muted fire activity observed during these interglacials (Laskar et al., 2004)(Figure 6.5). The charcoal records presented herein show that fire activity in North Africa during MIS 11 is more akin to that documented for pronounced interglacials MIS -1, -5e and -9, than to MIS 3, strongly suggesting that glacial state exerts an important influence on fire activity (Figure 6.5).

6.4.5 A fire activity peak associated with the MIS 11 termination?

A peak in fire activity is suggested by a singular data point is observed in the Mid-Brunhes, shown by the dotted line at 400 ka at the termination of the MIS 11 interglacial (Figure 6.5). Unfortunately, due to time restraints the reproducibility of the peak could not be verified by recounts, reprocessing or additional sampling. It must be conceded that the unexpectedly high charcoal flux values in this single sample might result from contamination during processing or potentially originate from an incorrect *Lycopodium* dose (half the expected *Lycopodium* dose effectively appears to double the

calculated charcoal flux). However, the timing of the peak relative to the other climatic proxies recorded at ODP site 658 is intriguing (Figure 6.5).

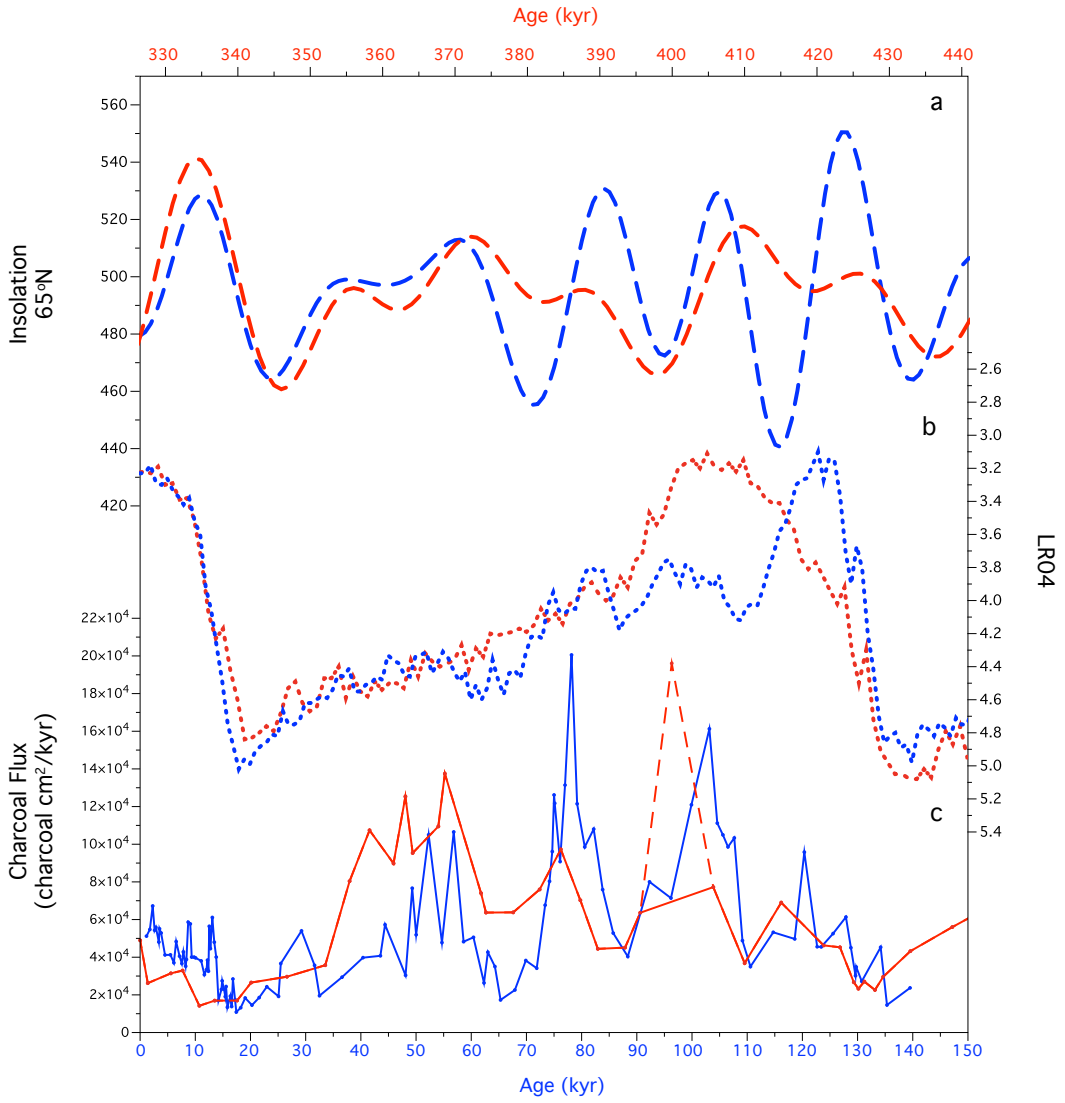

Figure 6.5: Overlay of the Charcoal Flux records from ODP 658 for the Last Glacial Cycle (Blue) and the Mid-Brunhes (Red). a) Insolation 65°N (JJA)(W/m^2) (Laskar *et al.,* 2004), b) LR04 Benthic Oxygen Isotope Stack (Lisiecki and Raymo, 2005), c) Charcoal Flux (this study). Dotted line shows trend to the outlier.

At the termination of the MIS 11 interglacial at *ca.* 400 ka a short slight aridification event is recorded in the dust flux (XRF) record as the decreasing insolation forcing produces a 2° southward shift in the position of the Saharan-Sahelian boundary as the ITCZ migrates towards the equator, crossing below 21°N (latitude of site 658) (Dupont, 2011; Dupont and Hooghiemstra, 1989). Reduction in vegetation coverage is inferred as pollen records indicate a rapid increase in Sahara indicative taxa (Figure 6.4). Tentatively, it is suggested that the interglacial GS-woody savanna type

landscape desiccates at *ca.* 400 ka allowing biomass to climatically cure and aided by woody plant presence increases biome flammability, to facilitate the short-lived period of high fire activity displayed in the charcoal flux record (Figure 6.5). This feature is yet to be resolved at interglacial at MIS -5 and -1 (Chapter 5) as the key termination point is not captured by current sampling, additional targeted sampling at the key interval would perhaps resolve this/a similar feature. The dust record suggests a more minor desiccation event than compared to the pollen record where significant floral turnover is indicated, a very rapid increase in Sahara taxa occurs the latitude of site 658 (Figure 6.4**Error! Reference source not found.**)(Dupont, 2011, 1993; Dupont and Hooghiemstra, 1989; Kleinen et al., 2014; Laskar et al., 2004).

6.4.6 An anthropogenic signature in fire activity at Site 658?

Schreuder *et al.*, (2019) invoke anthropogenic process including use of fire for hunting activities as a cause of increased fire activity between 50-60 ka from their fire biomarker (levoglucosan) record at GeoB9528-3 (Figure 3.9). Yet my records from nearby site 658 show (i) no correlative peak at 50-60 ka, (ii) no anomalous increase during the late Holocene, when we might expect the strongest anthropogenic influence and (iii) absolute values for charcoal flux during the LGC are broadly comparable to those of the Mid-Brunhes. These simple observations call into question the interpretations of Schreuder *et al.*, (2019).

6.5 Conclusions

A strong relationship between fire activity and rainfall regime in Northern Africa was documented in Chapter 4 and Chapter 5. Herein, I report records suggesting that this relationship also existed during the Mid-Brunhes. The over-arching pattern for both intervals is that periods of humidity driven by the northward penetration of the ITCZ sustains large fuel loads (C_4 grasses) and higher ignition success rates (C_3 woody plants), during partially glaciated states. On closer examination, however, a non-linear response between rainfall and fire activity is observed. My data indicates that fire activity increases with rainfall only up to a point. Consistently the wettest intervals in North Africa, the interglacial periods in the LGC and Mid-Brunhes charcoal flux records show modest peaks in fire activity compares to the peaks observed during partially glaciated conditions. The charcoal records presented herein show that fire activity in North Africa during MIS 11 is more akin to that documented for pronounced interglacials MIS -1, -5e and -9, than to MIS 3, strongly suggesting that

glacial state exerts an important influence on fire activity. We find no evidence in support of the suggested anthropogenic influence on North African fire activity during the last glacial cycle.

Chapter 7 Conclusions

In this thesis I have investigated the use of charcoal as a proxy and its robustness for reconstructing fire activity on North Western Africa. It was important to examine the intricacies of the charcoal as a proxy, through my investigations I produced several major findings. Comparing the ODP sites 658, 659 and 668 indicates that charcoal flux production, age, distance were not the cause of the lack of charcoal recovery from site 659. Secondly, the potential that charcoal is not impervious to degradation, oxidation may result in the loss of charcoal in marine geological archives. I suggest that heavy oxidation of the sedimentary column at site 659, suggested by the potential for oxidized iron in the "red beds" identified at this site's sedimentary column, caused charcoal degradation and charcoal loss. This finding led me to question the results of geochemical studies that oxidize sample to reconstruct fire activity, as heavy oxidation is used to extract charcoal. Resultantly, I determined that determined that microscopic methods of charcoal identification are more sensitive than geochemical methods, which potentially induce a loss of charcoal during processing.

The use of the charcoal proxy indicates that fire activity much like in the modern systems is spatially variable over the last 50kyr, this variability is intrinsically linked to changes in the hydrological cycle over both millennial and orbital time scales. Studying a transect of sites (ODP 658 (21°N), GeoB 9508-5 (15°N) and GeoB9528-3 (9°N)) enabled me to reconstruct fire activity over the last 50kyr across a range of ecosystems with differing modern fire activities and thereby gain a spatial overview of past fire activity on northwestern Africa. ODP site 658's longer sedimentary sequence allowed me to construct two records of fire activity, 0-140 kyr and 300-450kyr whose similarity in orbital geometry provided an opportunity to examine the fire activity shifts over orbital and millennial timescales in addition to determining a potential anthropogenic signal in the younger of the two records generated for this site.

Clear latitudinal variability is resolved in fire activity response to hydroclimatic shifts on the North West African Margin over the last 50kyr from examination of the transect. The northern end of the transect (ODP site 658, 21°N), humid conditions produce the highest fire activities, whilst the opposite response is observed at the southern end of the transect (GeoB9528-3, 9°N) peak fire occurring during periods of aridity. The difference in the biomes is attributed to the dramatically different fire activity responses between the two sites.

I postulate that an expansion of flammable grassy savanna into desert regions is driven by increased precipitation at site 658, the lower percentages (10-40%) of woody cover potentially facilitate an increased ignition likelihood if rainfall is sufficiently high, as observed at the end of AHP1 when an increase in C_3 vegetation was supported by ~1000 mm/yr Mean Annual Precipitation (Kuechler et al., 2013; Larrasoaña et al., 2013; Niedermeyer et al., 2010; Wang et al., 2006). Contrastingly, at higher humidity the likely increased woody plant coverage to high proportions at the expense of the more flammable grass biomass at GeoB9528-3, in addition to increasing the moisture content of the fuel, hence suppressing fire activity (Dupont, 2011; Niedermeyer et al., 2010; Ripley et al., 2010).

GeoB9508-5 (15°N) the intermediate latitude site, however, during the wettest (AHP1) and driest (H1-4) interval reduced charcoal fluxes are exhibited, with fire activity reaching maxima during periods of moderate humidity. This I explain by considering the transient nature of the of Sahara-Sahel Boundary, which has shifted north and south over the last 50kyr, to which GeoB9508-5 is proximal. The movement of the Sahara-Sahel boundary is accompanied by major biomes shifts in response to insolation and sea surface temperatures forcing. The high sensitivity of this region to latitudinal shifts in precipitation and thereby vegetation and by extension fuel availability is displayed by strong millennial-scale variability in the fire activity record. Temporal variability in fire activity over thousands of years largely seems to be driven by the same factors as modern spatial variability on the African continent.

Millennial-scale variability in hydrology is also shown to have a clear impact on fire activity during the last deglaciation at ODP site 658, although the smaller amplitude variations are recorded compared to the peaks occurring due to precession forcing. The preceding hydrological regime appears to be the strongest influencer of fire activity in northern Africa across the more rapid climate events resolved in this record. During the dramatic aridification documented at Heinrich Event 1, there is little change in the charcoal flux record, this is attributed to a lack of biomass and therefore fuel sources following on from the expansive desert conditions of the Last Glacial Maxima. The humid conditions of Bølling-Allerød coincide with an increase in fire activity, a short-lived increase in fire activity is registered coincident with a minor dust flux increase, associated with the arid 8.2 ka events, likely resulting from the curing of the abundant vegetation developed during AHP1.

This strong relationship between fire activity and hydrology in Northern Africa fire activity is not limited to the last 50kyrs, my new charcoal flux records for ODP site 659 indicates that this relationship is in effect across both the Last Glacial Cycle (LGC) as well as through the Mid-Brunhes. Consistently a pattern of higher fire activity is recorded during intervals of high humidity, when the Intertropical Convergence Zone (ITCZ) penetrates northwards sustaining large fuel loads (grasses) experiencing high ignition success rate (woody plants). An inflected relationship between rainfall climate and hydrology is however, resolved at closer inspection, increased precipitation only drives elevated fire activity up to a point. The very wettest intervals of the LGC (African Humid Periods (AHPs) -5 and -1) in Northern Africa display modest fire large peaks compared to AHP 3 and 4, the largest peak through the Mid-Brunhes interval during partially glaciated conditions, the exact cause of which is currently not understood and requires further exploration.

7.1 Future Work

Marine charcoal is currently a highly underexploited resource, but charcoal flux records have huge potential to inform on the changing behaviour of fire activity in geological time to enable future fire activity predictions, this is of particular interest to the large populations living in modern fire prone environments, notable in the agriculture dependent populations inhabiting the Sahel.

Marine charcoal has been shown to be a good proxy from which to determine fire activity variability, however very few records of this nature have been produced. Although, the absolute charcoal flux values should not be used and small amplitude variability (<12.5%) in the fire activity cannot be examined due to the internal error associated with charcoal counts, the overall larger scale trends are robust indicated for temporal changes in fire activity.

The production of higher-resolution charcoal flux records to allow for a greater level detail to be examined across climate change at all scales. Increasing the sampling density the records presented here in this work would be highly beneficial in order to examine fire activity response across millennial scale climate variability, specifically suggested are the GeoB9508-5 and GeoB9528-3 records for the Holocene, to further investigate spatial variability of fire activity across B/A, YD and H events as identified in the higher resolution charcoal flux record at ODP 658.

I also propose to increase sampling density at interglacial termination in order to investigate if a short-lived period of burning occurs following the wet interglacial at MIS -9, -5 and -1 conditions to test the finding of the MIS 11 termination at 400 ka. To this end, additional sampling and validation (reprocessing and counting) of the data point falling at 400 ka in the OPD 658 charcoal flux record would also be sensible.

Temporal extension of a number of the presented records would inform more on the spatial variability of fire activity across northwestern Africa, in particular the GeoB9508-5 and GeoB9528-3 charcoal flux records, to examine spatial fire activity response to AHP. In particular looking for co-variance or divergence in the fire activity records as observed during the deglacial and the Holocene. It would also present an opportunity to examine whether the muted fire activity during interglacial identified in the ODP 658 charcoal flux records for the Last Glacial Cycle and the Mid-Brunhes is specific to this site or forms part of a much wider spread pattern of low fire during the wettest intervals on the northwestern African Margin.

A spatial extension of the transect presented in Chapter 4, would also be highly interesting, to develop a better understanding of how different biomes boundaries respond to climate forcing by adding sites at latitudes north of 21°N on the northwest African margin. Extending the transect south across the equator would provide an opportunity to document whether in regions south of the Intertropical Convergence Zone (ITCZ) fire activity remains in phase with the charcoal flux records generated for the transect (Chapter 4) or occur anti-phase as indicated by other burning record in south Africa (Daniau et al., 2013; Hoetzel et al., 2013).

Connecting the LGM and Mid-Brunhes charcoal flux records presented here for ODP 658 has merit. This would have two benefits one it would provide a long uninterrupted record of burning at ODP 658, it would also cover an interval of time where insolation is unlike the Last Glacial Cycle and Mid-Brunhes which was selected because of similarity to the LGC.

In the wider context, I would like to generate a Late Miocene record of fire activity, specifically across the C_4 grassland expansion event observed, generating charcoal flux records from multiple sites globally would allow the hypothesis that a more active fire cycle drove this floral turnover to

be investigated in more detail. And whether like the C_4 expansion event was subject to regionally specific conditions including fire activity.

In the wider scientific context in order to better understand the inflected relationship between fire activity and high rainfall, it would be useful to have a greater agreement between the model and pollen derived rainfall estimates during interglacials. The generation of new high resolution palaeo-preciptation proxy records to be used in model parameters, would in some part, aid in the resolving the current discrepancies.

The generation of more biomarkers derived records of fire activity would also be interesting. Particularly it would be instructive to compare biomarker results to the optically derived fire activity records presented here, particularly for ODP 659 to see if a different method of "charcoal' identification could produce a record of fire activity for this site.

List of References

Accatino, F., De Michele, C., Vezzoli, R., Donzelli, D., Scholes, R.J., 2010. Tree-grass co-existence in savanna: Interactions of rain and fire. J. Theor. Biol. 267, 235–242. https://doi.org/10.1016/j.jtbi.2010.08.012

Adkins, J., DeMenocal, P., Eshel, G., 2006. The "African humid period" and the record of marine upwelling from excess 230 Th in Ocean Drilling Program Hole 658C. Paleoceanography 21, PA4203. https://doi.org/10.1029/2005PA001200

Aldersley, A., Murray, S., Cornell, S., 2011. Global and regional analysis of climate and human drivers of wildfire. Sci. Total Environ. 409, 3472–3481. https://doi.org/10.1016/j.scitotenv.2011.05.032

Alley, R., Mayewski, P., Sowers, T., Stuiver, M., Taylor, K., Clark, P., 1997. Holocene climatic instability: A prominent, widespread event 8200 yr ago. Geology 25, 483–486. https://doi.org/10.1130/0091-7613(1997)025<0483:HCIAPW>2.3.CO;2

Alley, R.B., Ágústsdóttir, A.M., 2005. The 8k event: cause and consequences of a major Holocene abrupt climate change. Quat. Sci. Rev. 24, 1123–1149. https://doi.org/10.1016/j.quascirev.2004.12.004

Andreae, M.O., Rosenfeld, D., Artaxo, P., Costa, A.., Frank, G.., Longo, K.., Silva-Dias, M.A.., 2004. Smoking rain clouds over the Amazon. Science (80-.). 303, 1337–1342.

Arbuszewski, J.A., deMenocal, P.B., Cléroux, C., Bradtmiller, L., Mix, A., 2013. Meridional shifts of the Atlantic intertropical convergence zone since the Last Glacial Maximum. Nat. Geosci. 6, 959–962. https://doi.org/10.1038/ngeo1961

Archibald, S., Hempson, G.P., 2016. Competing consumers: Contrasting the patterns and impacts of fire and mammalian herbivory in Africa. Philos. Trans. R. Soc. B Biol. Sci. 371, 20150309. https://doi.org/10.1098/rstb.2015.0309

Archibald, S., Lehmann, C.E.R., Gómez-Dans, J.L., Bradstock, R.A., 2013. Defining pyromes and global syndromes of fire regimes. PNAS 110, 6442–6447. https://doi.org/10.1073/pnas.1211466110/-/DCSupplemental.www.pnas.org/cgi/doi/10.1073/pnas.1211466110

Archibald, S., Roy, D.P., van Wilgen, B.W., Scholes, R.J., 2009. What limits fire? An examination of drivers of burnt area in Southern Africa. Glob. Chang. Biol. 15, 613–630.

https://doi.org/10.1111/j.1365-2486.2008.01754.x

Archibald, S., Staver, A., Levin, S., 2012. Evolution of human-driven fire regimes in Africa. Proc. Natl. Acad. Sci. 109, 847–852. https://doi.org/10.1073/pnas.1118648109

Armitage, S., Bristow, C., Drake, N., 2015. West African monsoon dynamics inferred from abrupt fluctuations of Lake Mega-Chad. Proc. Natl. Acad. Sci. 112, 8543–8548. https://doi.org/10.1073/pnas.1417655112

Ascough, P., Bird, M., Francis, S., 2011. Variability in oxidative degradation of charcoal: influence of production conditions and environmental exposure. Geochim. Cosmochim. Acta 75, 2361–2378. https://doi.org/10.1016/j.gca.2011.02.002

Ascough, P.L., Bird, M.I., Brock, F., Higham, T.F.G., Meredith, W., Snape, C.E., Vane, C.H., 2009. Hydropyrolysis as a new tool for radiocarbon pre-treatment and the quantification of black carbon. Quat. Geochronol. 4, 140–147. https://doi.org/10.1016/j.quageo.2008.11.001

Ascough, P.L., Bird, M.I., Scott, A.C., Collinson, M.E., Cohen-Ofri, I., Snape, C.E., Le Manquais, K., 2010. Charcoal reflectance measurements: Implications for structural characterization and assessment of diagenetic alteration. J. Archaeol. Sci. 37, 1590–1599. https://doi.org/10.1016/j.jas.2010.01.020

Bar-Matthews, M., Ayalon, A., Gilmour, M., Matthews, A., Hawkesworth, C.J., 2003. Sea-land oxygen isotopic relationships from planktonic foraminifera and speleothems in the Eastern Mediterranean region and their implication for paleorainfall during interglacial intervals. Geochim. Cosmochim. Acta 67, 3181–3199. https://doi.org/10.1016/S0016-7037(02)01031-1

Barker, S., Knorr, G., Vautravers, M., Diz Ferreiro, P., Skinner, L., 2010. Extreme deepening of the Atlantic overturning circulation during deglaciation. Nat. Geosci. 3, 567–571. https://doi.org/10.1038/NGEO921

Barnett, T., 2002. Rock-art , landscape and cultural transition in the Wadi al-Ajal , Fazzan. Libyan Stud. 33, 71–84.

Beckage, B., Ellingwood, C., 2008. Fire feedbacks with vegetation and alternative stable states. Complex Syst. 18, 159–173.

Beckage, B., Platt, W.J., Gross, L.J., 2009. Vegetation, Fire, and Feedbacks: A Disturbance-Mediated Model of Savannas. Am. Nat. 174, 805–818. https://doi.org/10.1086/648458

Beerling, D.J., Osborne, C.P., 2006. The origin of the savanna biome. Glob. Chang. Biol. 12, 2023–2031. https://doi.org/10.1111/j.1365-2486.2006.01239.x

Belcher, C.., McElwain, J.., 2008. Limits for Combustion in Low O2 Redfine Paleoatmospheric Predictions for the Mesozoic. Science (80-.). 321, 1197–1201.

Belcher, Claire M., Mander, L., Rein, G., Jervis, F.X., Haworth, M., Hesselbo, S.P., Glasspool, I.J., McElwain, J.C., 2010. Increased fire activity at the Triassic/Jurassic boundary in Greenland due to climate-driven floral change. Nat. Geosci. 3, 426–429. https://doi.org/10.1038/ngeo871

Belcher, Claire M, Yearsley, J.M., Hadden, R.M., McElwain, J.C., Rein, G., 2010. Baseline intrinsic flammability of Earth's ecosystems estimated from paleoatmospheric oxygen over the past 350 million years. Proc. Natl. Acad. Sci. U. S. A. 107, 22448–53. https://doi.org/10.1073/pnas.1011974107

Bereiter, B., Eggleston, S., Schmitt, J., Nehrbass-Ahles, C., Stocker, T.F., Fischer, H., Kipfstuhl, S., Chappellaz, J., 2014. Revision of the EPICA Dome C CO2 record from 800 to 600 kyr before present. Geophys. Res. Lett. 42, 542–549. https://doi.org/10.1002/2014GL061957

Bird, M.I., Ascough, P.L., 2012. Isotopes in pyrogenic carbon: A review. Org. Geochem. 42, 1529–1539. https://doi.org/10.1016/j.orggeochem.2010.09.005

Bird, M.I., Cali, J.A., 2002. A revised high-resolution oxygen-isotope chronology for ODP-668B: Implications for Quaternary biomass burning in Africa. Glob. Planet. Change 33, 73–76. https://doi.org/10.1016/S0921-8181(02)00062-0

Bird, M.I., Cali, J.A., 1998. A million-year record of fire in sub-Saharan Africa. Nature 394, 767–769.

Bird, M.I., Gröcke, D.R., 1997. Determination of the abundance and carbon isotope composition of elemental carbon in sediments. Geochim. Cosmochim. Acta 61, 3413–3423.

Bistinas, I., Harrison, S.P., Prentice, I.C., Pereira, J.M.C., 2014. Causal relationships versus emergent patterns in the global controls of fire frequency. Biogeosciences 11, 5087–5101. https://doi.org/10.5194/bg-11-5087-2014

Bobe, R., 2006. The evolution of arid ecosystems in eastern Africa. J. Arid Environ. 66, 564–584. https://doi.org/10.1016/j.jaridenv.2006.01.010

Bond, G.C., Showers, W., Elliot, M., Evans, M., Lotti, R., Hajdas, I., Bonani, G., Johnson, S., 1999. The North Atlantic's 1-2kyr Climatic Rhythm: Relation to Heinrich Events,

Dansgaard/Oeschger Cycles and the Little Ice Age. Geophys. Monogr. 112, 35–58. https://doi.org/10.1029/GM112

Bond, W.., Midgley, G.., 2000. A proposed CO2-controlled mechanism of woody plant invasion in grasslands and savannas. Glob. Chang. Biol. 6, 865–869.

Bond, W.J., 2015. Fires in the Cenozoic: a late flowering of flammable ecosystems. Front. Plant Sci. 5, 1–11. https://doi.org/10.3389/fpls.2014.00749

Bond, W.J., 2008. What Limits Trees in C4 Grasslands and Savannas? Annu. Rev. Ecol. Evol. Syst. 39, 641–659. https://doi.org/10.1146/annurev.ecolsys.39.110707.173411

Bond, W.J., Midgley, G.F., Woodward, F.I., 2003. The importance of low atmospheric CO2 and fire in promoting the spread of grasslands and savannas. Glob. Chang. Biol. 9, 973–982. https://doi.org/10.1046/j.1365-2486.2003.00577.x

Bond, W.J., Woodward, F.I., Midgley, G.F., 2005. The global distribution of ecosystems in a world without fire. New Phytol. 165, 525–538.

Boom, A., Marchant, R., Hooghiemstra, H., Sinninghe Damsté, J.S., 2002. CO2- and temperature-controlled altitudinal shifts of C4- and C3-dominated grasslands allow reconstruction of palaeoatmospheric pCO2. Palaeogeogr. Palaeoclimatol. Palaeoecol. 177, 151–168. https://doi.org/10.1093/jxb/eru155

Bouimetarhan, I., Dupont, L., Schefuß, E., Mollenhauer, G., Mulitza, S., Zonneveld, K., 2009. Palynological evidence for climatic and oceanic variability off NW Africa during the late Holocene. Quat. Res. 72, 188–197. https://doi.org/10.1016/j.yqres.2009.05.003

Bouimetarhan, I., Prange, M., Schefuß, E., Dupont, L., Lippold, J.J.J., Mulitza, S., Zonneveld, K., Schefu??, E., Dupont, L., Lippold, J.J.J., Mulitza, S., Zonneveld, K., 2012. Sahel megadrought during Heinrich Stadial 1: Evidence for a three-phase evolution of the low- and mid-level West African wind system. Quat. Sci. Rev. 58, 66–76. https://doi.org/10.1016/j.quascirev.2012.10.015

Bowman, D.M.J.S., Balch, J., Artaxo, P., Bond, W.J., Cochrane, M.A., D'Antonio, C.M., Defries, R., Johnston, F.H., Keeley, J.E., Krawchuk, M.A., Kull, C.A., Mack, M., Moritz, M.A., Pyne, S., Roos, C.I., Scott, A.C., Sodhi, N.S., Swetnam, T.W., 2011. The human dimension of fire regimes on Earth. J. Biogeogr. 38, 2223–2236. https://doi.org/10.1111/j.1365-2699.2011.02595.x

Bowman, D.M.J.S., Balch, J.K., Artaxo, P., Bond, W.J., Carlson, J.M., Cochrane, M.A., D'Antonio,

C.M., DeFries, R.S., Doyle, J.C., Harrison, S.P., Johnston, F.H., Keeley, J.E., Krawchuk, M.A., Kull, C.A., Marston, J.B., MaxA.Moritz, Prentice, I.C., Roos, C.I., Scott, A.C., Swetnam, T.W., Werf, G.R. van der, Pyne, S.J., 2009. Fire in the Earth System. Science (80-.). 324, 481–484. https://doi.org/10.1126/science.1163886

Braconnot, P., Otto-Bliesner, B., Harrison, S., Joussaume, S., Peterchmitt, J.-Y., Abe-Ouchi, A., Crucifix, M., Driesschaert, E., Fichefet, T., Hewitt, C.D., Kageyama, M., Kitoh, A., Loutre, M.-F., Marti, O., Merkel, U., Ramstein, G., Valdes, P., Weber, L., Yu, Y., Zhao, Y., 2007. Results of PMIP2 coupled simulaitons of the Mid-Holocene and Last Glacial Maximum - Part 2: feedback with emphasis on the location of the ITCZ and mid- and high latitudes heat budget. Clim. Past 3, 279–296. https://doi.org/10.5194/cp-3-279-2007

Bradtmiller, L.I., McGee, D., Awalt, M., Evers, J., Yerxa, H., Kinsley, C.W., DeMenocal, P.B., 2016. Changes in biological productivity along the northwest African margin over the past 20,000 years. Paleoceanography 31, 1–18. https://doi.org/10.1002/2015PA002862

Broecker, W., Bond, G., Klas, M., Clark, E., McManus, J., 1992. Origin of the northern Atlantic's Heinrich events. Clim. Dyn. 6, 265–273. https://doi.org/10.1007/BF00193540

Broecker, W.S., Putnam, A.E., 2013. Hydrologic impacts of past shifts of Earth's thermal equator offer insight into those to be produced by fossil fuel CO2. Proc. Natl. Acad. Sci. U. S. A. 110, 16710–5. https://doi.org/10.1073/pnas.1301855110

Bruun, S., Jensen, E.S., Jensen, L.S., 2008. Microbial mineralization and assimilation of black carbon: Dependency on degree of thermal alteration. Org. Geochem. 39, 839–845. https://doi.org/10.1016/j.orggeochem.2008.04.020

Bucini, G., Hanan, N.P., 2007. A continental-scale analysis of tree cover in African savannas. Glob. Ecol. Biogeogr. 16, 593–605. https://doi.org/10.1111/j.1466-8238.2007.00325.x

Candy, I., Schreve, D.C., Sherriff, J., Tye, G.J., 2014. Marine Isotope Stage 11: Palaeoclimates, palaeoenvironments and its role as an analogue for the current interglacial. Earth-Science Rev. 128, 18–51. https://doi.org/10.1016/j.earscirev.2013.09.006

Capotondi, A., Wittenberg, A., Newman, M., Di Lorenzo, E., Yu, J.-Y., Braconnot, P., Cole, J., Dewitte, B., Giese, B., Guilyardi, E., Jin, F.-F., Karnauskas, K., Lee, T., Schneider, N., Xue, Y., Yeh, S.-W., 2014. Understanding ENSO Diversity. Bull. Am. Meteorol. Soc. 96, 921–938. https://doi.org/10.1175/bams-d-13-00117.1

Carmona-Moreno, C., Belward, A., Malingreau, J.P., Hartley, A., Garcia-Alegre, M., Antonovskiy,

M., Buchshtaber, V., Pivovarov, V., 2005. Characterizing interannual variations in global fire calendar using data from Earth observing satellites. Glob. Chang. Biol. 11, 1537–1555. https://doi.org/10.1111/j.1365-2486.2005.01003.x

Castaneda, I.S., Mulitza, S., Schefuß, E., Lopes, R.A., Damste, J.S.S., Schouten, S., Castañeda, I.S., Mulitza, S., Schefuß, E., Lopes dos Santos, R.A., Sinninghe Damsté, J.S., Schouten, S., Castaneda, I.S., Mulitza, S., Schefuß, E., Lopes, R.A., Damste, J.S.S., Schouten, S., 2009. Wet phases in the Sahara/Sahel region and human migration patterns in North Africa. Proc. Natl. Acad. Sci. U. S. A. 106, 20159–63. https://doi.org/10.1073/pnas.0905771106

Cerling, T.E., 1992. Development of grasslands and savannas in East Africa during the Neogene. Palaeogeogr. Palaeoclimatol. Palaeoecol. 97, 241–247.

Cerling, T.E., Harris, J.M., Macfadden, B.J., Leakey, M.G., Quadek, J., Eisenmann, V., Ehleringer, J.R., 1997. Global vegetation change through the Miocene/Pliocene boundary. Nature 389, 153–158.

Cerling, T.E., Wang, Y., Quade, J., 1993. Expansion of C4 ecosystems as an indicator of global ecological change in the late Miocene. Nature 361, 344–345.

Cincotta, R.P., Wisnewski, J., Engelman, R., 2000. Human population in the biodiversity hotspots. Lett. to Nat. 404, 990–992. https://doi.org/10.1038/35010105

Clark, J.S., 1988. Particle Motion and the Theory of Charcoal Analysis: Source Area, Transport, Deposition, and Sampling. Quat. Res. 30, 67–80. https://doi.org/10.1016/0033-5894(88)90088-9

Claussen, M., Gayler, V., 1997. The Greening of the Sahara during the Mid-Holocene: Results of an Interactive Atmosperic-Biome Model. Glob. Ecol. Biogeogr. Lett. 6, 369–377.

Cochrane, M.A., 2003. Fire science for rainforests. Nature 421, 913–919.

Cohen, A.S., Stone, J.R., Beuning, K.R., Park, L.E., Reinthal, P.N., Dettman, D., Scholz, C.A., Johnson, T.C., King, J.W., Talbot, M.R., Brown, E.T., Ivory, S.J., 2007. Ecological consequences of early Late Pleistocene megadroughts in tropical Africa. Proc. Natl. Acad. Sci. 104, 16422–16427. https://doi.org/10.1073/pnas.0703873104

Cole, J.M., Goldstein, S.L., DeMenocal, P.B., Hemming, S.R., Grousset, F.E., 2009. Contrasting compositions of Saharan dust in the eastern Atlantic Ocean during the last deglaciation and African Humid Period. Earth Planet. Sci. Lett. 278, 257–266. https://doi.org/10.1016/j.epsl.2008.12.011

Collins, J., Govin, A., Mulitza, S., Heslop, D., Zabel, M., Hartmann, J., Röhl, U., Wefer, G., 2013. Abrupt shifts of the Sahara-Sahel boundary during Heinrich stadials. Clim. Past 9, 1181–1191. https://doi.org/10.5194/cp-9-1181-2013

Collins, J., Schefuß, E., Heslop, D., Mulitza, S., Prange, M., Zabel, M., Tjallingii, R., Dokken, T., Huang, E., Mackensen, A., Schulz, M., Tian, J., Zarriess, M., Wefer, G., 2010. Interhemispheric symmetry of the tropical African rainbelt over the past 23,000 years. Nat. Geosci. 4, 42–45. https://doi.org/10.1038/ngeo1039

Colombaroli, D., Ssemmanda, I., Gelorini, V., Verschuren, D., 2014. Contrasting long-term records of biomass burning in wet and dry savannas of equatorial East Africa. Glob. Chang. Biol. 20, 2903–2914. https://doi.org/10.1111/gcb.12583

Conedera, M., Tinner, W., Nefi, C., Meurer, M., Dickens, A.., Krebs, P., 2009. Reconstructing past fire regimes: methods, applications, and relevance to fire management and conservation. Quat. Sci. Rev. 28, 555–576. https://doi.org/10.1016/j.quascirev.2008.11.005

Cooke, W.F., Koffi, B., Grégoire, J.-M., 1996. Seasonality of vegetation fires in Africa from remote sensing data and application to a global chemistry model. J. Geophys. Res. Atmos. 101, 21051–21065. https://doi.org/10.1029/96JD01835

Cope, M.J., Chaloner, W.., 1980. Fossil charcoal as evidence of past atmospheric composition. Nature 283, 647–649.

Crawford, A.J., Belcher, C.M., 2014. Charcoal morphometry for paleoecological analysis: The effects of fuel type and transportation on morpholocial parameters. Appl. Plant Sci. 2, 1400004. https://doi.org/10.3732/apps.1400004

Czimczik, C.I., Preston, C.M., Schmidt, M.W.I., Werner, R.A., Schulze, E., 2002. Effects of charring on mass, organic carbon, and stable carbon isotope composition of wood. Org. Geochem. 33, 1207–1223.

D'Onofrio, D., von Hardenberg, J., Baudena, M., 2018. Not only trees: Grasses determine African tropical biome distributions via water limitation and fire. Glob. Ecol. Biogeogr. 1–12. https://doi.org/10.1111/geb.12735

Damnati, B., 2000. Holocene lake records in the Northern Hemisphere of Africa. J. African Earth Sci. 31, 253–262. https://doi.org/10.1016/S0899-5362(00)00089-0

Daniau, A.-L., Sánchez Goñi, M.F., Martinez, P., Urrego, D.H., Bout-Roumazeilles, V., Desprat, S., Marlon, J.R., 2013. Orbital-scale climate forcing of grassland burning in southern Africa. Proc.

Natl. Acad. Sci. U. S. A. 110, 5069–73. https://doi.org/10.1073/pnas.1214292110

Daniau, A.L., Harrison, S.P., Bartlein, P.J., 2010. Fire regimes during the Last Glacial. Quat. Sci. Rev. 29, 2918–2930. https://doi.org/10.1016/j.quascirev.2009.11.008

Daniau, A.L., Sánchez-Goñi, M.F., Beaufort, L., Laggoun-Défarge, F., Loutre, M.F., Duprat, J., 2007. Dansgaard-Oeschger climatic variability revealed by fire emissions in southwestern Iberia. Quat. Sci. Rev. 26, 1369–1383. https://doi.org/10.1016/j.quascirev.2007.02.005

Dansgaard, W., Johnsen, S.J., Clausen, H.B., Dahl-Jensen, D., Gundestrup, N.S., Hammer, C.U., Hvidberg, C.S., Steffensen, J.P., Sveinbjörnsdottir, a. E., Jouzel, J., Bond, G., 1993. Evidence for general instability of past climate from a 250-kyr ice-core record. Nature 364, 218–220. https://doi.org/10.1038/364218a0

Das, O., Wang, Y., Hsieh, Y.P., 2010. Chemical and carbon isotopic characteristics of ash and smoke derived from burning of C3 and C4 grasses. Org. Geochem. 41, 263–269. https://doi.org/10.1016/j.orggeochem.2009.11.001

Davis, B.A.S., Stevenson, A.C., 2007. The 8.2 ka event and Early-Mid Holocene forests, fires and flooding in the Central Ebro Desert, NE Spain. Quat. Sci. Rev. 26, 1695–1712. https://doi.org/10.1016/j.quascirev.2007.04.007

De Rouw, A., 2004. Improving yields and reducing risks in pearl millet farming in the African Sahel. Agric. Syst. 81, 73–93. https://doi.org/10.1016/j.agsy.2003.09.002

DeMenocal, P., Ortiz, J., Guilderson, T., Adkins, J., Sarnthein, M., Baker, L., Yarusinsky, M., 2000. Abrupt onset and termination of the African Humid Period: Rapid climate responses to gradual insolation forcing. Quat. Sci. Rev. 19, 347–361. https://doi.org/10.1016/S0277-3791(99)00081-5

di Lernia, S., Gallinaro, M., 2010. The date and context of Neolithic rock art in the Sahara: engravings and ceremonial monuments from Messak Settafet (south-west Libya). Antiquity 84, 954–975. https://doi.org/10.1017/S0003598X00067016

Drake, N.., Blench, R.., Armitage, S.., Bristow, C.., White, K.., 2011. Ancient watercourses and biogeography of the Sahara explain the peopling of the desert. Proc. Natl. Acad. Sci. 108, 458–462. https://doi.org/10.1073/pnas.1012231108

Dumont, H.J., 2017. A freshwater medusa (Limnocnida) pictured in the Neolithic rock art of the Central Sahara (Tan Zoumaitek, Tamrit, Algeria). Hydrobiologia 1–5. https://doi.org/10.1007/s10750-017-3290-4

Dupont, L., 2011. Orbital scale vegetation change in Africa. Quat. Sci. Rev. 30, 3589–3602. https://doi.org/10.1016/j.quascirev.2011.09.019

Dupont, L.M., 1993. Vegetation zones in NW Africa during the Brunhes Chron reconstructed from marine palynological data. Quat. Sci. Rev. 12, 189–202. https://doi.org/10.1016/0277-3791(93)90053-O

Dupont, L.M., Agwu, C.O.C., 1992. Latitudinal shifts of forest and savanna in N. W. Africa during the Brunhes chron: further marine palynological results from site M 16415 (9°;N 19°W). Veg. Hist. Archaeobot. 1, 163–175. https://doi.org/10.1007/BF00191556

Dupont, L.M., Beug, H.-J., Stalling, H., Tiedermann, R., 1989. 6. First Palynological Results From Site 658 at 21°N Off North West Africa: Pollen as Climate Indicators. Proc. Ocean Drill. Program, Sci. Results, Vol 108.

Dupont, L.M., Hooghiemstra, H., 1989. The Saharan-Sahelian boundary during the Brunhes chron. Acta Bot. Neerl. 38, 405–415. https://doi.org/10.1111/j.1438-8677.1989.tb01372.x

Dupont, L.M., Rommerskirchen, F., Mollenhauer, G., Schefuß, E., 2013. Miocene to Pliocene changes in South African hydrology and vegetation in relation to the expansion of C4 plants. Earth Planet. Sci. Lett. 375, 408–417. https://doi.org/10.1016/j.epsl.2013.06.005

Dupont, L.M., Schefuß, E., 2018. The roles of fire in Holocene ecosystem changes of West Africa. Earth Planet. Sci. Lett. 481, 255–263. https://doi.org/10.1016/j.epsl.2017.10.049

Ehleringer, J.R., Cerling, T.E., 2001. 1.21 Photosynthetic Pathways and Climate. Glob. Biogeochem. Cycles Clim. Syst. 267–277.

Ehleringer, J.R., Cerling, T.E., Helliker, B.R., 1997. C4 photosynthesis, atmospheric CO2, and climate. Oecologia 112, 285–299.

Ehleringer, J.R., Sage, R.F., Flanagan, L.B., Pearcy, R.W., 1991. Climate Change and the Evolution of C4 Photosynthesis. TREE 6, 95–99.

Ehrmann, W., Schmiedl, G., Seidel, M., Krüger, S., Schulz, H., 2016. A distal 145 ka sediment record of Nile discharge and East African monsoon variability. Clim. Past Discuss. 12, 713–727. https://doi.org/10.5194/cpd-11-4273-2015

El-Shenawy, M.I., Kim, S.-T., Schwarcz, H.P., Asmerom, Y., Polyak, V.J., 2018. Speleothem evidence for the greening of the Sahara and its implications for the early human dispersal out of sub-Saharan Africa. Quat. Sci. Rev. 188, 67–76. https://doi.org/10.1016/j.quascirev.2018.03.016

Enache, M.D., Cumming, B.F., 2006. Tracking recorded fires using charcoal morphology from the sedimentary sequence of Prosser Lake, British Columbia (Canada). Quat. Res. 65, 282–292. https://doi.org/10.1016/j.yqres.2005.09.003

Engelstaedter, S., Washington, R., 2007. Atmospheric controls on the annual cycle of North African dust. J. Geophys. Res. Atmos. 112, D03103. https://doi.org/10.1029/2006JD007195

Finsinger, W., Tinner, W., 2005. Minimum count sums for charcoal concentration estimates in pollen slides: accuracy and potential errors. The Holocene 15, 293–297. https://doi.org/10.1191/0959683605hl808rr

Flannigan, M.., Stocks, B.., Wotton, B.., 2000. Climate change and forest fires. Sci. Total Environ. 262, 221–229. https://doi.org/10.1016/S0048-9697(00)00524-6

Fromm, M., Bevilacqua, R., Servranckx, R., Rosen, J., Thayer, J.P., Herman, J., Larko, D., 2005. Pyro-cumulonimbus injection of smoke to the stratosphere: Observations and impact of a super blowup in northwestern Canada on 3-4 August 1998. J. Geophys. Res. D Atmos. 110. https://doi.org/10.1029/2004JD005350

Furley, P., Rees, R., Ryan, C., Saiz, G., 2008. Savanna burning and the assessment of long-term fire experiments with particular reference to Zimbabwe. Prog. Phys. Geogr. 32, 611–634. https://doi.org/10.1177/0309133308101383

Gallinaro, M., 2013. Saharan Rock Art: Local Dynamics and Wider Perspectives. Arts 2, 350–382. https://doi.org/10.3390/arts2040350

Garcin, Y., Vincens, A., Williamson, D., Buchet, G., Guiot, J., 2007. Abrupt resumption of the African Monsoon at the Younger Dryas-Holocene climatic transition. Quat. Sci. Rev. 26, 690–704. https://doi.org/10.1016/j.quascirev.2006.10.014

Gasse, F., 2000. Hydrological changes in the African tropics since the Last Glacial Maximum. Quat. Sci. Rev. 19, 189–211. https://doi.org/10.1016/S0277-3791(99)00061-X

Gasse, F., Stabell, B., Fourtanier, E., Van Iperen, Y., 1989. Freshwater Diatom Influx in Intertropical Atlantic: Relationships Continental Records from Africa. Quat. Res. 32, 229–243.

Giglio, L., van der Werf, G.R., Randerson, J.T., Collatz, G.J., Kasibhatla, P., 2006. Global estimation of burned area using MODIS active fire observations. Atmos. Chem. Phys. 6, 957–974. https://doi.org/10.5194/acp-6-957-2006

Glasspool, I.J., Edwards, D., Axe, L., 2004. Charcoal in the Silurian as evidence for the earliest

wildfire. Geology 32, 381. https://doi.org/10.1130/G20363.1

Goudie, A.S., Middleton, N.J., 2001. Saharan dust storms: nature and consequences. Earth-Science Rev. 56, 179–204. https://doi.org/10.1016/S0012-8252(01)00067-8

Grant, K.M., Grimm, R., Mikolajewicz, U., Marino, G., Ziegler, M., Rohling, E.J., 2016. The timing of Mediterranean sapropel deposition relative to insolation, sea-level and African monsoon changes. Quat. Sci. Rev. 140, 125–141. https://doi.org/10.1016/j.quascirev.2016.03.026

Grousset, F.E., Parra, M., Bory, A., Martinez, P., Bertrand, P., Shmmield, G., Ellam, R.M., 1998. Saharan wind regimes traced by the Sr-Nd isotopic composition of Subtropical Atlantic sediments: Last Glacial Maximum vs Today. Quat. Sci. Rev. 17, 395–409.

Hammes, K., Schmidt, M.W.I., Smernik, R.J., Currie, L. a., Ball, W.P., Nguyen, T.H., Louchouarn, P., Houel, S., Gustafsson, Ö., Elmquist, M., Cornelissen, G., Skjemstad, J.O., Masiello, C. a., Song, J., Peng, P., Mitra, S., Dunn, J.C., Hatcher, P.G., Hockaday, W.C., Smith, D.M., Hartkopf-Fröder, C., Böhmer, A., Lüer, B., Huebert, B.J., Amelung, W., Brodowski, S., Huang, L., Zhang, W., Gschwend, P.M., Flores-Cervantes, D.X., Largeau, C., Rouzaud, J.-N., Rumpel, C., Guggenberger, G., Kaiser, K., Rodionov, A., Gonzalez-Vila, F.J., Gonzalez-Perez, J.A., de la Rosa, J.M., Manning, D.A.C., López-Capél, E., Ding, L., 2007. Comparison of quantification methods to measure fire-derived (black/elemental) carbon in soils and sediments using reference materials from soil, water, sediment and the atmosphere. Global Biogeochem. Cycles 21, GB3016. https://doi.org/10.1029/2006GB002914

Handiani, D., Paul, A., Prange, M., Merkel, U., Dupont, L., Zhang, X., 2013. Tropical vegetation response to Heinrich Event 1 as simulated with the UVic ESCM and CCSM3. Clim. Past 9, 1683–1696. https://doi.org/10.5194/cp-9-1683-2013

Harding, I.C., Charles, A.J., Marshall, J.E.A., Pälike, H., Roberts, A.P., Wilson, P.A., Jarvis, E., Thorne, R., Morris, E., Moremon, R., Pearce, R.B., Akbari, S., 2011. Sea-level and salinity fluctuations during the Paleocene-Eocene thermal maximum in Arctic Spitsbergen. Earth Planet. Sci. Lett. 303, 97–107. https://doi.org/10.1016/j.epsl.2010.12.043

Harrison, S.P., Kohfeld, K.E., Roelandt, C., Claquin, T., 2001. The role of dust in climate changes today, at the last glacial maximum and in the future. Earth-Science Rev. 54, 43–80. https://doi.org/10.1016/S0012-8252(01)00041-1

Harrison, S.P., Sanchez Goñi, M.F., 2010. Global patterns of vegetation response to millennial-scale variability and rapid climate change during the last glacial period. Quat. Sci. Rev. 29, 2957–2980. https://doi.org/10.1016/j.quascirev.2010.07.016

Hawthorne, D., Courtney, C.J., Aleman, J.C., Blarquez, O., Colombaroli, D., Daniau, A., Marlon, J.R., Han, Y., Hantson, S., Kehrwald, N., Power, M., Vanni, B., Magi, B., Yue, X., Carcaillet, C., Marchant, R., Ogunkoya, A., Githumbi, E.N., Muriuki, R.M., 2017. Global Modern Charcoal Dataset (GMCD): A tool for exploring proxy- fire linkages and spatial patterns of biomass burning. Quaternay Int. 1–15. https://doi.org/10.1016/j.quaint.2017.03.046

Heinrich, H., 1988. Origin and consequences of cyclic ice rafting in the Northeast Atlantic Ocean during the past 130,000 years. Quat. Res. 29, 142–152. https://doi.org/10.1016/0033-5894(88)90057-9

Hély, C., Braconnot, P., Watrin, J., Zheng, W., 2009. Climate and vegetation: Simulating the African humid period. Comptes Rendus - Geosci. 341, 671–688. https://doi.org/10.1016/j.crte.2009.07.002

Hély, C., Lézine, A.M., Ballouche, A., Cour, P., Duzer, D., Guinet, P., Jahns, S., Maley, J., Mercuri, A.M., Pons, A., Ritchie, J.C., Salzmann, U., Schulz, E., Van Campo, M., Waller, M.P., 2014. Holocene changes in African vegetation: Tradeoff between climate and water availability. Clim. Past 10, 681–686. https://doi.org/10.5194/cp-10-681-2014

Hemming, S.R., 2004. Heinrich events: Massive late Pleistocene ditritus layers of the North Atlantic and their global climate imprint. Rev. Geophys. 42, RG1005. https://doi.org/10.1029/2003RG000128.1.INTRODUCTION

Herold, M., Lohmann, G., 2009. Eemian tropical and subtropical African moisture transport: An isotope modelling study. Clim. Dyn. 33, 1075–1088. https://doi.org/10.1007/s00382-008-0515-2

Herring, J.R., 1985. Charcoal Fluxes into sediments of the North Pacific Ocean: The Cenozoic Record of Burning. Geophys. Monogr. Ser. 32.

Higgins, S.I., Bond, W.J., Trollope, W.S.W., 2000. Fire, resprouting and variability: A recipe for grass-tree coexistence in savanna. J. Ecol. 88, 213–229. https://doi.org/10.1046/j.1365-2745.2000.00435.x

Hirota, M., Holmgren, M., Van Nes, E., Schetter, M., Van New, E., Scheffer, M., 2011. Global Resilience of Tropical Forest and Savanna to Critical Transitions. Science (80-.). 334, 232–235. https://doi.org/10.1126/science.1210657

Hoetzel, S., Dupont, L., Schefuß, E., Rommerskirchen, F., Wefer, G., 2013. The role of fire in Miocene to Pliocene C4 grassland and ecosystem evolution. Nat. Geosci. 6, 1027–1030.

https://doi.org/10.1038/ngeo1984

Hoffmann, W.A., Geiger, E.L., Gotsch, S.G., Rossatto, D.R., Silva, L.C.R., Lau, O.L., Haridasan, M., Franco, A.C., 2012. Ecological thresholds at the savanna-forest boundary: How plant traits, resources and fire govern the distribution of tropical biomes. Ecol. Lett. 15, 759–768. https://doi.org/10.1111/j.1461-0248.2012.01789.x

Hoogakker, B.A.A., Smith, R.S., Singarayer, J.S., Marchant, R., Prentice, I.C., Allen, J.R.M., Anderson, R.S., Bhagwat, S.A., Behling, H., Borisova, O., Bush, M., Correa-Metrio, A., De Vernal, A., Finch, J.M., Fréchette, B., Lozano-Garcia, S., Gosling, W.D., Granoszewski, W., Grimm, E.C., Grüger, E., Hanselman, J., Harrison, S.P., Hill, T.R., Huntley, B., Jiménez-Moreno, G., Kershaw, P., Ledru, M.P., Magri, D., McKenzie, M., Müller, U., Nakagawa, T., Novenko, E., Penny, D., Sadori, L., Scott, L., Stevenson, J., Valdes, P.J., Vandergoes, M., Velichko, A., Whitlock, C., Tzedakis, C., 2016. Terrestrial biosphere changes over the last 120 kyr. Clim. Past 111, 1031–1091. https://doi.org/10.5194/cp-12-51-2016

Hooghiemstra, H., Lézine, A.M., Leroy, S. a G., Dupont, L., Marret, F., 2006. Late Quaternary palynology in marine sediments: A synthesis of the understanding of pollen distribution patterns in the NW African setting. Quat. Int. 148, 29–44. https://doi.org/10.1016/j.quaint.2005.11.005

Hopcroft, P.O., Valdes, P.J., Harper, A.B., Beerling, D.J., 2017. Multi vegetation model evaluation of the Green Sahara climate regime. Geophys. Res. Lett. 44, 6804–6813. https://doi.org/10.1002/2017GL073740

Jahns, S., Huls, M., Sarnthein, M., Johns, S., Huls, M., Sarnthein, M., 1998. Vegetation and climate history of west equatorial Africa based on a marine pollen record off Liberia (site GIK 16776) covering the last 400,000 years. Rev. Palaeobot. Palynol. 102, 277–288. https://doi.org/10.1016/S0034-6667(98)00009-8

Jeltsch, F., Weber, G.E., Grimm, V., 2000. Ecological buffering mechanisms in savannas: A unifying theory of long-term tree-grass coexistence. Plant Ecol. 150, 161–171. https://doi.org/10.1023/A:1026590806682

Jennings, R.P., Singarayer, J., Stone, E.J., Krebs-Kanzow, U., Khon, V., Nisancioglu, K.H., Pfeiffer, M., Zhang, X., Parker, A., Parton, A., Groucutt, H.S., White, T.S., Drake, N.A., Petraglia, M.D., 2015. The greening of Arabia: Multiple opportunities for human occupation of the Arabian Peninsula during the Late Pleistocene inferred from an ensemble of climate model simulations. Quat. Int. 382, 181–199. https://doi.org/10.1016/j.quaint.2015.01.006

Jensen, K., Lynch, E.A., Calcote, R., Hotchkiss, S.C., 2007. Interpretation of charcoal morphotypes in sediments from Ferry Lake, Wisconsin, USA: Do different plant fuel sources produce distinctive charcoal morphotypes? Holocene 17, 907–915. https://doi.org/10.1177/0959683607082405

Jolly, D., Prentice, I.C., Bonnefille, R., Ballouche, A., Bengo, M., Brenac, P., Buchet, G., Burney, D., Cazet, J.P., Cheddadi, R., Edorh, T., Elenga, H., Elmoutaki, S., Guiot, J., Laarif, F., Lamb, H., Lezine, A.M., Maley, J., Mbenza, M., Peyron, O., Reille, M., Reynaud-Farrera, I., Riollet, G., Ritchie, J.C., Roche, E., Scott, L., Ssemmanda, I., Straka, H., Umer, M., Van Campo, E., Vilimumbalo, S., Vincens, A., Waller, M., 1998. Biome reconstruction from pollen and plant macrofossil data for Africa and the Arabian peninsula at 0 and 6000 years. J. Biogeogr. 25, 1007–1027. https://doi.org/10.1046/j.1365-2699.1998.00238.x

Justino, F., Peltier, W.R., Barbosa, H.A., 2010. Atmospheric susceptibility to wildfire occurrence during the Last Glacial Maximum and mid-Holocene. Palaeogeogr. Palaeoclimatol. Palaeoecol. 295, 76–88. https://doi.org/10.1016/j.palaeo.2010.05.017

Knaack J-J and Sarnthien M. (2005) 'Stable isotope of foraminifera of ODP Hole 108-658C' doi: 10.1594/PANGAEA.227736

Keeley, J.E., Fotheringham, C.J., 2000. Role of Fire in Regeneration from Seed, in: Seeds The Ecology of Regeneration in Plant Communities. pp. 311–330. https://doi.org/10.1079/9780851994321.0311

Keeley, J.E., Rundel, P.W., 2005. Fire and the Miocene expansion of C_4 grasslands. Ecol. Lett. 8, 683–690. https://doi.org/10.1111/j.1461-0248.2005.00767.x

Kehrwald, N., Zangrando, R., Gabrielli, P., Jaffrezo, J.L., Boutron, C., Barbante, C., Gambaro, A., 2012. Levoglucosan as a specific marker of fire events in Greenland snow. Tellus, Ser. B Chem. Phys. Meteorol. 64, 1–9. https://doi.org/10.3402/tellusb.v64i0.18196

Kleinen, T., Hildebrandt, S., Prange, M., Rachmayani, R., Müller, S., Bezrukova, E., Brovkin, V., Tarasov, P.E., 2014. The climate and vegetation of Marine Isotope Stage 11 - Model results and proxy-based reconstructions at global and regional scale. Quat. Int. 348, 247–265. https://doi.org/10.1016/j.quaint.2013.12.028

Koren, I., Kaufman, Y., Remer, L., Martins, J., 2004. Measurement of the Effect of Amazon Smoke on Inhibition of Cloud Formation. Science (80-.). 303, 1342–1345. https://doi.org/10.1126/science.1089424

Krull, E.S., Skjemstad, J.O., Graetz, D., Grice, K., Dunning, W., Cook, G., Parr, J.F., 2003. 13C-depleted charcoal from C4 grasses and the role of occluded carbon in phytoliths. Org. Geochem. 34, 1337–1352. https://doi.org/10.1016/S0146-6380(03)00100-1

Kuechler, R.R., Schefuß, E., Beckmann, B., Dupont, L., Wefer, G., 2013. NW African hydrology and vegetation during the Last Glacial cycle reflected in plant-wax-specific hydrogen and carbon isotopes. Quat. Sci. Rev. 82, 56–67. https://doi.org/10.1016/j.quascirev.2013.10.013

Lamb, H.F., Bates, C.R., Coombes, P. V., Marshall, M.H., Umer, M., Davies, S.J., Dejen, E., 2007. Late Pleistocene desiccation of Lake Tana, source of the Blue Nile. Quat. Sci. Rev. 26, 287–299. https://doi.org/10.1016/j.quascirev.2006.11.020

Lange, C.B., Romero, O.E., Wefer, G., Gabric, A.J., 1998. Offshore influence of coastal upwelling off Mauritania, NW Africa, as recorded by diatoms in sediment traps at 2195 m water depth. Deep. Res. Part I Oceanogr. Res. Pap. 45, 985–1013. https://doi.org/10.1016/S0967-0637(97)00103-9

Laris, P., Wardell, D.A., 2006. Good, bad or “necessary evil”? Reinterpreting the colonial burning experiment in the savanna landscapes of West Africa. Geogr. J. 172, 271–290.

Larrasoaña, J.C., Roberts, A.P., Rohling, E.J., 2013. Dynamics of Green Sahara Periods and Their Role in Hominin Evolution. PLoS One 8, e76514. https://doi.org/10.1371/journal.pone.0076514

Larrasoaña, J.C., Roberts, A.P., Rohling, E.J., Winklhofer, M., Wehausen, R., 2003. Three million years of monsoon variability over the northern Sahara. Clim. Dyn. 21, 689–698. https://doi.org/10.1007/s00382-003-0355-z

Laskar, J., Robutel, P., Joutel, F., Gastineau, M., Correia, a. C.M., Levrard, B., 2004. A long-term numerical solution for the insolation quantities of the Earth. Astron. Astrophys. 428, 261–285. https://doi.org/10.1051/0004-6361:20041335

Lasslop, G., Moeller, T., Onofrio, D.D., Hantson, S., Kloster, S., 2018. Tropical climate-vegetation-fire relationships: multivariate evaluation of the land surface model JSBACH. Biogeosciences Discuss. 1–23.

Lécuyer, C., Lézine, A.M., Fourel, F., Gasse, F., Sylvestre, F., Pailles, C., Grenier, C., Travi, Y., Barral, A., 2016. I-n-Atei palaeolake documents past environmental changes in central Sahara at the time of the “Green Sahara”: Charcoal, carbon isotope and diatom records. Palaeogeogr. Palaeoclimatol. Palaeoecol. 441, 834–844. https://doi.org/10.1016/j.palaeo.2015.10.032

Lehmann, C.E.R., Anderson, T.M., Sankaran, M., Higgins, S.I., Archibald, S., Hoffmann, W.A., Hanan, N.P., Williams, R.J., Fensham, R.J., Felfili, J., Hutley, L.B., Ratnam, J., San Jose, J., Montes, R., Franklin, D., Russell-smith, J., Ryan, C.M., Durigan, G., Hiernaux, P., Haidar, R., Bowman, D.M.J.S., Bond, W.J., Jose, J.S., Montes, R., Franklin, D., Russell-smith, J., Ryan, C.M., Durigan, G., Hiernaux, P., Haidar, R., Bowman, D.M.J.S., Bond, W.J., 2014. Savanna Vegetation-Fire-Climate Relationships Differ Among Continents. Science (80-.). 343, 548–552. https://doi.org/10.1126/science.1247355

Lezine, A.-M., 1989. Late Quaternary Vegetation and Climate of the Sahel. Quat. Res. 32, 317–334.

Lézine, A.M., 2009. Timing of vegetation changes at the end of the Holocene Humid Period in desert areas at the northern edge of the Atlantic and Indian monsoon systems. Comptes Rendus - Geosci. 341, 750–759. https://doi.org/10.1016/j.crte.2009.01.001

Lézine, A.M., Hély, C., Grenier, C., Braconnot, P., Krinner, G., 2011. Sahara and Sahel vulnerability to climate changes, lessons from Holocene hydrological data. Quat. Sci. Rev. 30, 3001–3012. https://doi.org/10.1016/j.quascirev.2011.07.006

Lisiecki, L.E., Raymo, M.E., 2005. A Pliocene-Pleistocene stack of 57 globally distributed benthic δ18O records. Paleoceanography 20, 1–17. https://doi.org/10.1029/2004PA001071

Lisiecki, L.E., Stern, J. V, 2016. Regional and global benthic δ18O stacks for the last glacial cycle. Paleoceanography 1368–1394. https://doi.org/10.1002/2016PA003002.Received

Lu, Z., Miller, P.A., Zhang, Qiong, Zhang, Qiang, Wårlind, D., Nieradzik, L., Sjolte, J., Smith, B., 2018. Dynamic Vegetation Simulations of the Mid-Holocene Green Sahara. Geophys. Res. Lett. 45, 8294–8303. https://doi.org/10.1029/2018GL079195

Lüthi, D., Le Floch, M., Bereiter, B., Blunier, T., Barnola, J.M., Siegenthaler, U., Raynaud, D., Jouzel, J., Fischer, H., Kawamura, K., Stocker, T.F., 2008. High-resolution carbon dioxide concentration record 650,000-800,000 years before present. Nature 453, 379–382. https://doi.org/10.1038/nature06949

Magny, M., Bégeot, C., 2004. Hydrological changes in the European midlatitudes associated with freshwater outbursts from Lake Agassiz during the Younger Dryas event and the early Holocene. Quat. Res. 61, 181–192. https://doi.org/10.1016/j.yqres.2003.12.003

Manning, K., Timpson, A., 2014. The demographic response to holocene climate change in the Sahara. Quat. Sci. Rev. 101, 28–35. https://doi.org/10.1016/j.quascirev.2014.07.003

Marlon, J.R., Bartlein, P.J., Walsh, M.K., Harrison, S.P., Brown, K.J., Edwards, M.E., Higuera, P.E.,

Power, M.J., Anderson, R.S., Briles, C., Brunelle, a, Carcaillet, C., Daniels, M., Hu, F.S., Lavoie, M., Long, C., Minckley, T., Richard, P.J.H., Scott, a C., Shafer, D.S., Tinner, W., Umbanhowar, C.E., Whitlock, C., 2009. Wildfire responses to abrupt climate change in North America. Proc. Natl. Acad. Sci. U. S. A. 106, 2519–2524. https://doi.org/10.1073/pnas.0808212106

Marlon, J.R., Kelly, R., Daniau, A.L., Vannière, B., Power, M.J., Bartlein, P., Higuera, P., Blarquez, O., Brewer, S., Brücher, T., Feurdean, A., Romera, G.G., Iglesias, V., Yoshi Maezumi, S., Magi, B., Mustaphi, C.J.C., Zhihai, T., 2016. Reconstructions of biomass burning from sediment-charcoal records to improve data-model comparisons. Biogeosciences 13, 3225–3244. https://doi.org/10.5194/bg-13-3225-2016

Marshall, M.H., Lamb, H.F., Huws, D., Davies, S.J., Bates, R., Bloemendal, J., Boyle, J., Leng, M.J., Umer, M., Bryant, C., 2011. Late Pleistocene and Holocene drought events at Lake Tana, the source of the Blue Nile. Glob. Planet. Change 78, 147–161. https://doi.org/10.1016/j.gloplacha.2011.06.004

Masiello, C., 2004. New directions in black carbon organic geochemistry. Mar. Chem. 92, 201–213. https://doi.org/10.1016/j.marchem.2004.06.043

Masiello, C., Druffel, E., 1998. Black carbon in Deep-Sea Sediments. Science (80-.). 280, 1911–1913. https://doi.org/10.1126/science.280.5371.1911

Maslin, M., Christensen, B., 2007. Tectonics, orbital forcing, global climate change, and human evolution in Africa: introduction to the African paleoclimate special volume. J. Hum. Evol. 53, 443–464. https://doi.org/10.1016/j.jhevol.2007.06.005

Maslin, M., Seidov, D., Lowe, J., 2001. Synthesis of the Nature and Causes of Rapid Climate Transitions During the Quaternary. Geophys. Monogr. 126 126, 9–52. https://doi.org/10.1029/GM126p0009

Maslin, M., Shackleton, N., Pflaumann, U., 1995. Surface water temperature, salinity, and density changes in the northeast Atlantic during the last 45, 000 years: Heinrich events, deep water formation, and climatic rebounds. Paleoceanography 10, 527–544.

Maslin, M.A., Brierley, C.M., Milner, A.M., Shultz, S., Trauth, M.H., Wilson, K.E., 2014. East African climate pulses and early human evolution. Quat. Sci. Rev. 101, 1–17. https://doi.org/10.1016/j.quascirev.2014.06.012

Matthews, J., 1969. The Assessment of a Method for the Determination of Absolute Pollen Frequencies. New Phytol. 68, 161–166. https://doi.org/10.1111/j.1469-8137.1969.tb06429.x

Mayewski, P.A., Rohling, E.E., Stager, J.C., Karlén, W., Maasch, K.A., Meeker, L.D., Meyerson, E.A., Gasse, F., van Kreveld, S., Holmgren, K., Lee-Thorp, J., Rosqvist, G., Rack, F., Staubwasser, M., Schneider, R.R., Steig, E.J., 2004. Holocene climate variability. Quat. Res. 62, 243–255. https://doi.org/10.1016/j.yqres.2004.07.001

McGee, D., Broecker, W.S., Winckler, G., 2010. Gustiness: The driver of glacial dustiness? Quat. Sci. Rev. 29, 2340–2350. https://doi.org/10.1016/j.quascirev.2010.06.009

McGee, D., deMenocal, P.B., Winckler, G., Stuut, J.B.W., Bradtmiller, L.I., 2013. The magnitude, timing and abruptness of changes in North African dust deposition over the last 20,000 yr. Earth Planet. Sci. Lett. 371–372, 163–176. https://doi.org/10.1016/j.epsl.2013.03.054

McGee, D., Donohoe, A., Marshall, J., Ferreira, D., 2014. Changes in ITCZ location and cross-equatorial heat transport at the Last Glacial Maximum, Heinrich Stadial 1, and the mid-Holocene. Earth Planet. Sci. Lett. 390, 69–79. https://doi.org/10.1016/j.epsl.2013.12.043

Meckler, A.N., Sigman, D.M., Gibson, K. a, François, R., Martínez-García, A., Jaccard, S.L., Röhl, U., Peterson, L.C., Tiedemann, R., Haug, G.H., 2013. Deglacial pulses of deep-ocean silicate into the subtropical North Atlantic Ocean. Nature 495, 495–498. https://doi.org/10.1038/nature12006

Melki, T., Kallel, N., Fontugne, M., 2010. The nature of transitions from dry to wet condition during sapropel events in the Eastern Mediterranean Sea. Palaeogeogr. Palaeoclimatol. Palaeoecol. 291, 267–285. https://doi.org/10.1016/j.palaeo.2010.02.039

Merlis, T.M., Schneider, T., Bordoni, S., Eisenman, I., 2013. Hadley circulation response to orbital precession. Part ii: Subtropical Continent. J. Clim. 26, 754–771. https://doi.org/10.1175/JCLI-D-11-00716.1

Meyers, P.A., 1994. Preservation of elemental and isotopic source identification of sedimentary organic matter. Chem. Geol. 114, 289–302. https://doi.org/10.1016/0009-2541(94)90059-0

Mohtadi, M., Prange, M., Steinke, S., 2016. Palaeoclimatic insights into forcing and response of monsoon rainfall. Nature 533, 191–199. https://doi.org/10.1038/nature17450

Moritz, M.A., Parisien, M.-A., Batllori, E., Krawchuk, M.A., Van Dorn, J., Ganz, D.J., Hayhoe, K., 2012. Climate change and disruptions to global fire activity. Ecosphere 3, Article 49. https://doi.org/10.1890/ES11-00345.1

Morley, R.J., Richards, K., 1993. Gramineae cuticle: a key indicator of Late Cenozoic climatic change in the Niger Delta. Rev. Palaeobot. Palynol. 77, 119–127.

Mulitza, S., Prange, M., Stuut, J.-B.B., Zabel, M., Von Dobeneck, T., Itambi, A.C., Nizou, J., Schulz, M., Wefer, G., 2008. Sahel megadroughts triggered by glacial slowdowns of Atlantic meridional overturning. Paleoceanography 23, PA4206. https://doi.org/10.1029/2008PA001637

Nelson, D.M., Verschuren, D., Urban, M.A., Hu, F.S., 2012. Long-term variability and rainfall control of savanna fire regimes in equatorial East Africa. Glob. Chang. Biol. 18, 3160–3170. https://doi.org/10.1111/j.1365-2486.2012.02766.x

Neumann, K., Fahmy, A., Lespez, L., Ballouche, A., Huysecom, E., 2009. The Early Holocene palaeoenvironment of Ounjougou (Mali): Phytoliths in a multiproxy context. Palaeogeogr. Palaeoclimatol. Palaeoecol. 276, 87–106. https://doi.org/10.1016/j.palaeo.2009.03.001

Niedermeyer, E.M., Prange, M., Mulitza, S., Mollenhauer, G., Schefuß, E., Schulz, M., 2009. Extratropical forcing of Sahel aridity during Heinrich stadials. Geophys. Res. Lett. 36, L20707. https://doi.org/10.1029/2009GL039687

Niedermeyer, E.M., Schefuss, E., Sessions, A.L., Mulitza, S., Mollenhauer, G., Schulz, M., Wefer, G., 2010. Orbital- and millennial-scale changes in the hydrologic cycle and vegetation in the western African Sahel: insights from individual plant wax delta D and delta C-13. Quat. Sci. Rev. 29, 2996–3005. https://doi.org/Doi 10.1016/J.Quascirev.2010.06.039

Nikolova, I., Yin, Q., Berger, A., Singh, U.K., Karami, M.P., 2013. The last interglacial (Eemian) climate simulated by LOVECLIM and CCSM3. Clim. Past 9, 1789–1806. https://doi.org/10.5194/cp-9-1789-2013

Olson, D.M., Dinerstein, E., Wikramanayake, E.D., Burgess, N.D., Powell, G.V.N., Underwood, E.C., D'amico, J. a., Itoua, I., Strand, H.E., Morrison, J.C., Loucks, C.J., Allnutt, T.F., Ricketts, T.H., Kura, Y., Lamoreux, J.F., Wettengel, W.W., Hedao, P., Kassem, K.R., 2001. Terrestrial Ecoregions of the World: A New Map of Life on Earth. Bioscience 51, 933–938. https://doi.org/10.1641/0006-3568(2001)051[0933:TEOTWA]2.0.CO;2

Osborne, A.H., Vance, D., Rohling, E.J., Barton, N., Rogerson, M., Fello, N., 2008. A humid corridor across the Sahara for the migration of early modern humans out of Africa 120,000 years ago. PNAS 105, 16444–16447. https://doi.org/10.1073/pnas.0804472105

Osborne, C.P., 2008. Atmosphere, ecology and evolution: What drove the Miocene expansion of C4 grasslands? J. Ecol. 96, 35–45. https://doi.org/10.1111/j.1365-2745.2007.01323.x

Osborne, C.P., Beerling, D.J., 2006. Nature's green revolution: the remarkable evolutionary rise of

C4 plants. Philos. Trans. R. Soc. Lond. B. Biol. Sci. 361, 173–194. https://doi.org/10.1098/rstb.2005.1737

Otto-Bliesner, B.L., Russell, J.M., Clark, P.U., Liu, Z., Overpeck, J.T., Konecky, B., DeMenocal, P.B., Nicholson, S.E., He, F., Lu, Z., 2014. Coherent changes of southeastern equatorial and northern African rainfall during the last deglaciation. Science (80-.). 346, 1223–1227. https://doi.org/10.1126/science.1259531

Oweis, T., Hachum, A., 2006. Water harvesting and supplemental irrigation for improved water productivity of dry farming systems in West Asia and North Africa. Agric. Water Manag. 80, 57–73. https://doi.org/10.1016/j.agwat.2005.07.004

Palliard D., Labeyrie L., and Yiuo. (1996) 'Macintosh program performs tie-series analysis', E*OS Trans AGU*, 77:379

Parkin, D.W., Phillips, D.R., Sullivan, R.A.L., Johnson, L., 1970. Airbourne Dust Collections over the North Atlantic. J. Geophys. Res. 75, 1782–1793.

Patterson, W.A., Edwards, K.J., Maguire, D.J., 1987. Microscopic charcoal as a fossil indicator of fire. Quat. Sci. Rev. 6, 3–23. https://doi.org/10.1016/0277-3791(87)90012-6

Pausas, J.G., Ribeiro, E., 2013. The global fire-productivity relationship. Glob. Ecol. Biogeogr. 22, 728–736. https://doi.org/10.1111/geb.12043

Pausata, F.S.R.R., Messori, G., Zhang, Q., 2016. Impacts of dust reduction on the northward expansion of the African monsoon during the Green Sahara period. Earth Planet. Sci. Lett. 434, 1–10. https://doi.org/10.1016/j.epsl.2015.11.049

Power, M.J., Marlon, J., Ortiz, N., Bartlein, P.J., Harrison, S.P., Mayle, F.E., Ballouche, A., Bradshaw, R.H.W., Carcaillet, C., Cordova, C., Mooney, S., Moreno, P.I., Prentice, I.C., Thonicke, K., Tinner, W., Whitlock, C., Zhang, Y., Zhao, Y., Ali, a. a., Anderson, R.S., Beer, R., Behling, H., Briles, C., Brown, K.J., Brunelle, A., Bush, M., Camill, P., Chu, G.Q., Clark, J., Colombaroli, D., Connor, S., Daniau, A.-L.L., Daniels, M., Dodson, J., Doughty, E., Edwards, M.E., Finsinger, W., Foster, D., Frechette, J., Gaillard, M.-J.J., Gavin, D.G., Gobet, E., Haberle, S., Hallett, D.J., Higuera, P., Hope, G., Horn, S., Inoue, J., Kaltenrieder, P., Kennedy, L., Kong, Z.C., Larsen, C., Long, C.J., Lynch, J., Lynch, E. a., McGlone, M., Meeks, S., Mensing, S., Meyer, G., Minckley, T., Mohr, J., Nelson, D.M., New, J., Newnham, R., Noti, R., Oswald, W., Pierce, J., Richard, P.J.H., Rowe, C., Sanchez Goñi, M.F., Shuman, B.N., Takahara, H., Toney, J., Turney, C., Urrego-Sanchez, D.H., Umbanhowar, C., Vandergoes, M., Vanniere, B., Vescovi, E., Walsh, M., Wang, X., Williams, N., Wilmshurst, J., Zhang, J.H., 2008. Changes in fire regimes since

the Last Glacial Maximum: an assessment based on a global synthesis and analysis of charcoal data. Clim. Dyn. 30, 887–907. https://doi.org/10.1007/s00382-007-0334-x

Preston, C.M., Schmidt, M.W.I., 2006. Black (pyrogenic) carbon: a synthesis of current knowledge and uncertainties with special consideration of boreal regions. Biogeosciences 3, 397–420.

Rachmayani, R., Prange, M., Schulz, M., 2015. North African vegetation-precipitation feedback in early and mid-Holocene climate simulations with CCSM3-DGVM. Clim. Past 11, 175–185. https://doi.org/10.5194/cp-11-175-2015

Raffi, I., Backman, J., Fornaciari, E., Pälike, H., Rio, D., Lourens, L., Hilgen, F., 2006. A review of calcareous nannofossil astrobiochronology encompassing the past 25 million years. Quat. Sci. Rev. 25, 3113–3137. https://doi.org/10.1016/j.quascirev.2006.07.007

Ratnam, J., Bond, W.J., Fensham, R.J., Hoffmann, W.A., Archibald, S., Lehmann, C.E.R., Anderson, M.T., Higgins, S.I., Sankaran, M., 2011. When is a “forest” a savanna, and why does it matter? Glob. Ecol. Biogeogr. 20, 653–660. https://doi.org/10.1111/j.1466-8238.2010.00634.x

Reddad, H., Etabaai, I., Rhoujjati, A., Taieb, M., Thevenon, F., Damnati, B., 2013. Fire activity in North West Africa during the last 30,000 cal years BP inferred from a charcoal record from Lake Ifrah (Middle atlas-Morocco): Climatic implications. J. African Earth Sci. 84, 47–53. https://doi.org/10.1016/j.jafrearsci.2013.03.007

Rhodes, A.N., 1998. A method for the preparation and quantification of microscopic charcoal from terrestrial and lacustrine sediment cores. The Holocene 8, 113–117.

Ridley, D.A., Heald, C.L., Ford, B., 2012. North African dust export and deposition: A satellite and model perspective. J. Geophys. Res. Atmos. 117, 1–21. https://doi.org/10.1029/2011JD016794

Ripley, B., Donald, G., Osborne, C.P., Abraham, T., Martin, T., 2010. Experimental investigation of fire ecology in the C3 and C4 subspecies of Alloteropsis semialata. J. Ecol. 98, 1196–1203. https://doi.org/10.1111/j.1365-2745.2010.01700.x

Ritchie, J.., Eyles, C.., Haynes, C.., 1985. Sediment and pollen evidence for an early to mid-Holocene humid period in the eastern Sahara. Lett. to Nat. 314, 352–355. https://doi.org/10.1038/314141a0

Rohling, E.J., Grant, K.M., Roberts, A.P., Larrasoaña, J.-C., 2013. Paleoclimate Variability in the Mediterranean and Red Sea Regions during the Last 500,000 Years. Curr. Anthropol. 54,

S000. https://doi.org/10.1086/673882

Rohling, E.J., Marino, G., Grant, K.M., 2015. Mediterranean climate and oceanography, and the periodic development of anoxic events (sapropels). Earth-Science Rev. 143, 62–97. https://doi.org/10.1016/j.earscirev.2015.01.008

Rohling, E.J.E., Cane, T.R.T., Cooke, S., Sprovieri, M., Bouloubassi, I., Emeis, K.C.K., Schiebel, R., Kroon, D., Jorissen, F.J.F., Lorre, a., Kemp, A. a. E.S., 2002. African monsoon variability during the previous interglacial maximum. Earth Planet. Sci. Lett. 202, 61–75. https://doi.org/10.1016/S0012-821X(02)00775-6

Rucina, S.M., Muiruri, V.M., Kinyanjui, R.N., McGuiness, K., Marchant, R., 2009. Late Quaternary vegetation and fire dynamics on Mount Kenya. Palaeogeogr. Palaeoclimatol. Palaeoecol. 283, 1–14. https://doi.org/10.1016/j.palaeo.2009.08.008

Ruddiman, W., Sarnthein, M., Baldauf, J., Al, E., 1988a. 3. Site 658, in: Proceedings of the Ocean Drilling Program, Initial Reports (Part A), ODP 108. pp. 105–219.

Ruddiman, W., Sarnthein, M., Baldauf, J., Al, E., 1988b. 13. SITE 668, in: Proceedings of the Ocean Drilling Program, Initial Reports (Part A), ODP 108.

Sage, R.F., 2004. The evolution of C4 photosynthesis. New Phytol. 161, 341–370. https://doi.org/10.1046/j.1469-8137.2004.00974.x

Sage, R.F., 2002. Variation in the kcat of Rubisco in C3 and C4 plants and some implications for photosynthetic performance at high and low temperature. J. Exp. Bot. 53, 609–620.

Sage, R.F., 2001. C4 Plants, Encylopedia. Academic Press.

Sankaran, M., Hanan, N.P., Scholes, R.J., Ratnam, J., Augustine, D.J., Cade, B.S., Gignoux, J., Higgins, S.I., Le Roux, X., Ludwig, F., Ardo, J., Banyikwa, F., Bronn, A., Bucini, G., Caylor, K.K., Coughenour, M.B., Diouf, A., Ekaya, W., Feral, C.J., February, E.C., Frost, P.G.H., Hiernaux, P., Hrabar, H., Metzger, K.L., Prins, H.H.T., Ringrose, S., Sea, W., Tews, J., Worden, J., Zambatis, N., 2005. Determinants of woody cover in African savannas. Nature 438, 846–849. https://doi.org/10.1038/nature04070

Sarnthein, M., Tetzlaff, G., Koopmann, B., Wolter, K., Pflaumann, U., 1981. Glacial and interglacial wind regimes over the eastern subtropical Atlantic and North-West Africa. Nature 293, 193–196. https://doi.org/10.1038/293193a0

Sarnthein, M., Tiedemann, R., 1989. 12 . TOWARD A HIGH-RESOLUTION STABLE ISOTOPE

STRATIGRAPHY OF THE LAST 3 4 MILLION YEARS: SITES 658 AND 659 OFF NORTHWEST AFRICA. Proc. Ocean Drill. Program, Sci. Results 108, 167–185.

Scerri, E.M.L., Blinkhorn, J., Groucutt, H.S., Niang, K., 2016. The Middle Stone Age archaeology of the Senegal River Valley. Quat. Int. 408, 16–32. https://doi.org/10.1016/j.quaint.2015.09.025

Schefuß, E., Ratmeyer, V., Stuut, J.B.W., Jansen, J.H.F., Sinninghe Damsté, J.S., 2003. Carbon isotope analyses of n-alkanes in dust from the lower atmosphere over the central eastern Atlantic. Geochim. Cosmochim. Acta 67, 1757–1767. https://doi.org/10.1016/S0016-7037(02)01414-X

Scheiter, S., Higgins, S.I., Osborne, C.P., Bradshaw, C., Lunt, D., Ripley, B.S., Taylor, L.L., Beerling, D.J., 2012. Fire and fire-adapted vegetation promoted C4 expansion in the late Miocene. New Phytol. 195, 653–666.

Schmidt, M., Noack, A., 2000. Black Carbon in soils and sediments: Analysis, distribution, implications, and current challenges. Global Biogeochem. Cycles 14, 777–793.

Schneider, T., Bischoff, T., Haug, G.H., 2014. Migrations and dynamics of the intertropical convergence zone. Nature 513, 45–53. https://doi.org/10.1038/nature13636

Scholes, R.J., Archer, S.R., 1997. Tree-Grass Interactions. Annu. Rev. Ecol. Syst.

Schreuder, L.T., Hopmans, E.C., Castañeda, I.S., Schefuß, E., Mulitza, S., Sinninghe Damsté, J.S., Schouten, S., 2019. Late Quaternary Biomass Burning in Northwest Africa and Interactions With Climate, Vegetation, and Humans. Paleoceanogr. Paleoclimatology. https://doi.org/10.1029/2018pa003467

Scott, A.C., 2010. Charcoal recognition, taphonomy and uses in palaeoenvironmental analysis. Palaeogeogr. Palaeoclimatol. Palaeoecol. 291, 11–39. https://doi.org/10.1016/j.palaeo.2009.12.012

Scott, A.C., Damblon, F., 2010. Charcoal: Taphonomy and significance in geology, botany and archaeology. Palaeogeogr. Palaeoclimatol. Palaeoecol. 291, 1–10. https://doi.org/10.1016/j.palaeo.2010.03.044

Ségalen, L., Lee-Thorp, J. a., Cerling, T., 2007. Timing of C4 grass expansion across sub-Saharan Africa. J. Hum. Evol. 53, 549–559. https://doi.org/10.1016/j.jhevol.2006.12.010

Sereno, P.C., Garcea, E.A.A., Jousse, H., Stojanowski, C.M., Saliège, J.F., Maga, A., Ide, O.A.,

Knudson, K.J., Mercuri, A.M., Stafford, T.W., Kaye, T.G., Giraudi, C., N'siala, I.M., Cocca, E., Moots, H.M., Dutheil, D.B., Stivers, J.P., 2008. Lakeside cemeteries in the Sahara: 5000 years of holocene population and environmental change. PLoS One 3, e2995. https://doi.org/10.1371/journal.pone.0002995

Severinghaus, J.P., Brook, E.J., 1999. Abrupt Climate Change at the End of the Last Glacial Period Inferred from Trapped Air in Polar Ice. Science (80-.). 286, 930–933. https://doi.org/10.1126/science.286.5441.930

Shanahan, T.M., Mckay, N.P., Hughen, K. a, Overpeck, J.T., Otto-bliesner, B., Heil, C.W., King, J., Scholz, C. a, Peck, J., 2015. The time-transgressive termination of the African Humid Period. Nat. Geosci. 8, 140–144. https://doi.org/10.1038/NGEO2329

Shanahan, T.M., Overpeck, J.T., Wheeler, C.W., Beck, J.W., Pigati, J.S., Talbot, M.R., Scholz, C.A., Peck, J., King, J.W., 2006. Paleoclimatic variations in West Africa from a record of late Pleistocene and Holocene lake level stands of Lake Bosumtwi, Ghana. Palaeogeogr. Palaeoclimatol. Palaeoecol. 242, 287–302. https://doi.org/10.1016/j.palaeo.2006.06.007

Shipboard Scientific Party, 1988a. Site 658. In Ruddiman, W., Sarnthein, M., Baldauf, J., et al., Proc. ODP, Init. Repts., 108: College Station, TX (Ocean Drilling Program), 105–219. doi:10.2973/odp.proc.ir.108.103.1988

Shipboard Scientific Party, 1988b. Site 659. In Ruddiman, W., Sarnthein, M., Baldauf, J., et al., Proc. ODP, Init. Repts., 108: College Station, TX (Ocean Drilling Program), 221–325. doi:10.2973/odp.proc.ir.108.104.1988

Shipboard Scientific Party, 1988c. Site 668. In Ruddiman, W., Sarnthein, M., Baldauf, J., et al., Proc. ODP, Init. Repts., 108: College Station, TX (Ocean Drilling Program), 931–946. doi:10.2973/odp.proc.ir.108.113.1988

Shinneman, D.J., Baker, W.L., 1997. Nonequilibrium dynamics between catastophic disturbances and old-growth forests in Ponderosa pine landscapes of the Black Hills. Conserv. Biol. 11, 1276–1288.

Shukla, Y., Mintz, J., 1982. Influence of Land-Surface Evapotranspiration on the Earth's Climate. Sci. New Ser. 215, 1498–1501. https://doi.org/10.2307/1688150

Sicre, M.-A., Ternois, Y., Paterne, M., Martinez, P., Betrand, P., 2002. Climatic changes in the upwelling region off Cap Blanc, NW Africa, over the last 70 kyear: a multi-biomarker approach. Org. Geochem. 32, 981–990. https://doi.org/10.1016/s0146-6380(01)00061-4

Simpson, K.J., Ripley, B.S., Christin, P., Belcher, C.M., Lehmann, C.E.R., Thomas, G.H., Osborne, C.P., 2016. Determinants of flammability in savanna grass species. J. Ecol. 104, 138–148. https://doi.org/10.1111/1365-2745.12503

Singarayer, J.S., Valdes, P.J., Roberts, W.H.G., 2017. Ocean dominated expansion and contraction of the late Quaternary tropical rainbelt. Sci. Rep. 7, 9382. https://doi.org/10.1038/s41598-017-09816-8

Sjolte, J., Hoffmann, G., 2014. Modelling stable water isotopes in monsoon precipitation during the previous interglacial. Quat. Sci. Rev. 85, 119–135. https://doi.org/10.1016/j.quascirev.2013.12.006

Skonieczny, C., Paillou, P., Bory, A., Bayon, G., Biscara, L., Crosta, X., Eynaud, F., Malaizé, B., Revel, M., Aleman, N., Barusseau, J.-P., Vernet, R., Lopez, S., Grousset, F., 2015. African humid periods triggered the reactivation of a large river system in Western Sahara. Nat. Commun. 6, 8751. https://doi.org/10.1038/ncomms9751

Stager, J.C., Mayewski, P.A., Meeker, L.D., 2002. Cooling cycles, Heinrich event 1, and the desiccation of Lake Victoria. Palaeogeogr. Palaeoclimatol. Palaeoecol. 183, 169–178. https://doi.org/10.1016/S0031-0182(01)00468-0

Stager, J.C., Ryves, D.B., Chase, B.M., Pausata, F.S.R., 2011. Catastrophic drought in the Afro-Asian monsoon region during Heinrich event 1. Science (80-.). 331, 1299–1302. https://doi.org/10.1126/science.1198322

Staver, A.C., Archibald, S., Levin, S., Staver, C., Archibald, S., Levin, S., 2011a. Tree cover in sub-Saharan Africa: Rainfall and fire constrain forest and savanna as alternative stable states. Ecology 92, 230–232. https://doi.org/10.1890/i0012-9658-92-5-1063

Staver, A.C., Archibald, S., Levin, S.A., 2011b. The global extent and determinants of savanna and forest as alternative biome states. Science (80-.). 334, 230–232. https://doi.org/10.1126/science.1210465

Stein, R., Haven, H.L., Littke, R., Rullkotter, J., Welte, D.H., 1989. 21. Accumulation of Marine and Terrigenous Organic Carbon At Upwelling Site 658 and Nonupwelling Sites 657 and 659: Implications for the reconstructions of Paleoenvironments in the Eastern Subtropical Atlantic through late Cenozoic Times. Proc. Ocean Drill. Program, Sci. Results, Vol 108 108, 361–385.

Stockmarr, J., 1971. Tablets with spores used in absolute pollen analysis. Pollen et Spores XIII, 615–621.

Stott, P., 2000. Combustion in tropical biomass fires: A critical review. Prog. Phys. Geogr. 24, 355–377. https://doi.org/10.1191/030913300701542679

Straub, M., Sigman, D.M., Ren, H., Martínez-García, A., Meckler, A.N., Hain, M.P., Haug, G.H., Marietta Straub Haojia Ren, Alfredo Martínez-García,\tA. Nele Meckler, Mathis P. Hain & Gerald H. Haug, D.M.S., 2013. Changes in North Atlantic nitrogen fixation controlled by ocean circulation. Nature 501, 200–203. https://doi.org/10.1038/nature12397

Swain, A., 1973. A History of Fire and Vegetation in Northeastern Minnesota as Recorded in Lake Sediments. Quat. Res. 396, 383–396.

Tabel, J., Khater, C., Rhoujjati, A.L.I., Dezileau, L., Bouimetarhan, I., Carre, M., Vidal, L., Benkaddour, A., 2016. Environmental changes over the past 25 000 years in the southern Middle Atlas, Morocco. J. Quat. Sci. 31, 93–102. https://doi.org/10.1002/jqs.2841

Thevenon, F., Williamson, D., Bard, E., Anselmetti, F.S., Luc, B., Cachier, H., 2010. Combining charcoal and elemental black carbon analysis in sedimentary archives: Implications for past fire regimes, the pyrogenic carbon cycle, and the human–climate interactions. Glob. Planet. Change 72, 381–389. https://doi.org/10.1016/j.gloplacha.2010.01.014

Tiedemann, R., Kiel, U., Shackleton, J., Sarnthein, M., Shackleton, J., 1994. Astronomic timescale for the Pliocene Atlantic d18O and dust flux records of Ocean Drilling Program site 659. Paleoceanography 9, 619–638.

Tiedemann, R., Sarnthein, M., Stein, R., 1989. 15. Climatic Changes in the Western Sahara: Aeolo-Marine Sediment Record of the last 8 Million Years (Sites 657-661), in: Proceedings of the Ocean Drilling Program, Scientific Results Vol 108. pp. 241–277.

Tierney, J.E., DeMenocal, P.B., Zander, P.D., 2017a. A climatic context for the out-of-Africa migration. Geology. https://doi.org/10.1130/G39457.1

Tierney, J.E., Pausata, F.S.R.R., De Menocal, P.B., 2017b. Rainfall regimes of the Green Sahara. Sci. Adv. 3, 1–9. https://doi.org/10.1126/sciadv.1601503

Tjallingii, R., Claussen, M., Stuut, J.-B.W., Fohlmeister, J., Jahn, A., Bickert, T., Lamy, F., Röhl, U., 2008. Coherent high- and low-latitude control of the northwest African hydrological balance. Nat. Geosci. 1, 670–675. https://doi.org/10.1038/ngeo289

Tolonen, K., 1986. Charred Particle Analysis, in: Handbook of Holocene Palaeoecology and Palaeohydrology. pp. 485–496.

Toucanne, S., Angue Minto'o, C.C.M., Fontanier, C., Bassetti, M.A., Jorry, S.J., Jouet, G., 2015. Tracking rainfall in the northern Mediterranean borderlands during sapropel deposition. Quat. Sci. Rev. 129, 178–195. https://doi.org/10.1016/j.quascirev.2015.10.016

Turner, R., Roberts, N., Jones, M.D., 2008. Climatic pacing of Mediterranean fire histories from lake sedimentary microcharcoal. Glob. Planet. Change 63, 317–324. https://doi.org/10.1016/j.gloplacha.2008.07.002

Umbanhowar, C., 2004. Interactions of climate and fire at two sites in the northern Great Plains, USA. Palaeogeogr. Palaeoclimatol. Palaeoecol. 208, 141–152. https://doi.org/10.1016/j.palaeo.2004.03.001

Vallé, F., Dupont, L.M., Leroy, S.A.G., Schefuß, E., Wefer, G., 2014. Pliocene environmental change in West Africa and the onset of strong NE trade winds (ODP Sites 659 and 658). Palaeogeogr. Palaeoclimatol. Palaeoecol. 414, 403–414. https://doi.org/10.1016/j.palaeo.2014.09.023

van der Werf, G.R., Randerson, J.T., Giglio, L., Collatz, G.J., Kasibhatla, P.S., Arellano, Avelino F., J., 2006. Interannual variability in global biomass burning emissions from 1997 to 2004. Atmos. Chem. Phys. 6, 3423–3441. https://doi.org/10.5194/acpd-6-3175-2006

Van Der Werf, G.R., Randerson, J.T., Giglio, L., Gobron, N., Dolman, A.J., 2008. Climate controls on the variability of fires in the tropics and subtropics. Global Biogeochem. Cycles 22, 1–13. https://doi.org/10.1029/2007GB003122

Verardo, D., 1997. Charcoal analysis in marine sediments. Limnol. Oceanogr. 42, 192–197.

Verardo, D.J., Ruddiman, W.F., 1996. Late Pleistocene charcoal in tropical Atlantic deep-sea sediments: Climatic and geochemical significance. Geology 24, 855–857. https://doi.org/10.1130/0091-7613(1996)024<0855

Verschuren, D., Sinninghe Damsté, J.S., Moernaut, J., Kristen, I., Blaauw, M., Fagot, M., Haug, G.H., Members, C. project, 2009. Half-precessional dynamics of monsoon rainfall near the East African Equator. Nature 462, 637–641. https://doi.org/10.1038/nature08520

Vierich, H.I.D., Stoop, W.A., 1990. Changes in West African Savanna agriculture in response to growing population and continuing low rainfall. Agric. Ecosyst. Environ. 31, 115–132. https://doi.org/10.1016/0167-8809(90)90214-X

Waliser, D.E., Gautier, C., 1993. A satellite-derived climatology of the ITCZ. J. Clim. https://doi.org/10.1175/1520-0442(1993)006<2162:ASDCOT>2.0.CO;2

Waller, M.P., Street-Perrott, F.A., Wang, H., 2007. Holocene vegetation history of the Sahel: Pollen, sedimentological and geochemical data from Jikariya Lake, north-eastern Nigeria. J. Biogeogr. 34, 1575–1590. https://doi.org/10.1111/j.1365-2699.2007.01721.x

Waller, S.S., Lewis, J.K., 1979. Occurrence of C3 and C4 Photosynthetic pathways in North American grasses. J. Range Manag. 32, 12–28.

Wang, P.X., Wang, B., Cheng, H., Fasullo, J., Guo, Z.T., Kiefer, T., Liu, Z.Y., 2014. The global monsoon across timescales: Coherent variability of regional monsoons. Clim. Past 10, 2007–2052. https://doi.org/10.5194/cp-10-2007-2014

Wang, X., Auler, A.S., Edwards, R.L., Cheng, H., Ito, E., Solheid, M., 2006. Interhemispheric anti-phasing of rainfall during the last glacial period. Quat. Sci. Rev. 25, 3391–3403. https://doi.org/10.1016/j.quascirev.2006.02.009

Wang, Y., Notaro, M., Liu, Z., Gallimore, R., Levis, S., Kutzbach, J.E., 2008. Detecting vegetation-precipitation feedbacks in mid-Holocene North Africa from two climate models. Clim. Past 4, 59–67. https://doi.org/10.5194/cp-4-59-2008

Watrin, J., Lézine, A.M., Hély, C., Cour, P., Ballouche, A., Duzer, D., Elenga, H., Frédoux, A., Guinet, P., Jahns, S., Kadomura, H., Maley, J., Mercuri, A.M., Pons, I.A., Reynaud-Farrera, I., Ritchie, J.C., Salzmann, U., Schulz, E., Tossou, M.G., Vincens, A., Waller, M.P., 2009. Plant migration and plant communities at the time of the “green Sahara.” Comptes Rendus - Geosci. 341, 656–670. https://doi.org/10.1016/j.crte.2009.06.007

Weaver, A.J., Saenko, O. a, Clark, P.U., Mitrovica, J.X., 2003. Meltwater pulse 1A from Antarctica as a trigger of the Bølling-Allerød warm interval. Science (80-.). 299, 1709–1713. https://doi.org/10.1126/science.1081002

Weldeab, S., Lea, D.D.W., Schneider, R.R.R., Andersen, N., 2007. 155,000 Years of West African Monsoon and Ocean Thermal Evolution. Science (80-.). 316, 1303–1307. https://doi.org/10.1126/science.1140461

Williams, M., 2009. Late Pleistocene and Holocene environments in the Nile basin. Glob. Planet. Change 69, 1–15. https://doi.org/10.1016/j.gloplacha.2009.07.005

Winkler, M.., 1985. Charcoal analysis for paleoenvironmental interpretation: a chemical assay. Quat. Res. 23, 313–326.

Zerboni, A., Trombino, L., Cremaschi, M., 2011. Micromorphological approach to polycyclic pedogenesis on the Messak Settafet plateau (central Sahara): Formative processes and

palaeoenvironmental significance. Geomorphology 125, 319–335. https://doi.org/10.1016/j.geomorph.2010.10.015

Zhao, M., Beveridge, N.A.S., Shackleton, N.J., Sarnthein, M., Eglinton, G., 1995. Molecular stratigraphy of cores off northwest Africa: sea surface temperature history over the last 80 ka. Paleoceanography 10, 661–675. https://doi.org/10.1029/94PA03354

Zhao, M., Dupont, L., Eglinton, G., Teece, M., 2003. n-Alkane and pollen reconstruction of terrestrial climate and vegetation for N.W. Africa over the last 160 kyr. Org. Geochem. 34, 131–143. https://doi.org/10.1016/S0146-6380(02)00142-0

Zhao, M., Eglinton, G., Haslett, S.K., Jordan, R.W., Sarnthein, M., Zhang, Z., 2000. Marine and terrestrial biomarker records for the last 35,000 years at ODP site 658C off NW Africa. Org. Geochem. 31, 919–930. https://doi.org/10.1016/S0146-6380(00)00027-9

Zielhofer, C., von Suchodoletz, H., Fletcher, W.J., Schneider, B., Dietze, E., Schlegel, M., Schepanski, K., Weninger, B., Mischke, S., Mikdad, A., 2017. Millennial-scale fluctuations in Saharan dust supply across the decline of the African Humid Period. Quat. Sci. Rev. 171, 119–135. https://doi.org/10.1016/j.quascirev.2017.07.010